Computational Study of Polymer Films Using A Monte Carlo Model of Vapor Deposition Polymerization

by

Sairam Tangirala

(Under the direction of David P. Landau)

Abstract

Polymer films are a subject of both technological importance and fundamental scientific interest. Very often polymer films are created under far-from-equilibrium conditions. Polymer film growth is a complex process due to polymer's complicated structure and interactions that include internal degrees of freedom, limited bonding sites, chain relaxation, chain-chain interactions, etc.

My doctoral research focusses on the computational study of polymer films grown by an experimental growth technique referred to as vapor deposition polymerization (VDP), where a $2D$ substrate is exposed to gas phase monomers from the top and a polymer film grows on the substrate through a polymerization reaction occurring during the growth process.

A lattice Monte Carlo (MC) model was used to study polymer film growth and to examine the effects of random angle deposition, monomer diffusion, monomer adsorption, and polymerization reaction in determining polymer film properties. In addition to the aforementioned stochastic processes, our model also implemented the processes of polymer chain initiation, extension, and merger.

In our analysis, the spatial and temporal behavior of kinetic roughening were extensively studied using finite-length scaling and height-height correlations. The scaling behaviors at

local and global length scales were found to be very different. The global and local scaling exponents for morphological evolution were evaluated for varying system parameters. A systematic study was performed to discover the universality class of our VDP growth model.

We also studied the aggregation mechanism of polymers grown by VDP. The behavior of polymer chain length distributions were carefully analyzed and the dynamic scaling approach was employed to highlight the dependence of polymer aggregation on the system parameters. As the ratio of diffusion rate to the deposition rate was increased in the VDP growth, we observed a systematic change in the aggregation mechanism that prevented the manifestation of a unique scaling function for chain aggregates.

Finally, we calculated the conformational properties of polymer chains and studied their dependence on system parameters. The structural studies were useful in understanding the bias in the preferred growth direction of the films as diffusion was increased in the system.

INDEX WORDS: Vapor deposition polymerization, Polymer films, Monte Carlo model, Stochastic processes, Growth models, Dynamic scaling analysis, Universality classes.

Computational Study of Polymer Films Using A Monte Carlo Model of Vapor Deposition Polymerization

by

Sairam Tangirala

M.Sc., Sri Sathya Sai Institute of Higher Learning, 2002

M.Tech., University of Hyderabad, 2004

A Dissertation Submitted to the Graduate Faculty

of The University of Georgia in Partial Fulfillment

of the

Requirements for the Degree

Doctor of Philosophy

Athens, Georgia

2011

Computational Study of Polymer Films Using A Monte Carlo Model of Vapor Deposition Polymerization

by

Sairam Tangirala

Approved:

Major Professor: David P. Landau

Committee: Steven P. Lewis
Craig Wiegert
Shan-Ho Tsai

Electronic Version Approved:

Maureen Grasso
Dean of the Graduate School
The University of Georgia
May 2011

Dedication

To my parents Ms. Sujatha, Mr. Ramakrishna and siblings Saikrishna and Sunitha.

Acknowledgments

I would like to express my gratitude to Bhagawan Sri Sathya Sai Baba for his ever present love and support through out my journey of life. I would not have been here with out Baba's blessings and support. I am grateful to all my family members for their ever-present enthusiasm and encouragement. My special thanks to my brother Saikrishna who in his subtle words showed his support through out my interactions with him.

This work could not have been completed with out the guidance and mentorship of my doctoral research supervisor Prof. David Landau. I am thankful to have benefited from his research expertise through out my research work. It has been a memorable experience to have been a member of the Center for Simulational Physics at the University of Georgia.

My doctoral committee, Dr. Shan-Ho Tsai, Dr. Craig Wiegert, and Dr. Steven P. Lewis, has also been very helpful throughout my graduate studies. I am thankful to all my committee member for having provided me their expertise and insights ranging from topics covering Physics to teaching pedagogy. I am glad to have met Dr. Michael Bachmann and to have learnt from his outlook towards the importance of simulations. A number of my colleagues have also helped me during my overall scientic learning, including Dr. V.S.S. Sastry, Dr. K.P.N. Murthy, Dr. Steven J. Mitchell, Dr. Joao Plascak, and Dr. Thomas Wüst. My learning has been a pleasant experience due to a number of peers whose interactions have played an important role in my graduate career, many thanks to Dr. Daniel Seaton, Dr. Kalyan Allada, Krishnareddy, Vijay Veeraghattam, Vikram Dhende, Kamal, and Srinivasa Murthy.

I would also like to acknowledge various funding agencies that have provided support throughout my doctoral studies. They include, The National Science Foundation, TeraGrid, and The Department of Physics and Astronomy of The University of Georgia.

Table of Contents

List of Figures

Chapter 1

Introduction

The work presented in this doctoral dissertation focuses on understanding the physical mechanisms that underlie a Chemical Vapor Deposition (CVD) experimental technique, popularly employed in the fabrication of linear polymer films grown via Vapor Deposition Polymerization (VDP). VDP refers to the growth of higher molecular weight products directly from lower molecular weight vapor precursors. Inside a reactor, the precursor vapor phase chemical material undergoes a polymerization reaction to form immobilized films on the desired substrate. The deposited films can be grown to desired thicknesses thus enabling ultrathin, pinhole-free coatings. Materials can also be deposited onto rough surfaces and complex geometries yielding conformal coatings. [1]. The advantages of VDP methods are their versatility in synthesizing both simple and complex polymers with relative ease and generally at relatively low temperatures (close to room temperature), along with precise control of the composition and architecture of the resulting products. Another much desired feature of vapor depositable polymers is its "green chemistry" that involves the absence of any other chemicals or catalysts, thereby offering inherent cleanliness and minimal hazardous waste [2].

The performances of devices based on VDP depend not only on the precursor material but also on the arrangement of the molecules in the resulting films [3]. To understand the film growth, the kinetic processes should be considered on a molecular scale. Developing a reliable, scalable, and low-cost method to grow nanostructures, with control over design

parameters like diameter, length, and morphology, is vital for the success of polymeric structures in technological applications and for improving the performance of the devices based on them.

The motivation for studying polymer film growth via VDP arises from their varied applications and the above mentioned advantages. For understanding the physical principles governing a typical VDP experiment, we developed a Monte Carlo (MC) model to simulate polymer film growth (via VDP) and studied the affects of inherent dynamical growth processes. Our simulations employed a lattice model approximation to a typical VDP experiment. The model was restricted to $1+1D$ dimensions and simulated many physical processes often observed in a VDP experiment. In particular, we implemented the processes of monomer deposition, adsorption, and diffusion along with other stochastic processes of polymer chain initiation, extension, and merger. This dissertation presents the results of our study of various aspects of VDP that include: an extensive investigation of interface width of deposited polymer films; the scaling of polymer chain length distributions; and a conformation analysis of polymer chains formed during VDP growth. Other related topics, including the structural properties of polymers and bulk films, are also discussed as appropriate to the understanding of the growth mechanism.

In the second chapter, we provide a motivation for studying polymer growth systems along with an introduction to some of the popular paradigms used in modeling polymer systems. It also includes a review of some of the contemporary experimental and simulation techniques that have been used in studying VDP systems.

The third chapter introduces the MC model that was developed during our research on the VDP growth process. The sections of this chapter present the details of our model and its implementation. A description of various MC moves and the probabilistic method used in making MC decisions during the growth process are also discussed in this chapter.

The fourth and following chapters are devoted to the results obtained from our simu-

lational study. The results discussed in this chapter were published in [4] and have been reproduced with permissions [1]. In particular, the fourth chapter concentrates on the scaling analysis of the polymer film's interface width. It provides details of the finite-length scaling analysis that was performed to understand the scaling behavior of interface width at local and global length scales. A comparison is made between our simulational findings and published results from the literature.

Chapter Five deals with the analysis of polymer chain aggregates using the study of chain length distribution functions for varying model parameters. Specifically, we examine the behavior of chain length distribution as a function of chain length, deposition time, and diffusion parameter. A systematic approach has been presented to discover the dependence of chain length distributions on relevant system parameters. The results discussed in this chapter were communicated to Physical Review E as a regular article and have been reproduced with permissions [2]. We conclude this chapter by mentioning the strong influence of monomer diffusion on the chain length distributions which prevents the appearance of a universal scaling function. It also includes a comparison of our polymer chain aggregates results to a contemporary VDP experiment.

Chapter Six presents the results on various structural quantities that are typically used in characterizing polymer chain configurations. It contains the calculations of quantities like radius of gyration, fractal dimensions, and other geometric properties of the chains formed during VDP growth. We also discuss the dependence of relevant structural quantities on the model parameters.

As a conclusion, chapter seven is reserved for closing remarks and summarization of our research findings pertaining to the growth of polymer films using the VDP method.

[1] Reprinted figures with permission from [4] ©2010 by the American Physical Society.

[2] Reprinted figures with permission from Sairam Tangirala and D.P. Landau, Phys. Rev. E (July 2010), ©2010 by the American Physical Society.

Chapter 2

Background

2.1 Motivation

Organic polymer films exhibit a number of interesting properties, and their current and potential applications are rather broad, ranging from biomedical devices to microelectronic devices. The advantages of VDP-based methods in producing polymers is their versatility in synthesizing both simple and complex polymers with relative ease and precise control of the composition and architecture of the resulting materials. Other benefits of VDP include solvent-free environments, excellent adhesion onto substrate, high coating fidelity, and the ability to accommodate custom-tailored surface modifications [5, 2]. Many experimental efforts have focussed on the formation of polymer films using VDP [6, 7, 8] as this technique has immense technological applications in microelectronic interconnects [9, 10], organic electronics [10], and biomedical applications [11]. In nanotechnologies too, ultrathin polymer coatings prepared by VDP are of particular interest. One of the materials made by VDP is Poly(P-Xylylene) (PPX, commercially known as Parylene), a crystalline polymer characterized by a set of useful physical and chemical properties. For example, PPX films have been applied as moisture-proof coatings for electronic and microelectronic devices [12]. The PPX coatings are also used in the protection of radio electronic and microelectronic devices (such as printed boards, microassemblies, bare semiconductor devices, etc.) against aggressive environments. Recent interest in PPX films has been driven by the development of film materials for the interlayer insulation in high-efficiency semiconductor devices. Such materials exhibit desirable characteristics of (relatively) low electric permittivity, thermal

stability, high mechanical characteristics, and low linear-expansion coefficient [13].

Another factor promoting the study of VDP in fabricating desired polymer deposits relates to the fact that the design of many components frequently used in microelectronics are close to their physical limits. The capabilities of current conventional approaches to fabricate new electronic components and materials seems almost exhausted. It is thought that the creation of new materials with desired properties can be made possible using the structural variations at molecular, submolecular, and nanosized levels. At submolecular and nanosized length scales, one can expect qualitative variations in the basic material properties such as thermal conductivity, electrical conductivity, plasticity, photoconductivity, permeability, etc. [13]. Because of the versatility and technological applicability of VDP in coating technology, it is potentially rewarding to understand the principles underlying VDP growth.

For some time now, the study of various properties of polymer films grown using VDP has been a subject of wide interest, primarily due to the special requirements on the surface roughness of functional coatings [14, 15]. It is also known that the surface characteristics of deposited materials can strongly affect the electrical and optical properties of coatings [16, 17]. In applications involving the improvement of catalytic or sensor characteristics, the active area of the functional surface needs to be increased; and consequently thin-film coatings with a maximally large surface structure are required [18, 19]. In such applications, the problem of controlling surface morphology is of great importance and a solution to this problem can be found by understanding the mechanisms that determine a coating's surface structure during its formation. Another popular research area has been to study the integration of polymer growth with conventional microfabrication processes. This hybrid approach hopes to combine the best aspects of well established fabrication techniques with the novel properties of polymers.

Many deposition methods like VDP [20, 21, 22], ionization-assisted polymer deposition [23], sputtering growth [24], pulsed laser deposition [25, 26], and organic molecular beam

deposition [27], have been developed to grow a variety of polymer films. However, polymer film growth is still an undeniably complex phenomenon compared to conventional inorganic film growth. The difficulties in understanding the behaviors of polymers arise from their complicated structures and interactions. These include many internal degrees of freedom, limited bonding sites, chain-chain interactions, and various relaxation mechanisms. Aside from a few small organic molecules that form films through van der Waals interaction or hydrogen bonds, most of the molecules are long-chain polymers formed as a result of polymerization reactions during film deposition. Although there has been much experimental work on surface characterization of films grown using VDP, much less effort has been devoted to determining the polymer growth mechanism itself.

We carried out a broad literature survey of VDP based systems and after familiarizing ourselves with the published experimental data on linear polymers, we developed a computational frame-work to model and study the complex process of polymer growth using VDP. Our ultimate goals were to compare our simulational data with available experimental results and to understand the underlying physics principles. Going forward, we focus on a typical example of VDP growth of Poly(P-Xylylene) (also known as PPX or Parylene).

2.2 Polymers and Coarse-Grained Models

Polymers are chemical compounds that are made up of repeating identical molecular units called monomers (monomer units) that are held together by chemical bonds. A polymer chain is a large macromolecule that is typically modeled as a chain of repetitive monomer units. The polymers we are interested in are homopolymers, in which the constituting units are all identical. Besides this basic aspect of the homogeneous character of the chain, real polymers are complex molecules typically fluctuating in shape and interacting with their (possible) solvent molecules, neighboring polymers, as well as with other portions of themselves. The interactions between the parts of the same polymer are commonly referred to

as "self-interactions" or "excluded volume interactions". More comprehensive information about polymers and polymer models can be found in the classical references [28] and [29].

Computer simulations of polymer systems are known to have computational and implementation difficulties because of the multiple length and time scales inherent in polymer systems. Such complexity increases many fold when considering the non-equilibrium growth of linear polymers such as VDP. Their inherent complexities can be appreciated by considering a typical example of flexible polymer chains in solution or melts. The polymers in solutions or melts exhibit nontrivial geometric structure that range from the scale of their chemical bond lengths to their coil size, and even larger length scales are known to occur due to their collective phenomena [30]. The computational resources required for performing atomistically realistic simulations for reasonable (with respect to polymer systems) length scales are extremely expensive, if at all feasible. For polymer chains, such simulations are generally not feasible as polymers tend to have much wider spread of relaxation times due to their varying bond lengths and bond angles.

For a computational method that captures the details of the dynamical processes, such as Molecular Dynamics (MD), the studies of non-equilibrated systems are beyond reach. Even for the case of a chemically simple polymer such as polyethylene, a MD simulation is restricted to melts of short chains [30]. We instead take an alternate approach and try to simplify the computational tasks by eliminating the fast-varying degrees of freedom, "integrating out" the local structure and focusing on the long length scale properties. This approach is commonly referred to as "coarse-graining" along the backbone of the polymer chain. In this approach several chemical bonds are integrated out and replaced by one "effective bond" [31]. This methodology is relatively well established and has been successfully applied to models of random or self-avoiding walks on a lattice [28, 29, 32], the "bead-spring chain" [33, 34], etc. As the coarse-graining approach is very hypothetical, we can use this formalism to deal with universal properties of polymer chains (macromolecules), irrespective of the specific chain

architecture. In spite of being highly idealized, lattice models such as the bond fluctuation models [35, 36] describe many local properties in a qualitatively reasonable way and can be considered as a starting point to model other non-universal (specific) properties of polymers. The studies of non-universal properties quite often require the use of effective potentials for the lengths of the effective bonds and bond angles between the monomer units of the specific polymers of interest [37, 38]. The effective potentials are constructed from more realistic models and ultimately rely on results from quantum-chemical calculations [31, 38].

As a compromise with the computational complexities of all-atom models, a number of multi-step coarse-grained simulation processes have been introduced [39, 40]. The concept of coarse-graining might have multiple meanings depending on the context and on the quantitative accuracy of the research study. In studying the equilibrium properties, initial coarse-graining in these methods typically approximates the fine atomic-level detail (side chains) by simulating only the coarse polymer backbone. Once the equilibrium states of the reduced chain structure have been identified, the previously removed atomic details are added back to the polymer backbone, and the equilibrium structure is further refined by simulations.

In computational studies using simple coarse-grained models, polymers are often reduced to a chain of connected balls (monomer units) on a lattice and the self-interaction is modeled by the self-avoiding constraint, implemented via an excluded volume condition. In our current simulations we used the "ball-and-stick" model to represent a polymer chain. This modeling paradigm has the characteristics of lattice-centered positions of monomers and the presence of rigid bonds between them. The monomers were represented by circles (in $2D$ simulations), were connected by "sticks" that represented the chemical bonds between two nearest neighboring monomers. In a realistic model, the angles between the rods (chemical bonds) should be the same as the angles between the actual bonds, and the distances between the centers of the spheres should be proportional to the distances between the corresponding

monomers. However, for the sake of simplicity and as a consequence of using a lattice model, we decided to restrict all chemical bond angles to 90° or 180° and fix the bond lengths between all the nearest neighboring monomers of the chain to be identical to the unit lattice distance. More information about the specifics of our model are discussed in Chapter 3.

2.3 Vapor Deposition Polymerization

The deposition of Parylene (PPX) onto a surface using a gaseous precursor was first reported by Szwarc [41] in 1947. Since its discovery, Parylene has attracted a great deal of interest because of its many technologically desirable properties discussed earlier in Section 2.1. Parylene is one of the products that formed in the vacuum due to the thermal decomposition (pyrolysis) of Para-Xylylene[42]. The yields of polymer film from this method were only a few percent even at relatively high pyrolysis temperatures, ranging from 700°C to 900°C [43]. The dry preparation of PPX by chemical VDP via vapor phase pyrolysis received considerable interest after the work of Szwarc [41] and initiated a number of experiments studying the feasibility and mechanistic considerations of this process. Later Gorham found an efficient way of depositing Parylene films using the vacuum pyrolysis of di-para-Xylylene (dimer molecule) [44]. As shown in Fig. 2.1 [1], each molecule of Poly-Para-Xylylene (Parylene-N) is composed of an aromatic group with methylene groups attached at the para positions. At temperatures greater than $550°C$ and at pressures of less than 1 Torr, the dimer gets broken (pyrolized) into two Para-Xylylene monomer units which are then adsorbed onto the film surface at room temperature. Consequently, spontaneous polymerization results in the formation of high molecular weight Parylene polymers.

[1] Figure 2.1 was taken from pg. 5 of [45]. Reproduced with kind permission from Kluwer Academic Publishers.

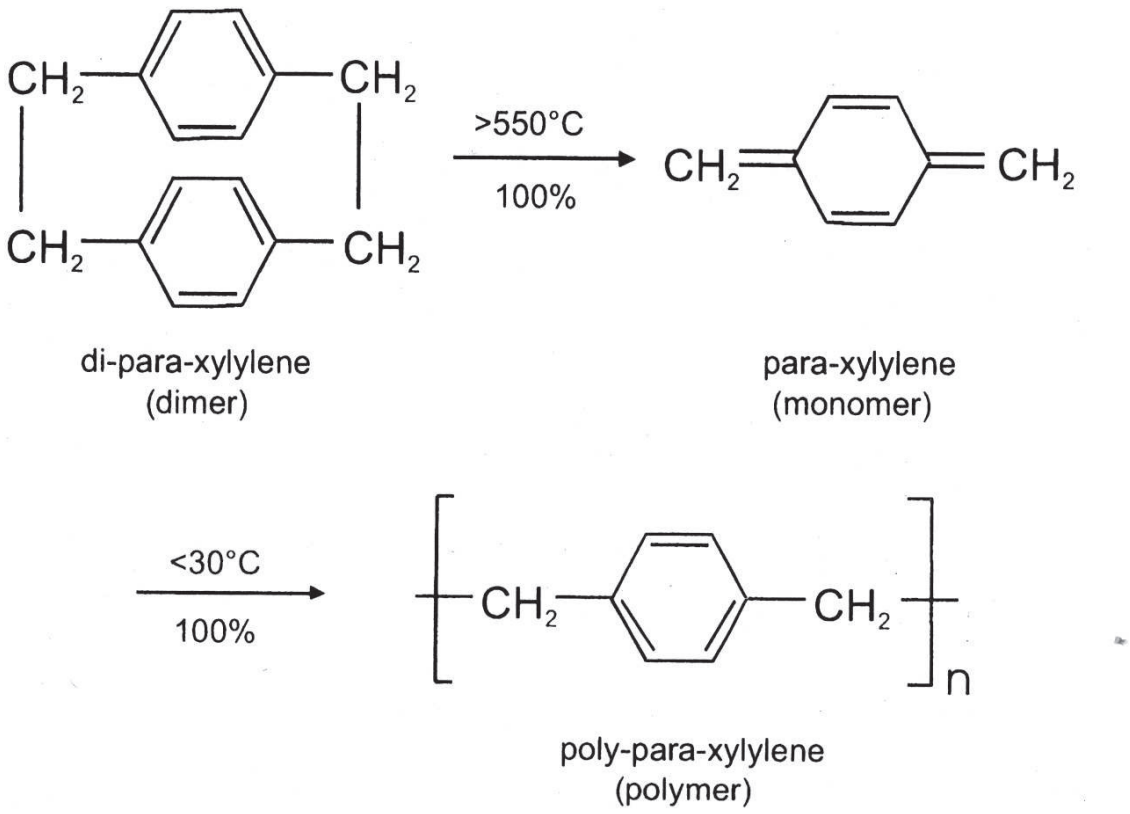

Figure 2.1: The polymerization mechanism of Parylene-N.

2.3.1 Polymerization Mechanism

Polymers are often categorized based on the polymerization kinetics occurring during their growth. Typically, all polymerization mechanisms can be classified into two types: Step growth and Chain growth [45]. In step growth polymerization, a chemical bond forms between any two random molecules. The reacting molecules can be any combination of a monomer, an oligomer (chain with less than 10 units), or another chain. Whereas, a chain growth polymerization refers to the growth of a polymer chain by one monomer unit at a time. The chain growth of a linear polymer occurs due to the attachment of a monomer to either of the two ends of the chain. The chain end could be a radical, a cation, or an anion. The chain growth polymerization takes place in three common steps: initiation, propagation, and termination. The details of chain growth polymerization are discussed in the following Chapter 3. The topic of our interest is Parylene growth that results from chain growth polymerization, except that the chains are not terminated during the growth. The chain ends (also referred to as active ends) of the polymers can however be buried within the film as it grows. Subsequent termination of the radical chain ends can occur post-deposition via reactions such as with atmospheric oxygen that generally diffuses into the polymer film [12].

2.3.2 Basic Processes in Vapor Deposition Polymerization

As suggested by Beach et al. [12, 46], both condensation and diffusion of monomers seem to occur during a VDP process. In a typical VDP experiment, a highly smooth wafer ($2D$ substrate) is exposed to one or more volatile gas phase precursors that produce monomers. The monomers are released from the top of the deposition chamber and travel down towards the substrate at random angles and locations. The deposited monomers may react and/or diffuse on the substrate surface to produce the desired deposit. Polymer thin films grown by VDP are made up of long polymer chains formed through chain growth polymerization reaction occurring during the growth process. The polymerization process involves the interaction of

two monomer molecules in a chemical reaction to initiate a dimer (polymer chain of length 2). The monomers travelling towards the substrate are eventually used up by one of the following processes: chain initiation in which new polymer molecules are generated; and chain propagation in which the existing polymer chains are extended to higher molecular weight. Besides these two physical processes, monomer adsorption, diffusion, and polymer merger can also occur during the growth and can be considered as relevant mechanisms that determine the overall film growth. As we were interested in studying linear polymer films (such as Parylene), chemical bonding restrictions were introduced in the polymer growth process. A monomer was only allowed to bond to either of the two active ends of a linear polymer, or to another nearest neighboring monomer. The bonding restrictions of linear polymers are very different from conventional physical vapor deposition (PVD) processes [47], where atoms can bond to their nearest neighboring nucleated clusters and atomistic processes such as surface diffusion, edge diffusion, step barrier effect, etc. affect the growth, resulting in the films being compact and dense [48, 49, 50, 51]. Investigations by Zhao et al. [52] have shown that the submonolayer growth behavior of VDP is very different from that of PVD due to long chain confinement and limited bonding sites, indicating that the detailed molecular configuration can drastically change the growth behavior [53].

2.4 Review of VDP Research

Since the discovery of VDP by Szwarc in 1947 [43], there have been a number of studies concentrating on understanding the VDP process used in the fabrication of a variety of polymer films. A brief summary of some of the contemporary studies pertaining to VDP is presented in this section. Although the literature results presented here are not comprehensive, they are meant to be representative of many scientific articles and are being discussed here for providing a review of the status quo in VDP research.

With a vast increase in the applications of PPX, there have been efforts to develop innovative ways to produce this polymer. The Refs. [54, 55] provide an overview of various synthetic approaches to produce Parylene. They also provide perspectives on the possible relationship between polymer film's structure and their characteristic properties. Commercially driven research includes reports on the synthesis of PPX and its derivatives from readily available compounds like α, $\alpha^{'}$-diether of P-Xylene [56]. The experimental results of Streltsov et al. [57] include Atomic Force Microscopy (AFM) studies of the surface morphology of Poly(P-Xylylene) thin films prepared by VDP for a range of polymerization temperatures. They analyzed the roughness of polymer films and reported that an increase in the substrate temperature results in a decrease in the roughness exponent at temperatures higher than the PPX glass transition temperature. They also studied the effect of the type of substrate, growth rate of polymer film, and the substrate temperature on the scaling coefficients of the synthesized films. In general they found that an increase in the growth rate of the polymer film resulted in an increased roughness exponent. There have been other studies dealing with the behavior of interface width of the films. For example, Ref. [58] quantified the evolution of growth front roughness of Parylene films using AFM measurements and reported a new universality class for the scaling behavior of polymer growth that was believed to arise from monomer bulk diffusion present in VDP. A similar study by Lee et al. [59] found drastic changes in the dynamic roughening behavior, involving unusually high growth exponent in the initial growth regime, followed by a growth regime characterized by growth exponent being zero, and finally a crossover to a different growth exponent value. Although both the mentioned experiments analyzed the films generated by VDP of same precursor material, the differences in their experimental observations have not yet been understood.

Apart from many experimental studies, there have been rigorous theoretical studies on understanding the initiation reaction and propagation steps of Parylene polymerization (up to pentamer) using different quantum-chemical methods [60]. Molecular Dynamics (MD)

simulations in this area include the studies of bulk phases of PPX and its isolated chains, the calculation of thermodynamic properties, molecular mobility, and structural characteristics [61]. Fortin et al. [8] developed a kinetic model for CVD of Parylene thin films using a multistep approach that includes physisorption of monomers on the film surface followed by their subsequent chemisorption. A comparison between their model predictions was found to fit experimental kinetic data well for a large range of pressures and temperatures.

Along with the development of more "accurate" first-principles and MD-based simulational studies, there have been a number of coarse-grained MC studies of VDP concentrating on various aspects of the growth process, ranging from the behavior of polymer film morphology, to interface width evolution, to the analysis of the multi-affine nature of the polymer films. Zhao et al. [52] proposed a stochastic MC model for the initial growth of polymer films and reported the existence of three distinct growth regimes: a low-coverage initiation regime, a chain propagation regime, and a saturation regime. Their growth regimes of initiation and propagation were found to be similar to the Molecular Beam Epitaxy (MBE) model, whereas the saturation regime was found to predict very different kinetics than MBE. There have been other MC based studies reporting the behavior of polymer chain length, interface width, the film thickness, as well as the interfacial depth as a function of relevant model parameters [53, 4, 62].

The lack of sufficient theoretical studies coupled with inconsistencies in the experiments motivated us to have a closer look at modeling VDP. Our current study performs an extensive analysis of the roughening mechanism, aggregation phenomena, chain conformations, etc., that occur during polymer film growth. We also have made comparisons of our simulational data with earlier reported experiments where ever possible.

Chapter 3

Model and Methods

For studying VDP process using computer simulations, we mimicked the real-time polymer film growth in terms of a simple $1+1D$ lattice model. In a bell-jar type deposition chamber of a typical VDP experiment, the monomer transport from the source to a $2D$ substrate is similar to that of a conventional physical vapor deposition (PVD) of molecular beam epitaxy (MBE). However, there are many differences in the nucleation and growth processes after the monomers are deposited on the substrate. In a PVD process, after the monomers reach the film surface they become chemically inert by diffusing and forming islands (clusters) with the nearest neighboring monomers. There are many atomistic processes such as surface diffusion, edge diffusion, step barrier effect, etc. that can affect PVD growth. Consequently, the PVD generated films are observed to be dense and compact with an increase in monomer diffusion. In contrast, in a VDP process the deposited monomers become stable only when they interact with other neighboring monomers or with either of the two active ends of the linear polymers present in the system. In this dissertation we use the term "active ends" to refer to either of the two ends of a linear polymer. The chain ends are considered to be "active" because, in addition to an existing chemical bond with the rest of the chain, they can form an one more chemical bond. Whereas a "monomer" in the system can form a maximum of two chemical bonds. Besides monomer diffusion, other surface dynamics that can affect the growth mechanisms in VDP are inter-molecular interactions, chain-chain interactions, and chain relaxations.

While developing our Monte Carlo (MC) simulation model, such characteristics of VDP

were carefully considered and included in our growth model. In the following section we discuss the details of polymer growth as implemented in our VDP model.

3.1 Details of Polymer Growth

The VDP growth was implemented on a $2D$ lattice on which MC simulations were performed. The monomer diameter that sets the length scale of the system was chosen to be the same as the lattice constant of the system. The growth dynamics of our simulations proceeded as follows: the simulations began at deposition time $t = 0$, with an unoccupied flat $1D$ substrate with L lattice sites. The monomers were released from above the substrate with a constant deposition rate F (in units of monomers per site per unit time) at random launch angles with respect to the substrate normal and travelled towards the $1D$ substrate located at $y = 0$. We used the KISS random number generator [63] in our simulations to make all stochastic decisions of the VDP growth. The KISS random number generator is a combination of (a) a congruential generator, (b) a 3-shift shift-register generator, and (c) two 16-bit multiply-with-carry generators; its overall period is known to be greater than 2^{123}. We also tested our program with the standard ISO C random number function *rand()* included in the GNU library. This *rand()* function uses a simple (single state) linear congruential generator only in case that the state is declared as 8 bytes. If the state is larger (an array), the generator becomes an additive feedback generator. The results from both random number generators were found to be identical to within statistical errors. In our model, for a $1D$ substrate of length L, one MC time unit ($t = 1$) corresponded to the deposition of L monomers in the $1 + 1D$ system.

The VDP growth model employed in our study is similar to the square-lattice disk model studied by Ref. [64] along with additional constraints that are specific to VDP growth. The depositing monomers followed a lattice approximation of a straight line trajectory until contacting the surface. The depositing monomers were then moved to the lattice position

nearest to the point of contact. If final landing position of the depositing monomer has a nearest neighboring monomer or an active end, the monomer is bonded permanently there and stops diffusing. Otherwise, the newly deposited monomer was allowed to diffuse via equally probable nearest-neighbor hops with a diffusion rate D (nearest neighbor hops per monomer per unit time). A monomer that was deposited on top of an existing polymer chain was physically adsorbed on the chain and was allowed to diffuse with same rate D. The monomers arrived towards the surface with a probability of deposition p_F and were allowed to diffuse with a probability of diffusion p_D discussed later in Section 3.3. In our simulations, the deposition and diffusion processes did not take place simultaneously but were implemented independently depending on the values of p_F and p_D. Our diffusion approach resembles the full (or collective) diffusion models [53, 65], where simultaneous diffusion of many atoms or molecules is simulated. This is in contrast to limited mobility models for molecular beam epitaxy (MBE) where the successive (multiple) diffusion of only one monomer is simulated in any diffusion step [66, 67]. The full diffusion models are considered to be more realistic as they avoid the possibility of finding many isolated monomers in energetically unfavorable positions after their diffusion hops, which is a possible concern of the limited mobility assumption. With the passage of MC time, as the monomer coverage increases on the substrate, the polymer film grows along a direction perpendicular to the substrate. This "two dimensional" growth is often referred to as the $1 + 1D$ growth in literature. In our model, the excluded volume constraint was implemented by rejecting the diffusion or deposition moves to an already occupied site. We also neglected chain-relaxation moves which are expected in real-time VDP experiments even for rapid deposition. Our assumption is a logical starting point for studying the role of monomer diffusion, independent of other processes. The detailed description of various MC moves that were implemented in our model are presented in the Section 3.3.

3.2 Probabilities of Deposition and Diffusion

At each stage of the simulation, either a deposition or a diffusion step was performed depending on the current state of the system. For keeping track of the competing rates of diffusion and deposition we used the method suggested by Amar et al. [68] and carried out the deposition with a probability p_F,

$$p_F = \frac{1}{1 + N_1 G}, \tag{3.1}$$

where N_1 is the total number of monomers present in the system and $G = D/F$. The diffusion was carried out with the probability p_D,

$$p_D = 1 - p_F = \frac{N_1 G}{1 + N_1 G}. \tag{3.2}$$

As it can be observed from the Eqns. (3.1) and (3.2), the probabilities of deposition and diffusion are not constant thoughout the simulation. The probabilities p_F and p_D keep varying throughout the simulation depending on the number of monomers N_1 available in the system at a given time. In our simulations the incoming monomer flux F was fixed ($F = 1/L$) for different diffusion rate D, and an increase in D was parametrized as an increase in $G = \frac{D}{F}$. Throughout the growth process the lists of all monomers and polymer chains were continually updated. If a monomer encountered another monomer or an active end of a polymer chain as its nearest neighbor, it was added to the polymer chain and removed from the monomer list.

3.3 Monte Carlo Moves

In our work, a number of MC moves were employed to simulate various dynamical processes occurring during the VDP growth. The physical processes that were implemented in our model are described below.

Deposition:

At each deposition step, a monomer was introduced into the system. The deposited monomers were released from a height three lattice units above the highest occupied position on the substrate with an initial x-value (horizontal position) randomly chosen from $1 \leq x \leq L$. The launch angle distribution of the downward travelling monomers did not follow a collimated flux, but instead had a uniform distribution which corresponds to a nonuniform flux distribution $J(\theta) \propto 1/\cos(\theta)$ often referred to as a "cosine flux" in literature [69, 70]. Here θ was defined as the angle between the direction of the impinging monomer and the positive x-axis (the symbol θ is later used for "coverage" in Section 5.3). The monomers travelled downwards, and for avoiding very shallow deposition angles θ was chosen randomly from the interval $(\pi + 0.2, 2\pi - 0.2)$ with uniform probability. We chose to deposit the monomers from three lattice units above the highest point on the surface, after testing different release heights. We found the results to be independent of the release heights of the monomers. In addition, by choosing a smaller release height, we saved the additional computational time spent on calculating the trajectories of all the deposited particles.

Surface Diffusion:

After the deposited monomers arrive onto the surface, they typically undergo finite diffusion hops to their nearest neighboring locations depending on the value of p_D. They can get deposited either onto a polymer body or on the substrate and subsequently wander from one site to another site along the absorbent. The surface growth is determined by the ratio of the diffusion coefficient to the deposition flux, G. As mentioned earlier, in our simulations we set $F = 1/L$ for convenience, such that $G \propto D$.

Chain Initiation/Nucleation:

When two monomers meet on the substrate or on polymer bodies as nearest neighbors, they undergo chemical polymerization and form a dimer. This process is called polymer chain-initiation or nucleation. In contrast to MBE growth where atoms can attach to any of the nucleated sites, in the VDP a stabilization reaction occurs only at the active ends (active

sites) of a polymer chain. Such active bonding in VDP growth is a key characteristic, in addition to the cosine flux for monomer deposition. A trimer can also form during nucleation, resulting from a deposition of a monomer between two adjacent neighboring monomers.

Chain Propagation:

When a monomer reaches either one of the active ends of a polymer, it is bonded to that active end of the chain. This increases the chain length by one unit and at the same time the newly added monomer becomes an active end of the polymer. This mechanism of an increase in the chain length of a polymer is referred to as chain propagation.

Polymer Merger:

This is a type of chain propagation in which an active end of one polymer meets that of another polymer as its nearest neighbor. Subsequently two distinct polymers are merged into one long polymer. It is important to note that for linear polymers studied here, only the two ends of the chain are active, and can react with monomers or other polymers. In special cases, where an active end of a polymer meets the other active end of the same polymer, the two active ends are not allowed to merge into a stabilized polymer loop and such a trial is rejected. This restriction avoids the formation of closed polymer loops and is motivated from the experimental observations of long polymers in the experiments. In special cases where a monomer was the nearest neighbor to the active ends of more than two polymers, we selected a random pair of polymers and performed polymer merger.

The Fig. 3.1 shows the schematics of various processes occurring during the non-equilibrium VDP growth on a $1D$ substrate of length L with periodic boundary conditions. Specific examples of the aforementioned dynamical processes are discussed here using Fig. 3.1. In Fig. 3.1, process 1(a) shows the vapor phase monomers depositing onto the substrate at random locations with uniform launch angle distribution. We neglected re-emission effects and the downward travelling monomers were made to always stick to the first nearest neighboring particle that comes on its deposition path. The monomers may get adsorbed

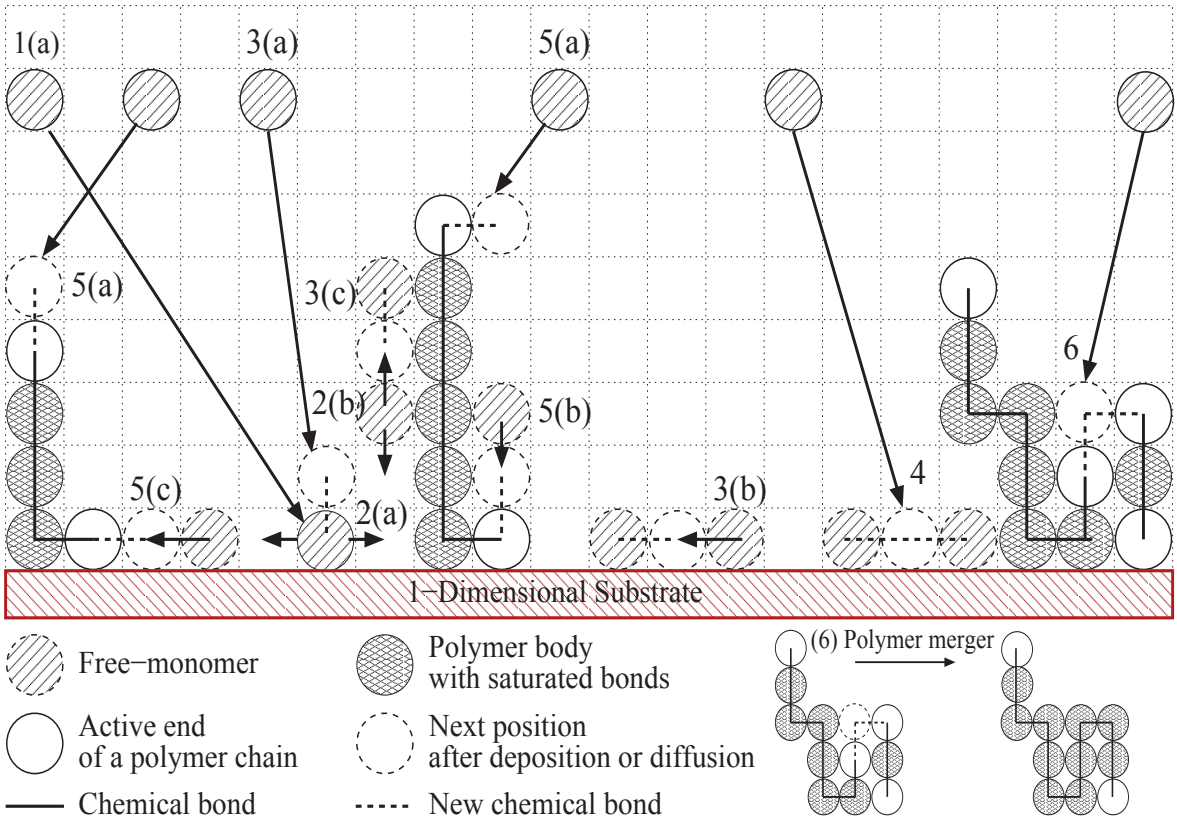

Figure 3.1: Schematic of our 1+1D VDP growth model. Various processes implemented in our model are explained using following labels; 1(a): monomer deposition at random angles. 2(a,b): Adsorbed monomer diffuses on the substrate and a polymer chain respectively. 3(a), 4: Polymer chain initiation resulting from random angle deposition. 3(b,c): Chain initiation resulting from monomer diffusion on the substrate and polymer chain respectively. 5(a): Chain propagation resulting from monomer deposition onto the active end of a polymer chain; 5(b,c) Chain propagation due to monomer diffusion on polymer chain and substrate respectively. 6: Polymer merger resulting from deposition. In all processes, the straight lines with arrows represent the trajectory of monomers.

either on the substrate (as shown by process 2(a)) or on polymer chains (indicated by process 2(b)), depending on what they encounter on their deposition path. Adsorbed monomers can diffuse along the adsorbent to any of the nearest-neighboring unoccupied sites with equal probability. The polymer chain length s refers to the number of monomers forming a polymer chain. As seen in process 3(a), when an impinging monomer encounters another monomer on the substrate as its nearest neighbor, both become immobile and undergo a chemical reaction to form a dimer ($s = 2$). Dimers can also be formed due to monomer diffusion on substrate or existing polymer chains as shown in processes 3(b) and 3(c) respectively. Polymers with $s = 3$ (trimers) can also be formed after deposition of monomer between two monomers as shown by process 4. When a downward travelling monomer encounters an active end of a polymer chain, it attaches itself to the chain and increases s by one unit as shown in a couple of processes labeled as 5(a). A diffusing monomer may encounter an active end of a chain in its neighborhood and get bonded to that polymer chain there by propagating the chain by one unit as shown in processes 5(b) and 5(c). In the linear polymer system studied here, the monomers were allowed to form a maximum of two chemical bonds. At any given time, only the two ends of the polymer chain were chemically active, resulting in the chain propagation at these two end locations only. The chain portion (of the polymer), excluding the two chemically active ends, was not allowed to form chemical bonds with neighboring monomers. Monomers can, however, be physisorbed on the chain and later diffuse along the chain as shown in processes 2(b) and 5(b). The process labeled 6 shows *polymer merger* occurring during the growth when the active ends of two different polymers meet as nearest neighbors and react chemically to join the two polymers into one longer polymer chain with a higher molecular weight. The resulting polymer chain is left with two active ends, one from each of the parent polymers. As mentioned earlier, a chemical bond between the active ends of the same polymer was prohibited. Also, we assumed that the impinging monomers would always stick to the particle that comes on its deposition path as shown in processes 5(a).

This criterion of sticking to the nearest-neighboring particle results in the development of overhang structures, which are discussed at length in Chapter 4.

3.4 Algorithm Outline

After having described the details of polymer growth and listing the various Monte Carlo moves present in our VDP model, the final segment of this "Model and Methods" chapter concentrates on providing an overall functionality of the computer model developed in the current study. The Fig. 3.2 shows a flowchart representation of the algorithm used in performing the simulation study. The flowchart has been presented with the intention of simplifying the understanding of program flow in our simulational study.

Before beginning the computations, a number of model parameters are input to the program. A list of relevant input parameters include: the substrate length L, the maximum Monte Carlo deposition time, the ratio between diffusion rate, the deposition rate G, etc. After reading the input parameters, the program initializes all the variables and data structures used in the program. At this point, we also initialize the random number generator with a "time seed" obtained from the system clock. Initially, the $1D$ substrate is unoccupied and the number of monomers N_1 is set to zero. Then the program uses Eqns. (3.1) and (3.2) to calculate the probabilities of deposition (p_F) and diffusion (p_D) and makes a MC decision to perform either a deposition or a diffusion move with probabilities p_F and p_D respectively. As discussed in the Section 3.2, the deposition and diffusion processes were performed depending on the dynamically varying probabilities p_F and p_D. At each deposition step only one monomer was deposited and during the diffusion process one of the N_1 monomers was selected randomly to perform a diffusion hop to its nearest neighboring location. Each of the deposition and diffusion steps can lead to one of the many MC moves ranging from simple diffusion to polymer merger (discussed in Section 3.3). After each deposition and diffusion

decision, a subroutine is called to evaluate the consequence of the chosen MC move and subsequently, various lists pertaining to monomers, polymer chains, and other state variables are updated. As the simulation progress, another subroutine is periodically called after each MC time step (depositoin of L monomers) to calculate the physical quantities of interest. The sequence of deposition or diffusion steps, followed by variable updates and data calculations, repeats until the desired maximum MC deposition time is reached. At the end of the simulation, various averaged quantities are output to data files. The data files also contain information about the standard error of the mean for various calculated quantities. The final step of the study includes analyzing the data and looking for the evidence of systematic behaviors and for physical explanations for the obtained data.

3.5 Estimation of Error-bars

In order to provide quantitative error estimates for the quantities calculated in this work, data obtained from multiple independent simulations were considered. All data presented in various plots in this dissertation were a result of multiple independent simulations, which were averaged together. For the physical quantities that were directly obtained from the simulations (unlike the fit-analysis quantities), the statistical error bars were calculated using the standard error of the mean. For a physical quantity denoted by O, the standard error of its mean value $\bar{O}$ was calculated using,

$$O_{error} = \frac{\sigma_O}{\sqrt{N}}. \tag{3.3}$$

Here N represents the number of independent runs used in calculating the mean $\bar{O}$, and σ_O is the standard deviation. The quantity σ_O was calculated using the root-mean square fluctuations of the multiple independent estimates O_i,

$$\sigma_O = \sqrt{\frac{\sum_{i=1}^{N} \left(O_i - \bar{O}\right)^2}{(N-1)}}. \tag{3.4}$$

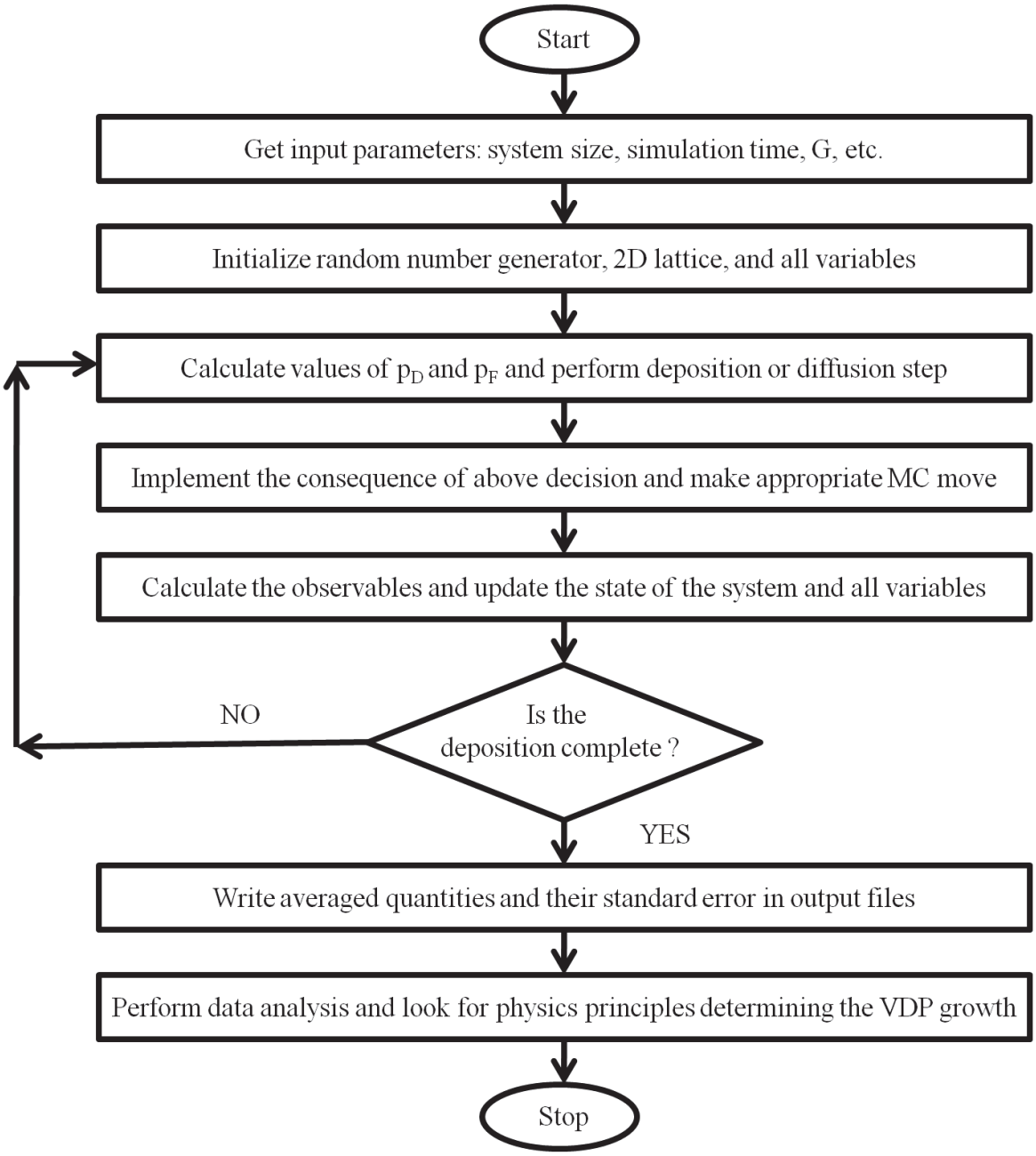

Figure 3.2: Flowchart representation of the algorithm used in the simulational study of VDP growth.

We obtained the error estimates of various exponents calculated in our study by using regression analysis that was performed using the *Xmgrace* program available under Linux OS. The regression analysis was used for predicting the exponents that quantified the dependence of measured (dependent) quantities on their corresponding independent variables. In the following chapters, the captions of the included figures clarify the error estimates as appropriate to the presented data.

Chapter 4

Polymer Film Properties

This chapter discusses the study of bulk properties of polymer films generated using our VDP model. The conclusions presented in this chapter are aimed at providing an understanding of the effects of substrate size L, deposition time t, and ratio G on the behavior of overall film properties. The various film properties studied in this chapter range from their qualitative appearance to the quantitative scaling behavior of the interface width. We performed the scaling analysis of a film's growth front by calculating interface widths and height distributions of the polymer films. We also studied the spatial and temporal behavior of interface width roughening using finite-length scaling and height-height correlations. The scaling behaviors at local and global length scales were found to be very different and are discussed in detail. All data presented beyond this point are averaged results of multiple independent simulations, unless otherwise specified.

4.1 Surface Morphology

An intuitive and qualitative understanding of VDP growth process can be obtained from observing a sequence of snapshots of the polymer films at various times during the film growth. We generated six snapshots of the deposited polymer films at varying deposition times for selected values of the ratio $G(= D/F)$. The Fig. 4.1 shows typical snapshots of the films generated using $L = 512$ substrate at two extreme cases: $G = 10$ (Figs. 4.1a, b, c) and $G = 10^6$ (Figs. 4.1d, e, f) after deposition times of $t = 15$ (Figs. 4.1a, d), $t = 30$ (Figs. 4.1b, e), and $t = 60$ units (Figs. 4.1c, f) respectively.

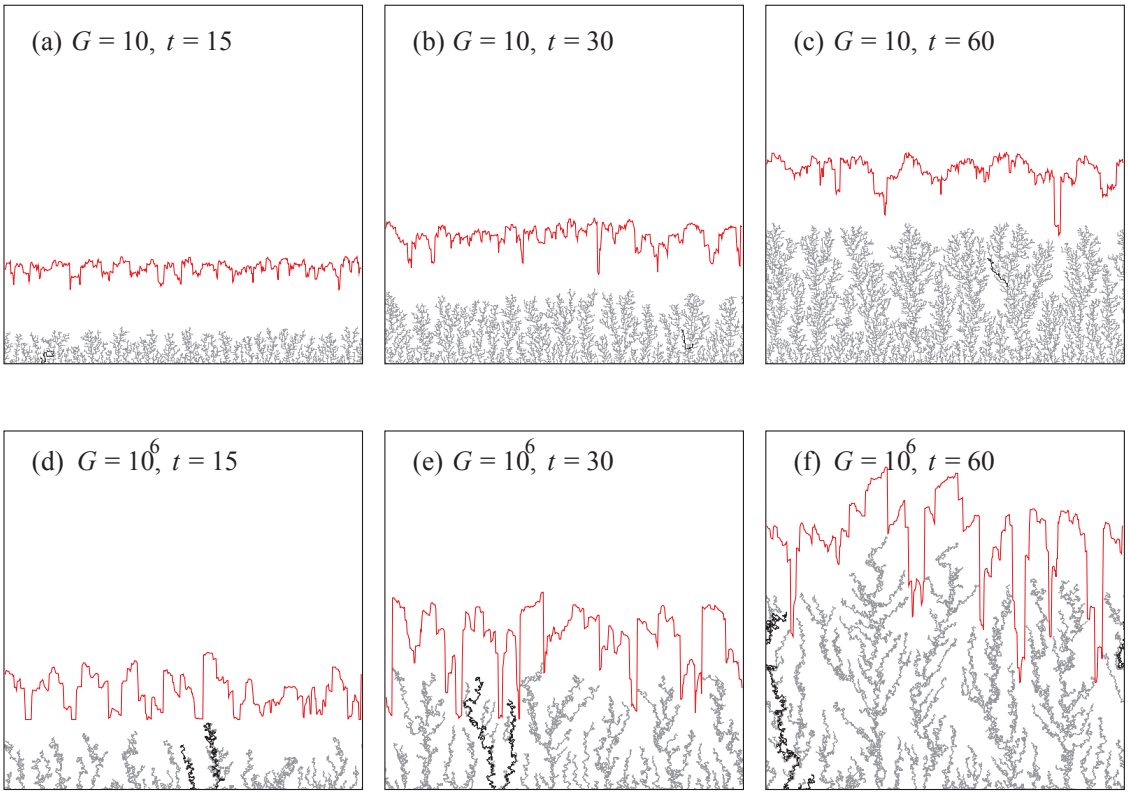

Figure 4.1: Snapshots of the polymer films grown on a $L = 512$ substrate. Figs. (a, b, c) were obtained for $G = 10$ at deposition times $t = 15$, 30, and 60 units respectively; whereas Figs. (d, e, f) were obtained for $G = 10^6$ and deposition times $t = 15$, 30, and 60 units, respectively. One deposition time unit corresponds to a deposition of L monomers. For a clear view, the growth front (shown in red) is displaced vertically by 100 pixels and the longest polymer chain is highlighted in black.

An observation of all the six snapshots in Fig. 4.1 indicates the presence of columnar structures, overhangs, and unoccupied regions during the VDP growth. These columnar structures were observed to persist throughout the growth process, independent of the values of G and deposition time t. The appearance of tree-like columnar structures in Fig. 4.1 is the effect of the $\cos\theta$ launch angle distribution of the downward travelling monomer flux [69, 71, 72, 73, 74] that results in a "shadowing effect" during the growth process. The shadowing effect arises when the relatively taller columnar structures of the surface "stick out" and shadow their neighboring sites, thus inhibiting the growth of their neighboring sites. In accordance with the experimental set-up, the deposition of monomers in our VDP model was not collimated. The monomers were instead deposited with uniform launch angles as discussed in Section 3.3. As the deposition of monomers in our model was not collimated, the rate of increase in the height of the deposited film was not uniform along the $1D$ substrate. This results in taller portions of the film to stick out and prevent the incoming monomer flux from entering the lower lying areas of the polymer film.

In Fig. 4.1, we find that for a fixed t, the films grown at $G = 10$ (Figs. 4.1a, b, c) are characterized by shallower unoccupied regions and short polymer chains, resulting in shorter, denser, and compact films; whereas for a larger diffusion case with $G = 10^6$ (Figs. 4.1d, e, f), the films are observed to contain deeper unoccupied regions, and longer polymer chains resulting in taller, more porous, and less dense films. Also, in Fig. 4.1, it is interesting to note that the longest polymer chains at each time (highlighted in black) occurring in simulations with $G = 10^6$ are much longer than for those occurring in simulations with $G = 10$. We were interested in understanding the phenomenon that promotes an increase in the polymer chain length as G is increased in the simulations. With this goal, we generated a sequence of snapshots and traced the diffusion path of the monomers after they arrive onto the surface. By observing the diffusion of monomers, we found that for a relatively low diffusion rate of $G = 10$, the monomers deposited on the film surface have a higher probability

of encountering another downward impinging monomer as nearest neighbor and initiating new polymers (chain initiation) on the film surface. Many such chain initiation events on the surface tend to fill up the void spaces in the films, thereby inhibiting the occurrence of deeper unoccupied-regions. Consequently the films at $G = 10$ were observed to be dense and compact. In contrast, in simulations with a higher diffusion rate of $G = 10^6$, the monomers present on the surface have a higher probability to diffuse. A larger number of diffusion hops were observed to transport the monomers in an upward direction towards the growth front. This additional flux of upward diffusing monomers eventually end up binding to the active ends of the polymers, thereby resulting in chain propagation. Consequently, the increase in chain propagation MC move results in larger chains observed at larger $G = 10^6$. A similar phenomenon of material transport has been observed in kinetic Monte Carlo studies where an upward diffusion of monomers was found to be favorable due to the non-symmetric nature of the lattice potential associated with diffusion over a step [48]. Even though our model does not incorporate any energy based calculations, the effects of non-symmetric upward diffusion were also observed in VDP growth.

Another systematic feature observed in Fig. 4.1 is that, for a fixed t even though the films have the same number of particles, the average "jaggedness" of the growth front looks very different for $G = 10$ and $G = 10^6$. The differences arise from the variations in the position of the growth front $h(x, t)$, defined as the set of highest occupied sites in the film for each column, where x is the position of the column on the substrate. In Fig. 4.1 the growth fronts are shown in red and are vertically displaced by 100 pixels in the growth direction for clarity. The fluctuations in the values of $h(x, t)$ are observed to occur at different length scales depending on the ratio G. For a fixed t, it is intuitive to think that the growth front profiles corresponding to $G = 10^6$ (Figs. 4.1d, e, f) are rougher than those obtained using $G = 10$ (Figs. 4.1a, b, c). Until this point in the chapter, the intriguing differences have been explained qualitatively with the intention of motivating a more rigorous later study. A

detailed, quantitative analysis of the dynamics of interface roughness evolution is presented in Section 4.3.

After having discussed the qualitative differences in the appearances of polymer films grown at different values of G, it is of interest to obtain relevant statistical quantities that give an indication of how completely the film structures appear to fill the surrounding $2D$ space, as one zooms down to finer and finer length scales. In this regard, the qth-order generalized height-height correlation function $H_q(r,t)$ (defined below) is commonly used in characterizing the "space-filling" property of $2D$ structures [75, 48]:

$$H_q(r,t) = \{\langle \mid h(x+r,t) - h(x,t) \mid^q \rangle\}^{(1/q)}, \tag{4.1}$$

where r varies from 0 to $L/2$, $\langle ... \rangle$ refers to a spatial average over the entire system, and $\{...\}$ is used to denote the statistical average. For the film interfaces typically obtained in VDP and shown in Figs.4.1, we were interested in finding if rescaling a part of the interface anisotropically results in an interface that is statistically indistinguishable from the whole. This study requires the calculation of $H_q(r,t)$ and determining if the interfaces are self-affine or multi-affine. If the interface were to be self-affine, then an anisotropic rescaling of a part of the interface using a single exponent q would result in a statistically similar interface again. However, if the scaling properties of the interface are describable only in terms of an infinite set of exponents, such an interface is referred to as *multi-affine*. The scaling properties of multi-affine surfaces can be described in terms of an infinite set of *Hurst exponents* [49, 76], h_q, which can be obtained using

$$H_q(r,t) \sim r^{h_q}. \tag{4.2}$$

For multi-affine interfaces, the exponents h_q are known to vary with the numerical value q [49] used in calculating the generalized height-height correlation function $H_q(r,t)$. Typically, in many diffusion mediated growth processes in $2D$, the values of Hurst exponents for growing structures tend to lie between 0 and 1, and a larger Hurst exponent indicates the presence

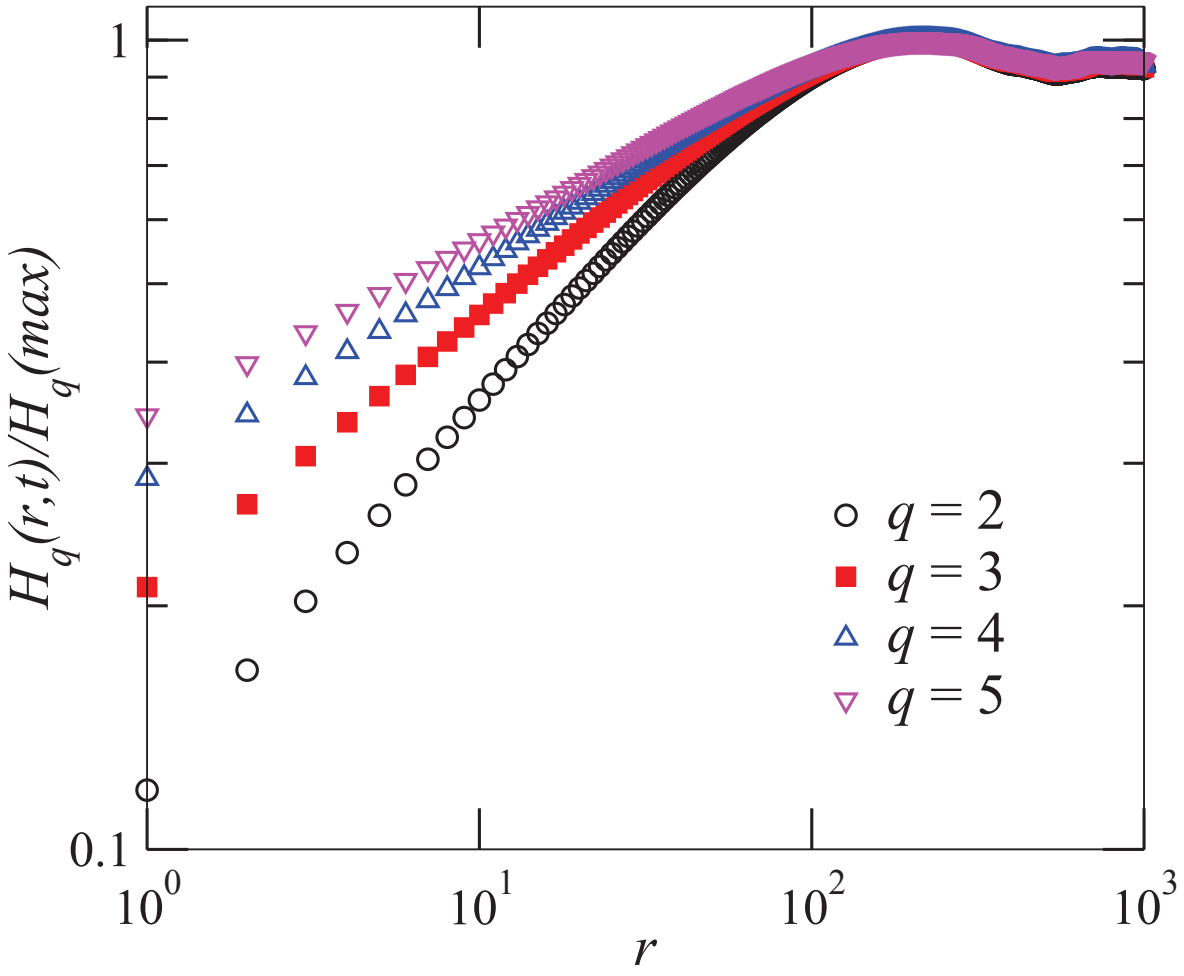

Figure 4.2: Generalized correlation function $H_q(r,t)$ calculated for $L = 2000$ and $t = 1000$. The data are averaged over 200 independent runs and the error-bars are smaller than the symbol size.

of a smoother surface with less roughness.

In this context, we calculated the generalized correlation function $H_q(r,t)$ using $q = 2$, 3, 4, and 5, for $G = 10$ at deposition time $t = 10^3$. Figure 4.2 shows the dependence of $H_q(r,t)$ on the chosen q indices. For smaller length scale r, we observed a power-law dependence of $H_q(r,t)$ on r in accordance with Eqn. (4.2). The slopes of the log-log plots shown in Fig. 4.2 were observed to depend on q and indicates the presence of multi-scaling in the film interfaces generated by our VDP growth model. A similar multi-affine property of the film interfaces was also observed in the polymers grown at other G values.

4.2 Average Film Height and Growth Rate

From Fig. 4.1, we observed that for both values of $G = 10$ and 10^6, the average height of the film increased with an increase in deposition time from $t = 15$ to $t = 60$ units. Another feature we observed is that, for comparable t (same column images), the average height of the films appears to be larger for $G = 10^6$ as compared to those films obtained at $G = 10$. The average film height also depended on the ratio G chosen in the simulations, in addition to deposition time t. In this section, we present the quantitative approach used in studying the dependence of average film height on G and t.

The average height of the growth front $h_{avg}(t)$ was calculated using the definition,

$$h_{avg}(t) = \frac{1}{L}\sum_{x=1}^{L} h(x,t), \tag{4.3}$$

and used in quantifying the overall thickness (height) of the film. Figure 4.3 shows the variation of h_{avg} with an increase in t for $G = 10$, 10^3, and 10^5 and $L = 512$. For all the indicated values of G, the h_{avg} versus t plots showed a linear relationship. This linear increase in h_{avg} with t was a consequence of restricting the growth to $1+1D$ and the excluded volume constraint implemented in the growth model. With an increase in t, the number of particles keeps increasing in the system; and due to the restriction of growth along the lateral x-axis

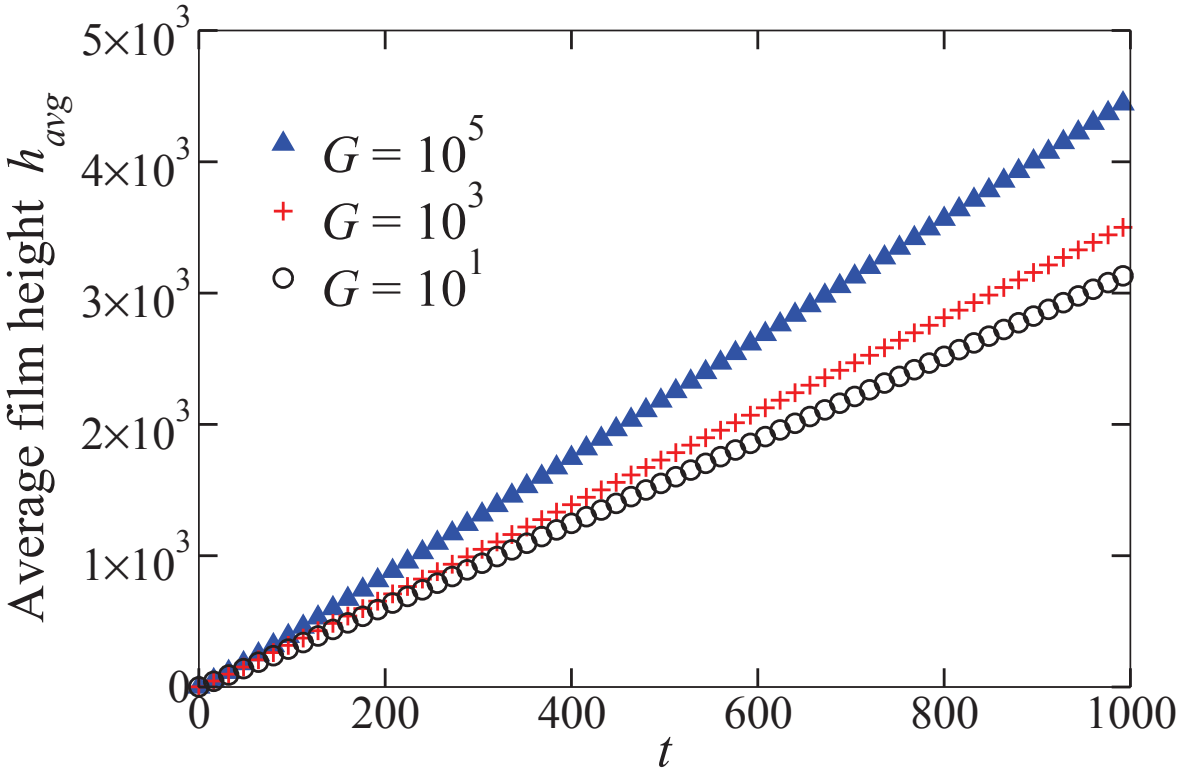

Figure 4.3: Variation of h_{avg} as a function of deposition time t for different G and $L = 512$. The data are averaged over 500 independent runs. The statistical errors are smaller than the symbol size.

(imposed by periodic boundary conditions), the polymer film is forced to grow along the vertical y-direction. As a result, the h_{avg} of the film was observed to increase linearly with t.

Another interesting feature observed in Fig. 4.3 was a systematic increase in the slope of the h_{avg} versus t data as G was increased from 10 to 10^5. For obtaining an explanation of the observed increase in the rate of increase of h_{avg} with G, we calculated the *growth rate* R of the polymer film given by,

$$R = \frac{dh_{avg}}{dt}. \tag{4.4}$$

In general, the overall film's growth rate is proportional to the incoming monomer flux only i.e. $R \propto F$, and it is natural to expect R to be independent of $G(= D/F)$ since $F(= 1/L)$ is a constant for a fixed L. However, in Fig. 4.3 our simulations showed a strong dependence of R on G as well, and the growth rate R was observed to increase systematically with an increase in G. This G dependent growth rate R indicates that the growth rate is affected by monomer diffusion directly, i.e., there is a net uphill monomer diffusion current that is responsible for the observed $R - G$ dependence. We thus incorporated an additional term, $r(G)$, that determined the growth rate $R(t)$ given by Eqn. (4.4) , in addition to its dependence on monomer flux F. From our observations, the growth rate could be obtained using our prescription,

$$R(G) = R_0 + r(G), \tag{4.5}$$

where R_0 is the growth rate due to the random deposition flux F only and $r(G)$ accounts for the growth rate induced only by the uphill diffusion of monomers. The value of R_0 was determined by measuring the growth rate $\frac{dh_{avg}}{dt}$ of the polymer film height by turning-off the monomer diffusion. In Fig. 4.4 we show the variation of $r(G)$ as a function of G. We found a systematic increase in $r(G)$ as a consequence of an increase in the independent parameter G. This observation establishes the strong influence of G in determining the polymer film's growth rate. In Fig. 4.4, for $G > 10^5$, we found a power law dependence given by $r(G) \propto G^{0.162(3)}$; the error estimate of the exponent was obtained from the regression analysis. This

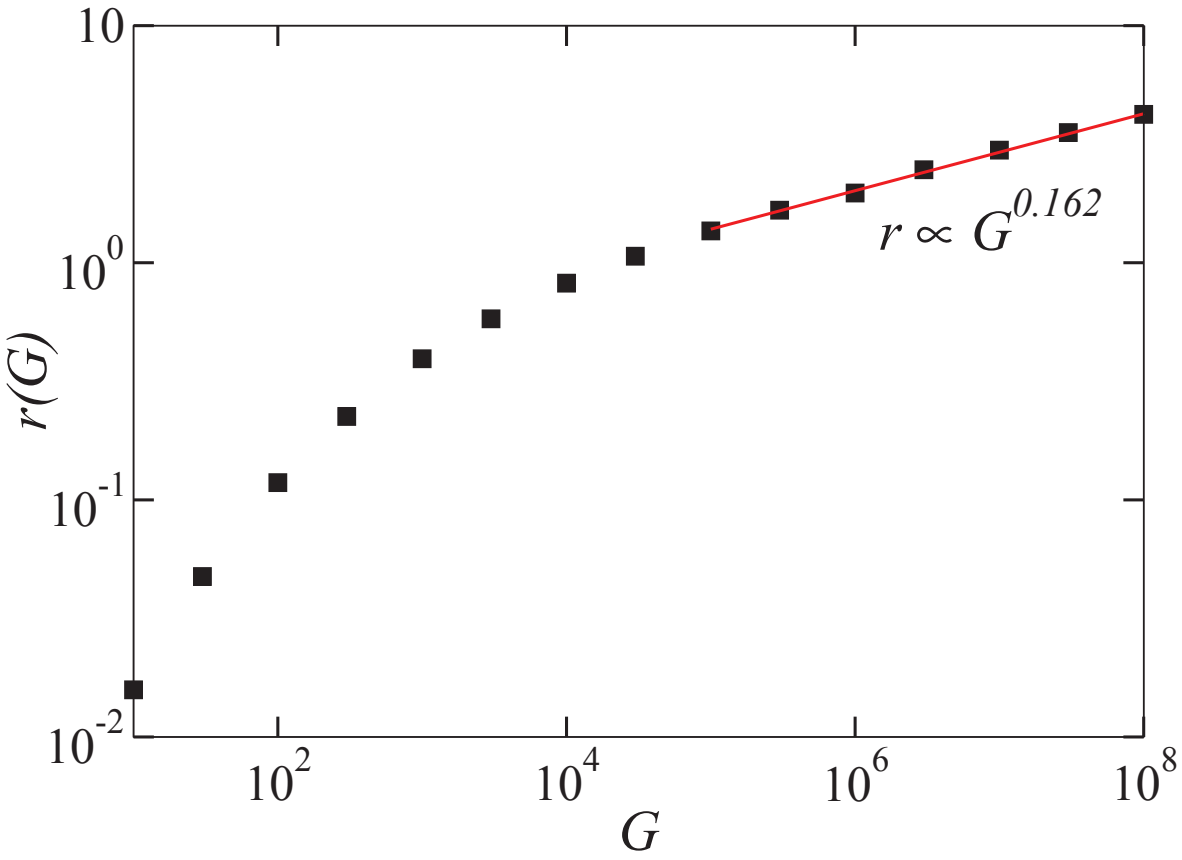

Figure 4.4: Variation of $r(G)$ as a function of G. The data were obtained for $L = 512$ and averaged over 500 independent runs. The statistical errors are smaller than the symbol size.

indicates that the growth rate due to uphill diffusion $r(G)$ asymptotically follows a power law dependence on G.

4.3 Characterization of the Growth Front Roughening

For studying the morphological evolution of any non-equilibrium stochastic growth process including VDP, it is essential to identify its steady growth regime. In a stochastic system whose behavior is non-deterministic, the steady state gives us a handle to study and characterize the system. In a steady-state growth, the probabilities that various different states of the system are repeated remains a constant. As a system attains a steady state, its recently observed behavior often continues into the future and many physical observables do not vary much with time. In many systems, a steady state is not achieved until some time gets elapsed after the system is started or initiated. In the following sections we discuss the observed growth regimes of VDP growth and calculate various properties of the films in their steady state.

4.3.1 Steady State Growth

As the VDP growth is known to be a non-equilibrium stochastic process, performing a reasonable characterization of the VDP based polymer film growth required the identification of the steady state of the growth process. To understand the steady-state growth regime in VDP, we calculated the *lateral film density* $\rho(y)$ (at a height y lattice units) of film defined as,

$$\rho(y) = \frac{N(y)}{L}, \tag{4.6}$$

where $N(y)$ represents the total number of occupied lattice sites at a height y lattice units above the substrate. Figure 4.5 shows the variation of $\rho(y)$ with t for polymer films generated with $L = 512$, $G = 10$ at deposition times of $t = 10$, 20, 40, and 60 units respectively. Similar lateral density profile plots were obtained for other G and L values also. In the Fig. 4.5, three

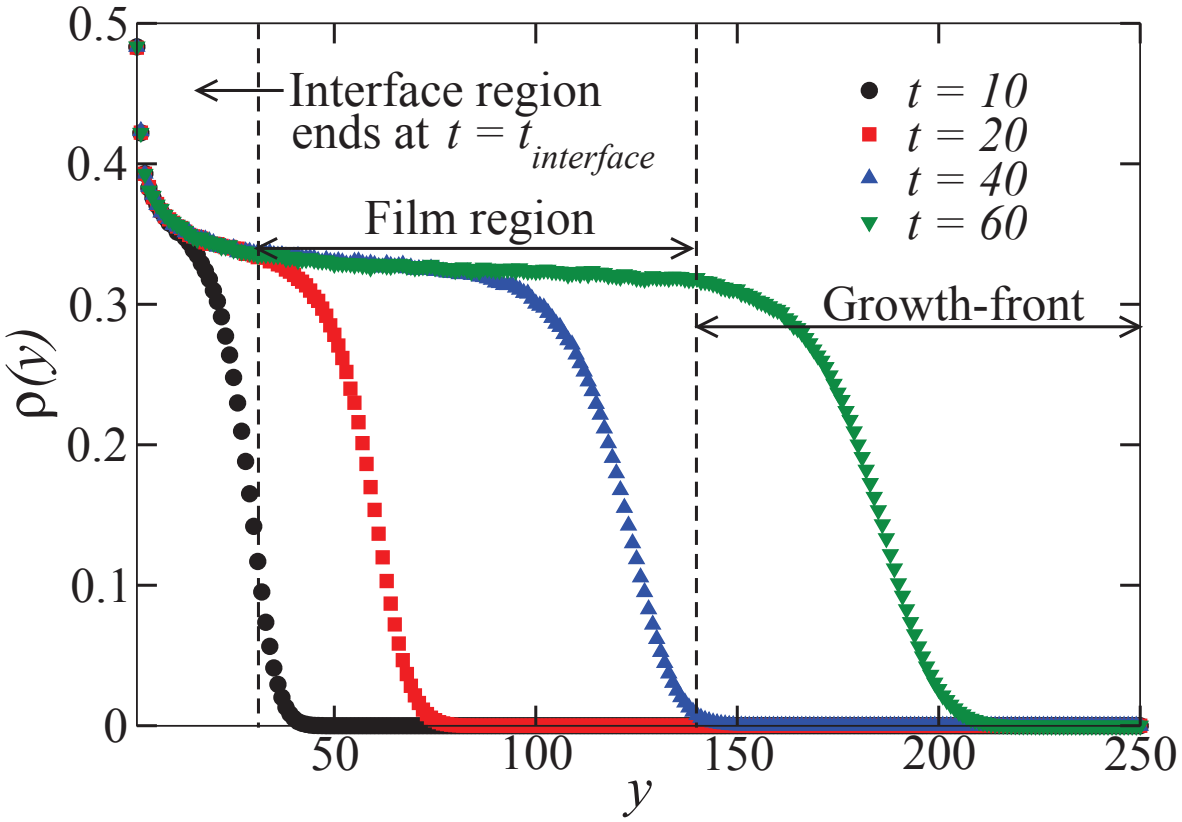

Figure 4.5: Lateral film density profiles $\rho(y)$ of polymer films grown on a $L = 512$ substrate with $G = 10$ at deposition times of $t = 10$, 20, 40, and 60 respectively. The statistical errors are smaller than the symbol size.

distinct regions of polymer film growth referred to as the *interface region*, the steady-state *film region* and the *growth front* were identified. Fig. 4.5 shows that the interface region is a transient or start-up growth phase where the lateral film density $\rho(y)$ decreases sharply from its maximum value until it attains a steady state value characterized by a nearly constant $\rho(y)$. The non-varying $\rho(y)$ region of the film has been indicated as the "film region" regime in Fig. 4.5. Finally in the "growth front" regime, the film density was observed to decrease from its steady state value until it became zero gradually. The values of y over which the steady state, and the growth front regimes of the film extend were observed to depend on t. The following sections of this chapter concentrate on films at deposition times $t \gg t_{interface}$ and discuss the characteristics of growth beyond the interface (start-up) region.

The roughening mechanism of the growth front can be characterized by studying its spatial and temporal evolution. In morphological scaling studies, typically two kinds of behaviors are associated with the roughening kinetics of the growth front depending on the length scales involved in the scaling. These two classes of roughening mechanisms are referred to as the global scaling and the local scaling [77, 78, 79]. The local roughness exponents are often used in the experimental analysis and have been employed in studying irregularly growing mound morphologies [58, 80].

In general, the exponents characterizing the local roughness α_l and the global roughness α_g take on different values depending on the type of scaling exhibited by the growth process. In the case of super-rough surfaces generated by non-equilibrium MBE growth models [81] and growth models with horizontal diffusion [82], an assumption of the equivalence between the global and local descriptions of the surface is not always valid. The scaling behaviors where the scaling exponents characterizing the local and the global scales are not the same are termed as anomalous scaling [81, 83]. The differences in the global and local scaling exponents have been attributed to the *super-roughening* and *intrinsically anomalous* spectrum

observed in the anomalous scaling of surfaces [84]. The following sections discuss the above mentioned roughening mechanisms (as applicable to VDP) in further detail.

4.3.2 Global Roughening Behavior

The global scaling behavior of growth fronts of polymer films was determined by studying the dependence of *interface width* $w(L,t)$ on substrate length L, and deposition time t. The interface width $w(L,t)$ was defined as,

$$w(L,t) = \sqrt{\frac{1}{L}\sum_{i=1}^{L}[h(i) - h_{avg}]^2}. \tag{4.7}$$

In many $2D$ morphological growth processes such as ballistic deposition [85, 86], the Eden model [86], and solid-on-solid models [87], $w(L,t)$ usually follows a scaling law given as

$$w(L,t) \sim t^{\beta} \qquad (t \ll t_X), \tag{4.8}$$

where the exponent β is known as the *growth exponent* that is often used in characterizing the time dependence of surface roughening. For any given L, the power law increase in $w(L,t)$ does not continue indefinitely with increasing t, but instead is followed by a saturation regime where the $w(L,t)$ reaches a steady value w_{sat}. The power law growth and the saturation regime are separated by a *crossover time* t_X. Inside the saturation regime ($t \gg t_X$), it is known that as L increases, w_{sat} also typically follows a power law [48] given by

$$w(L,t) = w_{sat} \sim L^{\alpha_g} \qquad (t \gg t_X), \tag{4.9}$$

where the exponent α_g is referred to as the *global roughness exponent* [48]. The crossover time t_X at which the behavior of $w(L,t)$ crosses over from growth regime (characterized by Eqn. (4.8)) to that of saturation regime (characterized by Eqn. (4.9)) depends on L and scales as,

$$t_X \sim L^{z_g}, \tag{4.10}$$

where z_g is called the *global dynamic exponent*.

Due to the non-equilibrium nature and the inherent stochastic nature of VDP growth, it might appear that the scaling behavior of interface width is sensitive to the details of the growth process. However, the exponents that characterize the scaling behavior are typically found to be independent of the specific interactions involved in the growth and instead depend on the dimensionality and symmetries of the system being studied [86, 88, 48, 49]. The term *universality class* is often used to refer to a specific set of scaling exponents that characterize a group of growth models that have the same (numerical valued) scaling exponents. For some growth processes, the characteristic exponents α_g, β, and z_g are unified using the *dynamic scaling hypothesis* [86] (also known as the *Family-Vicsek scaling*) given as,

$$w(L,t) \sim L^{\alpha_g} \Psi\left(t/L^{z_g}\right), \tag{4.11}$$

where $\Psi\left(t/L^{z_g}\right)$ is referred to as the *scaling function* and satisfies,

$$\Psi(x) = \begin{cases} x^{\beta} & (x \ll 1) \\ const & (x \gg 1), \end{cases} \tag{4.12}$$

and

$$z_g = \alpha_g/\beta. \tag{4.13}$$

In Fig. 4.6 we show two representative plots of $w(L,t)$ versus t on a log-log scale for (a) $G = 10$, (b) $G = 10^3$ and varying L. From both Figs. 4.6(a) and 4.6(b), for $t \ll t_X$, the $\log(w(L,t))$ versus $\log(t)$ shows a linear dependence implying a power-law behavior. Also, for the same G and $t \ll t_X$, the $w(L,t)$-t plots were found to overlap with one another for different L. We estimated β by fitting Eqn. (4.8) to the plots of $w(L,t)$ in Fig. 4.6 for the film region $t \ll t_X$. We obtained average $\beta = 0.509(8)$ and $0.51(2)$ for $G = 10$ and 10^3 respectively. For other G values, the β obtained was close to 0.50 and we observed an invariance of β (within the error-bars) with G. The statistical average and error bars in β were obtained from 1.8×10^3 independent simulations.

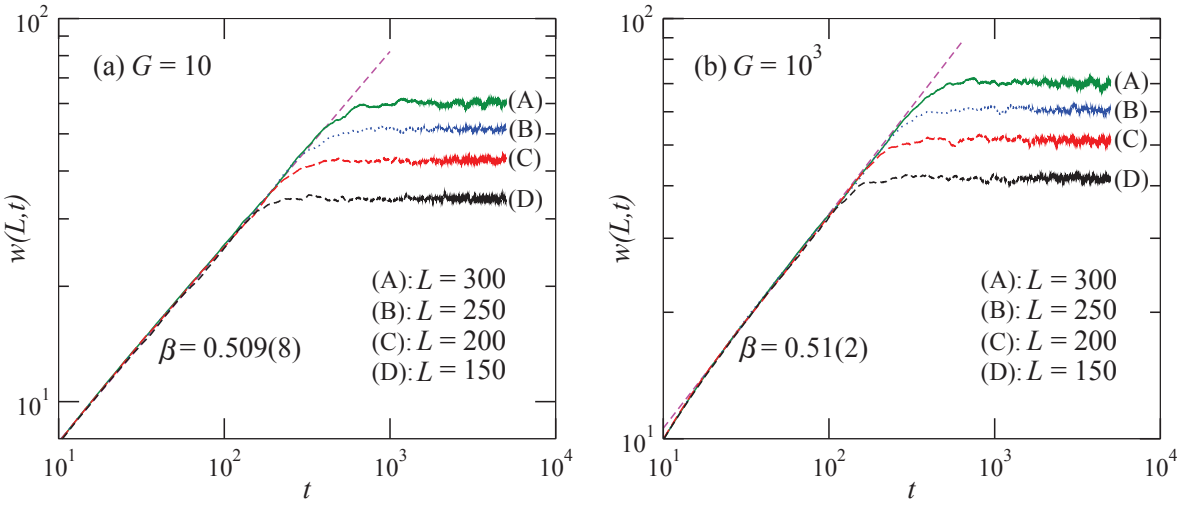

Figure 4.6: Time variation of the interface width $w(L,t)$ for (a) $G = 10$ and (b) $G = 10^3$ with $L = 100$, 200, and 300. The data are averaged over 1.8×10^3 independent runs.

The VDP model studied here is similar to the ballistic deposition model with additional degrees of freedom including diffusion, polymer initiation, extension, and merger that were discussed in Section 3.3. However it is important to note that, unlike the atomic diffusion in MBE growth, the monomer diffusion is confined by the linear geometry of the polymer chain. From Fig. 4.1 one can observe that in most cases the polymer chains are more or less perpendicular to the substrate. Since the monomers can only move along the polymer chain, most of the diffusion happens in the vertical direction rather than in the lateral direction (which is the case for MBE growth). Yet, the vertical diffusion does not contribute significantly to extra roughness in the growth front due to the porous nature of the film as compared to the random deposition model. Thus, it is natural to expect that the growth exponent of our VDP model will be close to that of random ballistic deposition model ($\beta = 0.50$) [49].

For studying the nature of interface roughening in saturation regime, we calculated w_{sat}

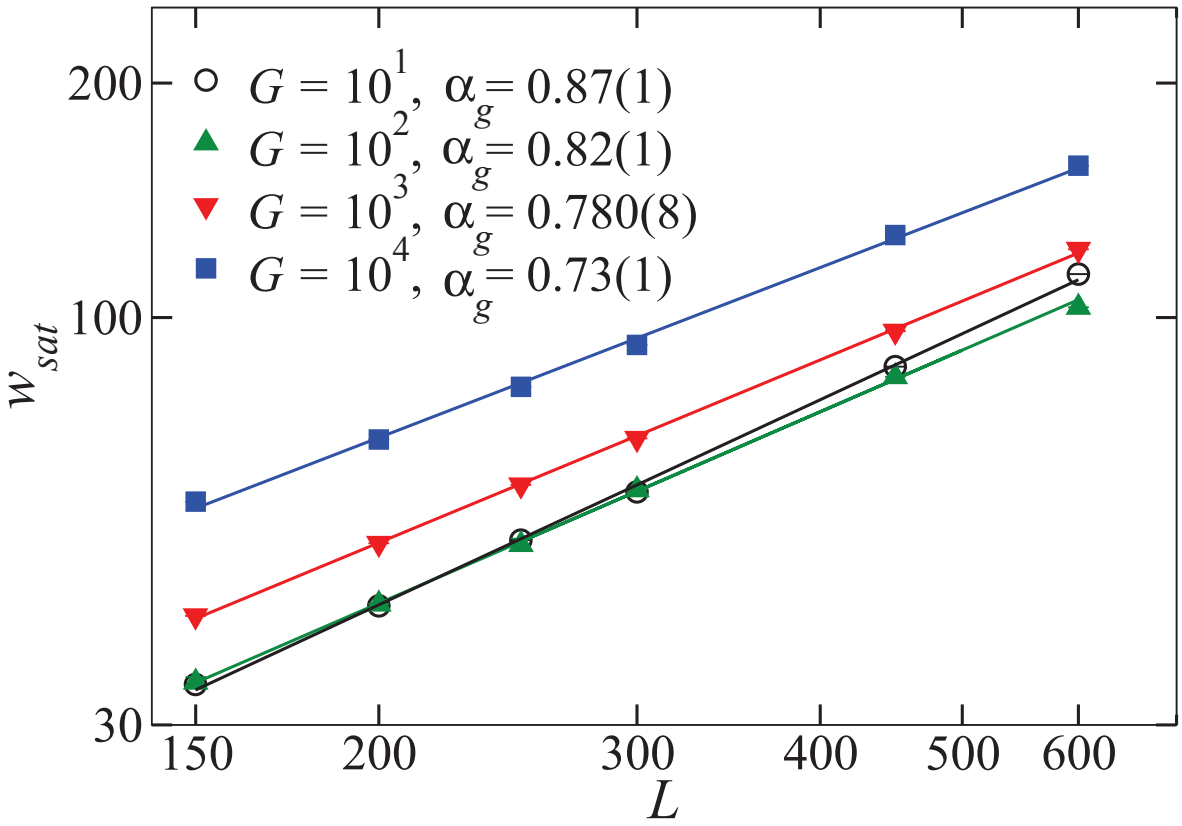

Figure 4.7: Variation of w_{sat} with L for G varying from 10 to 10^4. The data are averaged over 1.8×10^3 independent runs and the statistical errors are smaller than the symbol size. The error in the exponents were obtained from the curve fit.

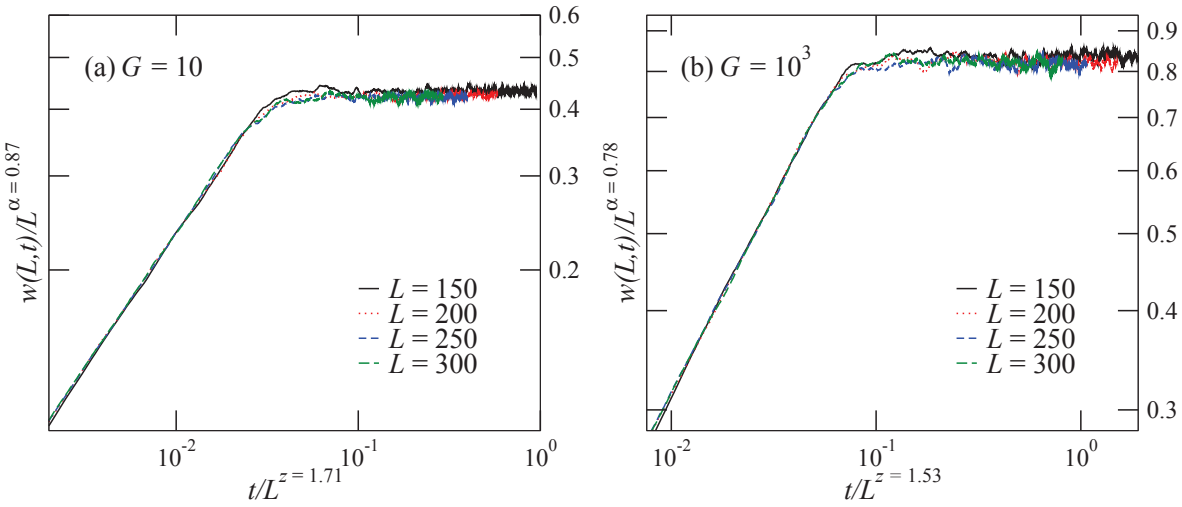

Figure 4.8: Rescaled plots of $w(L,t)/L^{\alpha_g}$ versus t/L^{z_g}. The "collapsed" curves shown in the plots are the scaling functions for (a) $G = 10$, (b) $G = 10^3$ and indicate the presence of dynamic scaling. The data are averaged over 1.8×10^3 independent runs.

by averaging $w(L,t)$ for $t \gg t_X$ from the data shown in Figs. 4.6(a) and 4.6(b). Figure 4.7 shows the plot of w_{sat} versus L on the log-log scale for G varying from 10 to 10^4. The exponent α_g was estimated for each G using Eqn. (4.9). With an increase in G from 10 to 10^4, α_g was found to decrease from 0.87(1) to 0.73(1), the error-bars in α_g were obtained from the curve fitting. The exponent α_g is known to be closely related to the surface fractal dimension [48]. The smaller the α_g, the larger is the fractal dimension. Our observation of a decrease in α_g with an increase in G shows that the fractal dimension of the growth front increases with G, i.e. there are more spatial fluctuations in the film morphology with an increase in G. This finding is consistent with the growth front profiles shown in Fig. 4.1. This result also demonstrates that G induces a large effective vertical growth rate $R(G)$ (shown in Fig. 4.4) and the large $R(G)$ in turn produces a much rougher film surface.

Finally, to determine whether the VDP process obeys the dynamic scaling hypothesis

in the global roughening mechanism, we start with an assumption that VDP growth follows the dynamic scaling hypothesis and obtain z_g through Eqn. (4.13). As $w(L,t)$ scales with both t (Eqn. (4.8)) and L (Eqn. (4.9)) we can rescale the $w(L,t)$ curve shown in Fig. 4.6 by plotting w/L^{α_g} versus t/L^{z_g} to see whether those curves "collapse". For $G = 10$ we obtain $\alpha_g = 0.87(1)$, $\beta = 0.509(8)$ and according to Eqn. (4.13) $z_g = 1.71(1)$ and for $G = 10^3$ we get $\alpha_g = 0.780(8)$, $\beta = 0.51(2)$, and $z_g = 1.53(2)$. We use the data from Figs. 4.6(a) and 4.6(b) and divide $w(L,t)$ by L^{α_g}. This shifts the curves of varying L vertically on the log-log scale. According to Eqn. (4.9), these curves now saturate at the same value of the ordinate w/L^{α_g}, however their saturation times do not overlap. We then rescale the time axis and plot t/L^{z_g} for both cases of G. This rescaling of time axis according to Eqn. (4.10) leads to a horizontal shift of the curves and the curves now saturate at the same abscissa t/L^{z_g}. In Figs. 4.8(a) and 4.8(b) we show the rescaled plots of $w(L,t)$ for $G = 10$, 10^3 and consequently observe the "collapse" of individual curves for varying L onto a single curve. This characteristic "collapsed" curve shown in Figs. 4.8(a) and 4.8(b) is the *scaling function* $\Psi\left(t/L^{z_g}\right)$ mentioned in the Eqn. (4.12). The scaling functions obtained in Figs. 4.8(a) and 4.8(b) were observed to follow Eqn. (4.12) for both cases of $G = 10$ and 10^3. For other G values, we observed similar "collapse" behavior indicating the global dynamic scaling of growth fronts of the polymer films grown using VDP.

4.3.3 Local Behavior

The local scaling behavior of the growth fronts can be understood from analyzing the spatial correlation functions. Two popular quantities used in describing the short length range properties of growing interfaces are: the auto-correlation function $C(r,t)$ and the height-height correlation function $H(r,t)$, defined as,

$$C(r,t) = \langle h(x+r,t) \cdot h(x,t) \rangle, \tag{4.14}$$

$$H(r,t) = \{\langle [h(x+r,t) - h(x,t)]^2 \rangle\} = 2[w^2 - C(r,t)], \tag{4.15}$$

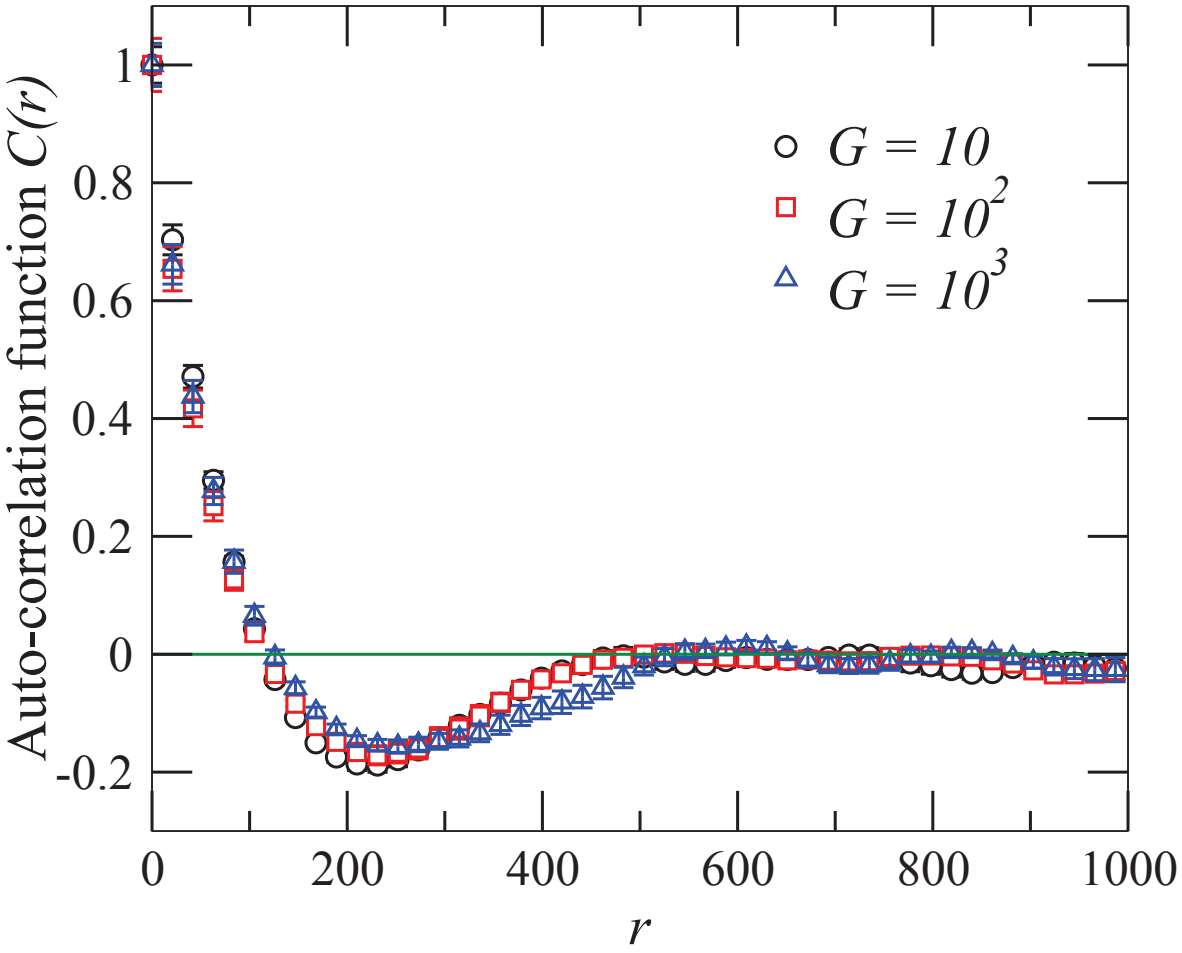

Figure 4.9: Auto-Correlation function $C(r,t)$ calculated for $L = 2000$ and $t = 1000$ (averaged over 200 independent runs).

where r is the translation distance also referred to as the lag or slip [89] and $\langle ... \rangle$ denotes a spatial average over the entire system. The functions $C(r,t)$ and $H(r,t)$ are directly related as shown in Eqn. (4.15). The $H(r,t)$ scales in the same way as the interface width $w(L,t)$ and is often used in studying the kinetic roughening on the local length scales [48].

In order to obtain reliable conclusions from the correlation functions, it is important to

account for the accuracy of statistical averages. In the case of correlation functions involving multiple summations over the translation distance r, accuracy depends not only on the number of data points, but also on the substrate length L. For a system with dimension d and lateral correlation length ξ, it is the ratio ξ/L, not the number of data points, that determines the accuracy. For example, in the case of the random Gaussian model surface studied by Ref. [89], converging $H(r,t)$ were obtained within an order of $(\xi/L)^{d/2}$. Once the ratio ξ/L is known, one may not be able to increase the accuracy no matter how many data points are collected [89]. This rule is different from the law of large numbers for independent random variables. This important difference needs to be recognized while studying spatially correlated systems. For improving the accuracy of correlation function data, ideally one would like to have $\sqrt{\xi/L} \ll 1$, i.e, $L \to \infty$. However, due to limited computational resources, we have to restrict the system size and choose a trade-off between accuracy and the computational feasibility. In the particular case of our $1+1D$ VDP model, we performed calculations using $L = 2000$ and $t = 1000$.

Coarsening Study

The nature and shape of the decay of $C(r,t)$ depends on the type of the surface and the decay rate depends on the distance over which two points x, $x+r$ become uncorrelated. For example, in the case of a random self-affine surface, $C(r,t)$ usually decays to zero with an increase in r. In Fig. 4.1 the growth fronts of the six snapshots do not appear to be random rough surfaces; instead they are observed to have correlated fluctuations of the columnar structures. By using multiple independent growth fronts generated by our VDP model, we calculated the correlation functions and analyzed the data to study the roughening mechanism at short length scales.

Figure 4.9 shows the auto-correlation function $C(r,t)$ for $L = 2000$ after a deposition time $t = 1000$ for $G = 10$, 10^2, and 10^3. This function can be used to characterize the

film morphology as a function of t. For the purpose of measuring the average distances between the columnar structures present in the polymer films, we defined two different lateral length scales: the lateral correlation length ξ, and the average column separation λ. The lateral correlation length ξ defines a representative lateral dimension of a rough surface and was estimated from $C(r,t)$ by using $C(r=\xi,t) = C(0,t)/e$. Within a distance of ξ the surface heights of any two points are strongly correlated. Whereas the parameter λ characterizes a wavelength-selection of a surface and was determined by measuring the value of r corresponding to the first zero-crossing of $C(r,t)$ [89]. The variation of λ with t represents how the columnar structures coarsen with progress in t. In general, the evolution of the columnar feature size follows a power law with t given by [64],

$$\lambda \propto t^p, \tag{4.16}$$

and the exponent p can be referred to as the *coarsening exponent*, that determines how the columnar structures coarsen during the growth process.

In Fig. 4.10 we plot λ and ξ versus t for $L = 2000$ and $G = 10$ and 10^3 along with the estimates for p. With an increase in G from 10 to 10^3, the exponent p was found to remain close to 0.57. The invariance of p indicates that the coarsening of the columnar structures follow a power law that is unaffected by the ratio G. We believe that the coarsening process mostly results from the effect of incoming monomer flux and is thought to be dominated by the "void-filling" property and the shadowing effect of monomer vapors coming from different launch angles.

Local Roughening Behavior

The *local roughness exponent* α_l of the growth front can be obtained from $H(r,t)$ using [48, 77]

$$H(r,t) \sim r^{2\alpha_l} \qquad (r \ll \xi). \tag{4.17}$$

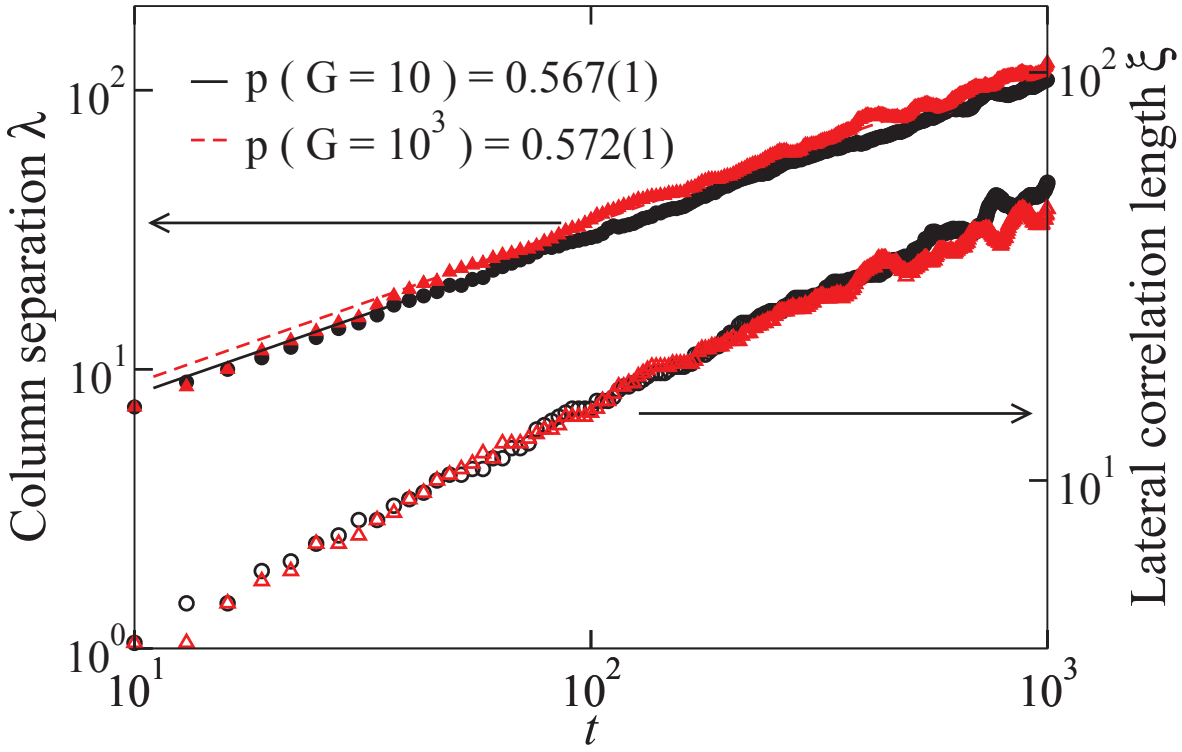

Figure 4.10: Estimates for column separation λ and lateral correlation length ξ obtained for $G = 10(circles)$ and $G = 10^3(triangles)$. Open symbols correspond to ξ and filled symbols correspond to λ. The data are averaged over 200 independent simulations with $L = 2000$ and $t = 1000$. The error in the exponents were obtained from the curve-fit.

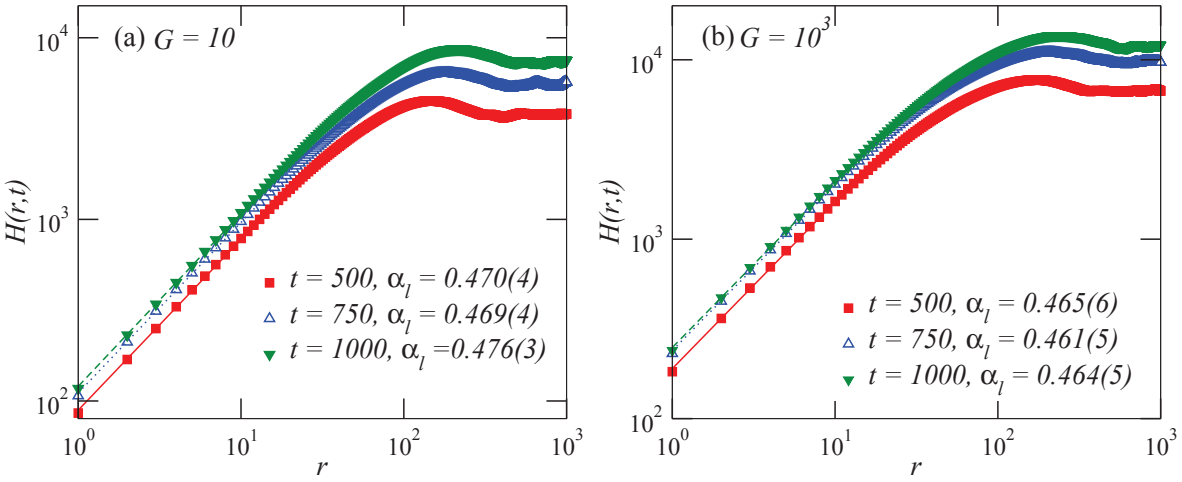

Figure 4.11: Height-height correlation function $H(r,t)$ for (a): $G = 10$, (b): $G = 10^3$ using $L = 2000$ at $t = 500$, 750, and 1000. The data are averaged over 200 independent runs and error in the exponents were obtained from the curve-fit.

In Figs. 4.11(a) and 4.11(b) we plot $H(r,t)$ for t = 500, 750, and 1000 along with the estimates for α_l for $L = 2000$ and $G = 10$, 10^3 respectively. For a given G and varying t, the estimates of α_l were observed to remain invariant within statistical errors. From Figs. 4.11(a) and 4.11(b), we obtained an average α_l of 0.470(3) and 0.460(3) for $G = 10$ and 10^3 respectively.

A comparison between α_g and α_l (shown in Fig. 4.7 and Fig. 4.11) shows that the roughness exponents at the global and local length scales are not the same. We find that $\alpha_g > \alpha_l$ for studied G and the scaling behavior of the interface width was observed to be different at short and large length scales. Also, for small r, the plots of $H(r,t)$ do not overlap at varying deposition times, and show the presence of non-stationary anomalous scaling [49]. The vertical temporal shift in the $H(r,t)$ observed in Fig 4.11 is due to the difference between α_g and α_l and indicates the presence of anomalous scaling in our VDP model.

The *anomalous* growth exponent defined as, $\beta_* = (\alpha_g - \alpha_l)/z_g$ [84] is often used to measure the difference between α_g, α_l. The exponent β_* can be obtained from the scaling behavior of $H(r,t)$ [90],

$$H(r,t) = r^{2\alpha_g} g_A(r/t^{1/z_g}), \tag{4.18}$$

where the *anomalous* scaling function $g_A(u)$ [90, 84] satisfies,

$$g_A(u) \sim \begin{cases} u^{-\kappa_1} & (u \ll 1) \\ u^{-\kappa_2} & (u \gg 1) \end{cases} \tag{4.19}$$

$$\kappa_1 = 2(\alpha_g - \alpha_l) \tag{4.20}$$

$$\kappa_2 = 2\alpha_g. \tag{4.21}$$

In Figs. 4.12(a) and 4.12(b) we show the plot of Eqn.(4.18), and show the rescaled data of $H(r,t)/r^{2\alpha_g}$ versus $r/t^{1/z_g}$. The rescaled data of $H(r,t)$ leads to the unique "data-collapse" function for $G = 10$ and 10^3 respectively. The "collapsed" curves shown in Figs. 4.12(a) and 4.12(b) are the anomalous scaling functions $g_A(u)$ (for $G = 10$ and 10^3) mentioned

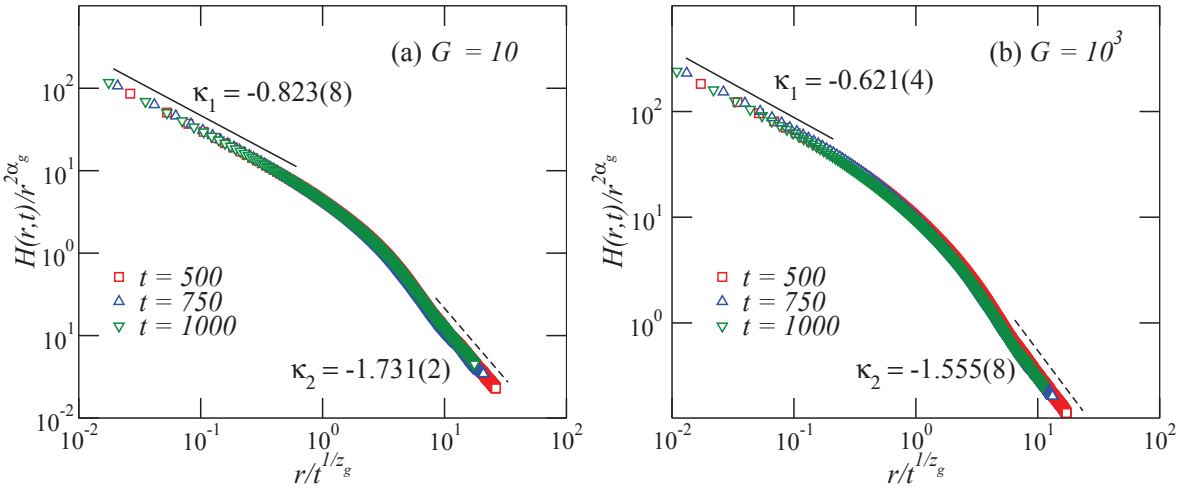

Figure 4.12: Plots of rescaled $H(r,t)$ showing the data collapse for (a): $G = 10$, and (b): $G = 10^3$ using $L = 2000$ at $t = 500$, 750, and 1000. The data are averaged over 200 independent runs and error in the exponents were obtained from the curve-fit. The straight lines are plotted as a guide to the eye. The scaling agrees with Eqn. (4.19).

in Eqn. (4.18). For both G, the scaling functions obtained in Fig. 4.12 satisfy Eqn. (4.19) in accordance with the theory for anomalous scaling [90, 84]. The exponents κ_1 and κ_2 were obtained from $g_A(u)$ plots using Eqn. (4.19). For $G = 10$ we have $\kappa_1 = 0.823(8)$, $\kappa_2 = 1.731(2)$ and for $G = 10^3$ we obtained $\kappa_1 = 0.621(4)$, $\kappa_2 = 1.555(8)$. For both G, we find that the exponents κ_1 and κ_2 obtained from the curve-fit satisfy Eqns. (4.20) and (4.21) for the numerical estimates of α_g and α_l obtained from Eqn. (4.9) and Eqn.(4.17).

4.3.4 Comparison of Global and Local Exponents

The dynamic scaling exponents of the local and global kinetic roughening are summarized in Figs. 4.13(a), 4.13(b), and 4.13(c) which shows the variation of global scaling exponents α_g, β, z_g and local exponents α_l, β_* with G. With an increase in G from 10 to 10^4, we found $\beta \approx 0.50$, α_g decreased from 0.87(1) to 0.73(1), and z_g decreased from 1.71(1) to 1.38(2). On

the local length scale, an increase in G did not cause a noticeable change in α_l ($\alpha_l \approx 0.46$) and β_* was observed to vary from 0.23(4) to 0.18(8). The small variation in β_* was found to be within statistical errors.

4.4 Conclusions

From the extensive studies of polymer films grown via VDP, the ratio G of the monomer diffusion coefficient D to the deposition rate F was found to have a strong influence on the film's growth morphology. The growth rate $R(G)$ of the polymer film was found to increase with an increase in G. This was due to the consequence of an upper diffusion flux of monomers. The detailed analysis of the surface morphology indicated the presence of very different scaling behavior at global and local length scales. The kinetic roughening study of film interface indicated the presence of anomalous scaling and multiscaling.

With an increase in G from 10 to 10^4, the global growth exponent $\beta \approx 0.50$ was found to be invariant, whereas the global roughness exponent α_g decreased from 0.87(1) to 0.73(1) along with a corresponding decrease in the global dynamic exponent z_g from 1.71(1) to 1.38(2). The global scaling exponents were found to follow the dynamic scaling hypothesis with $z_g = \alpha_g/\beta$ for various G. With an increase in G from 10 to 10^4, the average local roughness exponent α_l remained close to 0.46 with $\alpha_l \neq \alpha_g$ and the anomalous growth exponent β_* varied very slightly from 0.23(4) to 0.18(8) and was found to be invariant within statistical errors.

Even though our model is in $1+1D$ as compared to the $2+1D$ experiments, our estimates of α_l and β_* are close to the experimental findings of $\alpha = 0.5$ to 0.7 and $\beta = 0.25 \pm 0.03$ obtained from the AFM studies of linear PA-N films grown by VDP [58, 57]. The similarity between the experimental and simulational estimates appears to be a coincidence since the dimensions of the two systems are totally different. We also did not observe the changes in the dynamic roughening behavior reported by Ref. [59], perhaps due to the limitations of our

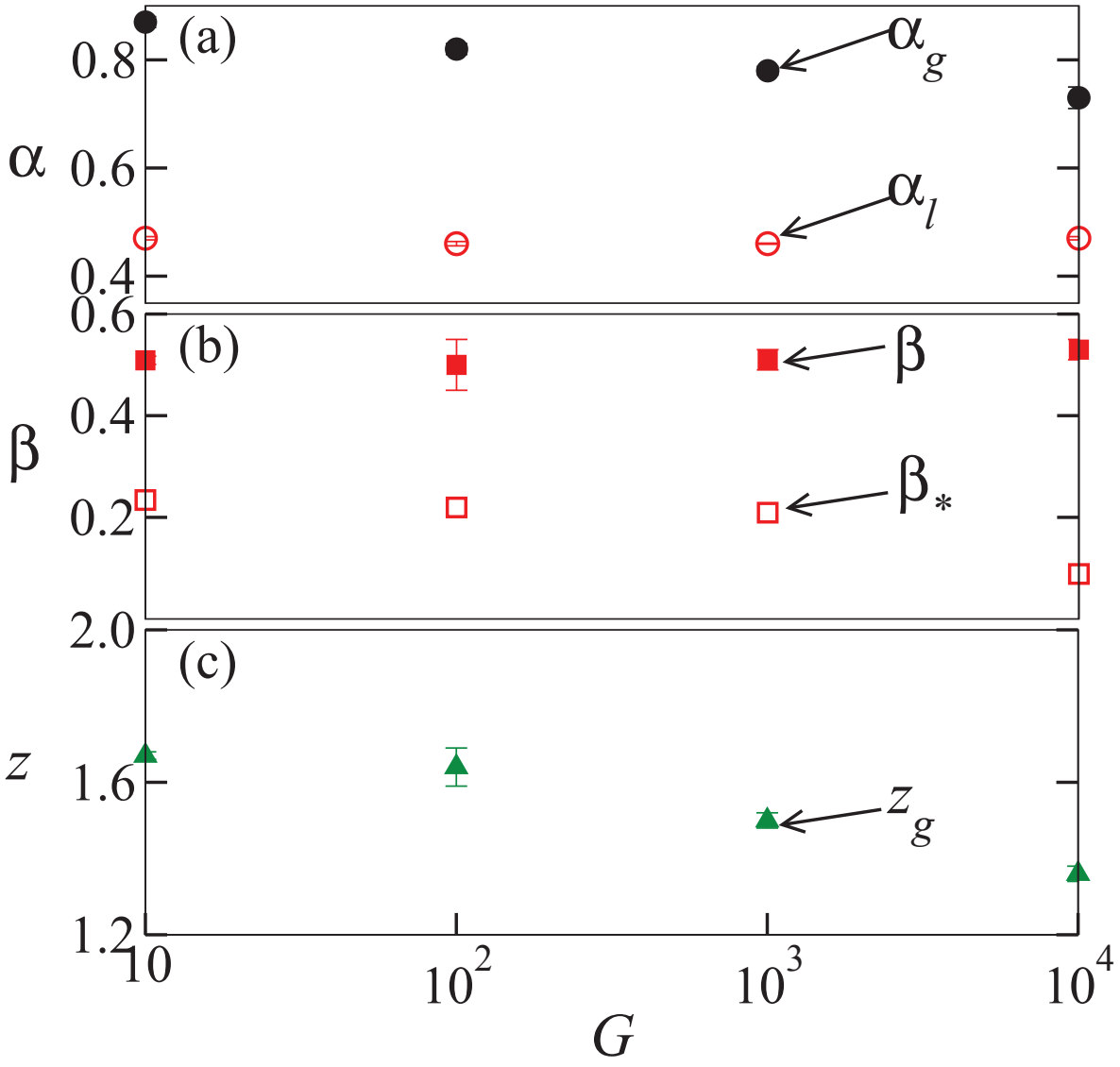

Figure 4.13: Variation of exponents α_g, β, z_g, α_l, and β_* with G. The global exponents were calculated after $t = 5000$ and the data were averaged over 1.8×10^3 independent runs. The local exponents were calculated using $L = 2000$ and $t = 1000$. The data were averaged over 200 runs and the error in the exponents were obtained from the curve-fit.

current simulation model in considering the effect of monomer diffusion only. This leads us to believe that the kinetic roughening of the polymer films is sensitive to the specific molecular-level interactions, relaxations of polymer chains through inter-polymer interactions, and the intrinsic nature of polymerization process that need to be accounted for in future simulations.

Chapter 5

Scaling of Polymer Chain Aggregates

In the preparation of polymer-based film materials like PPX, the polymer aggregation occurring during the film growth plays a key role in the VDP process. A theoretical understanding of the growth of polymer films including the formation of polymer aggregates (chains) and their temporal evolution is a topic of substantial interest. The mechanism of polymer film growth by VDP is known to be quite different from that of conventional PVD. Polymer film growth involves monomer reaction in the bulk of the film, which needs to be considered in growth models of VDP [91]. During film growth by VDP, the biradical nature of monomer molecules [92] likely plays an interesting role and may lead to distinctive growth behaviors that are very different from what one would expect from an atomistic PVD film growth. The polymer chains grow in both the lateral and vertical directions with the help of the chain propagation and polymer merger reactions that were discussed in Section 3.3. The relative rates of chain propagation and merger reactions are generally a function of the substrate temperature. It is also known that the rate of consumption of monomers by the chain propagation is several orders of magnitude greater than the consumption rate by the chain initiation at room temperature [92].

The development of AFM based methods have allowed a direct visualization of the morphology of such polymer films with a high spatial resolution. There have been interesting AFM studies [93, 94] that have examined how the surface morphologies of PPX films and its derivatives are affected by the rate of monomer deposition from the gas phase, the chemical nature of the monomer, and the substrate temperature [95, 96].

Although vapor transfer is a widely used method in growing organic nanostructures, literature on the size controllable growth of the constituting nanostructures themselves is very limited. In spite of the importance of understanding the aggregation mechanism on the molecular level, such an understanding is quite poor in polymerization driven processes as compared to those of metals and semiconductors. Many recent studies have focused on the behavior of overall polymer films properties like film density, interface width, end-to-end distance, etc [53, 52, 4, 97, 59]. But still, there remains an inadequate understanding of the aggregation process of polymer chains themselves apart from literature on submonolayer studies of VDP [52] that reported the existence of three distinct growth regimes: initiation (I), chain propagation (P), and saturation regime (S) and the recent experimental work on island nucleation during VDP [93] that indicates a new type of surface growth governed by reaction-limited aggregation in the films grown by VDP. Despite the availability of experimental data from many $3D$ growth processes, most computer modeling studies have been restricted to $1+1D$ for their simplicity. In general, $1+1D$ models can be used to explore a larger range of length scales and the results can be more easily visualized and explained. In non-equilibrium growth models, the sensitivity of polymer aggregation process and geometric scaling properties to the model details is an important aspect from a theoretical and practical point of view. There seems to be no generalized approach for a detailed, quantitative prediction of the geometry of the aggregates generated by growth models from the growth rules alone.

In many cases, the "surfaces" of polymer chains or clusters are important in both the cluster growth processes and in simulations that are carried out to explore the physical and chemical properties of the structures that they represent. Unfortunately, there is no well established convention used in defining the surface of a cluster; and instead there are multiple ways of defining the surface of various structures encountered in the growth processes. In most cases the "physics" of the research problem suggests a natural definition of the sur-

face of a cluster. In many non-equilibrium growth and aggregation processes, the growing structures are represented by collection of filled ("connected") sites on a lattice. We followed a similar definition in our analysis and a polymer chain or cluster was defined as a set of chemically bonded monomers. In VDP growth models, this description of cluster in terms of occupied bonded monomer sites is natural, and is very commonly used.

In this chapter, we present a systematic study of the evolution of polymer chains (clusters) during the VDP growth of linear polymer films on flat substrates. To obtain insight into the mechanism governing the growth of chains due to various allowed MC moves, we employed the dynamic scaling analysis which has been often used in investigating various forms of aggregates ranging from one-dimensional metal rows to three-dimensional droplet patterns.[98, 99]. Interestingly, the application of dynamic scaling analysis to a recent experimental growth of PPX-C (a derivative of PPX) [93] strongly indicates that film growth by VDP belongs to a new type of surface growth governed by reaction-limited aggregation process in which the competition between diffusion and deposition defines the time scale of film growth. While the possibility of observing the conventional dynamic scaling behavior is rather surprising given that the cluster formation by VDP involves processes very different from those associated with the usual inorganic film PVD growth, it provides a reasonable starting point for applying the concepts of dynamic scaling theory to the polymer growth studied in this work. We therefore use this as a starting point to study the chain aggregation processes in VDP.

5.1 Average Chain Length

A widely used method for the description of growing aggregates (clusters) is the determination of distribution function of aggregates, which, in the studies of polymers, is referred to as the polymer chain length distribution function $n_s(t) = N_s(t)/L$, where $N_s(t)$ is the number of polymer chains containing s monomers at time t [68, 100, 101]. The quantity $n_s(t)$ is often

used in the kinetic description of chain growth and gives the density (per site) of the chains of size s at time t.

The average linearized chain length $S(t)$ is commonly used in characterizing polymer chain lengths and is defined as the first moment of $n_s(t)$ [68],

$$S(t) = \frac{\sum_{s>1} n_s(t)s}{\sum_{s>1} n_s(t)}. \tag{5.1}$$

By definition, it is an average of the molecular weights of all the individual homopolymers present in the system at a given time t. It is a common way of determining the molecular weight of a polymer. Experimentally, the average molecular weight of a polymer can be determined by gel-permeation chromatography [102], viscometry, vapor pressure osmometry, etc.

5.1.1 Time Evolution

For getting an understanding of the growth of polymer chain aggregates in a VDP system, we studied the time evolution of $S(t)$ for $G = 10$, 10^2, and 10^3. Figure 5.1 shows the variation of $S(t)$ for $G = 10$, 10^2, and 10^3 as the deposition time t was increased from 0 to 10^4. For a given G, as t increases, the average chain length was observed to increase from its initial value of zero (at $t = 0$) and attain a maximum value at around $t = 1000$. For deposition time $t > 1000$ units, the $S(t)$ was observed to have a steady value that does not seem to vary much with an increase in t. The Fig. 5.1 indicates the presence of two distinct growth regions based on the evolution of $S(t)$. During early deposition times, the average chain length of the polymers present in the system increased until it attains an asymptotic value S_{sat} for large t. The presence of a nearly constant S_{sat} for $t > 1000$ indicates a steady state saturation regime, as labeled in Fig. 5.1. Also, from Fig. 5.1 we can observe that at any given t, the values of $S(t)$ and S_{sat} depend on the ratio G used in the simulation. As G was increased from 10 to 10^3, values of $S(t)$ and the steady state value S_{sat} was observed to increase systematically; the average S_{sat} for a larger G was found to be greater than that obtained for simulations

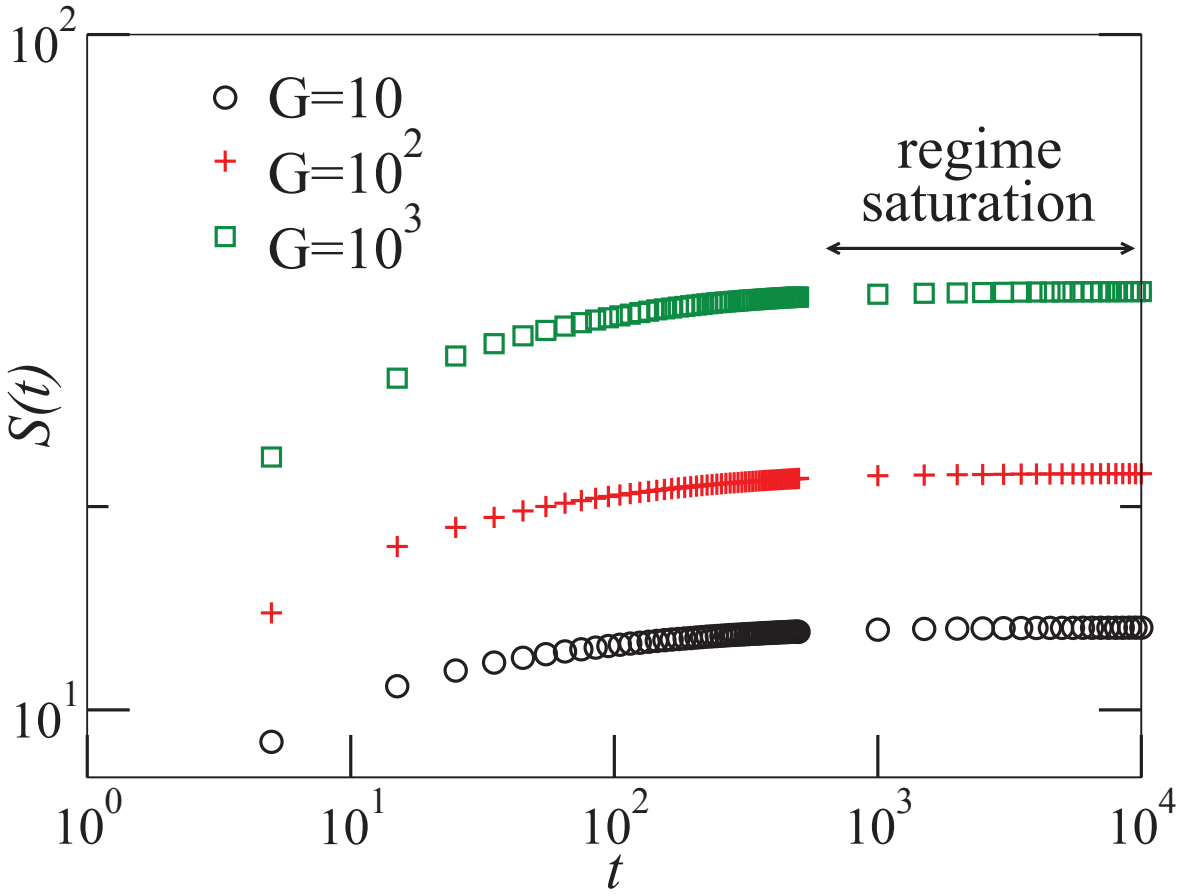

Figure 5.1: The mean chain length $S(t)$ as a function of t for $L = 200$ and $G = 10$, 10^2, and 10^3. The indicated saturation regime is characterized by a nearly constant $S(t)$ and demonstrates a steady state VDP growth.

with lower G. A similar increase in the values of $S(t)$ was also observed with an increase in G. This observation leads us to believe that the ratio G is a critical system parameter that determines and limits the overall average polymer chain lengths present in the VDP growth. More on this behavior is discussed in the following sections.

5.1.2 Variation of Average Chain Length With G

After having observed a definite influence of G on $S(t)$, we were interested in studying the dependence of S_{sat} on the ratio G. From the data plotted in Fig. 5.1 we calculated the average S_{sat} and observed its behavior as G was increased from 10 to 10^5. In Fig. 5.2 we show the variation of S_{sat} as G was increased systematically. From our analysis, we found a power law dependence of $S_{sat} \propto G^{0.273(5)}$. This observation quantifies the sensitivity of the steady state average chain length S_{sat} on the parameter G. The average chain lengths of the polymers were observed to increase as G was increased, a conclusion that is in agreement with our earlier qualitative finding from Fig. 4.1 in Section 4.1, where the longest chain (highlighted in black color) for $G = 10^6$ was much larger than that obtained for $G = 10$.

In the remaining part of this chapter we concentrate on the steady-state growth and study the scaling of polymer chain aggregates in the saturated regime of VDP.

5.2 Chain Length Distributions

In general it is known that any diffusion bias present in the aggregate growth process leads to the appearance of scaling behavior in $n_s(t)$; and if diffusion were independent of s then a diffusive-like kinetic universality class is manifested [103]. The VDP process studied in this work is an interesting stochastic growth model that is a combination of varying deposition probabilities (p_F), diffusion probabilities (p_D), coupled with many possible MC moves. We were interested in exploring the effect of various complex dynamic processes on the behavior of $n_s(t)$, our ultimate interest being to quantitatively understand the underlying polymer aggregation process.

5.2.1 Dependence on G

In this section, we present our results on the sensitivity of polymer chain length distribution function $n_s(t)$ to the changes in G. As a representative substrate, we chose $L = 200$ and

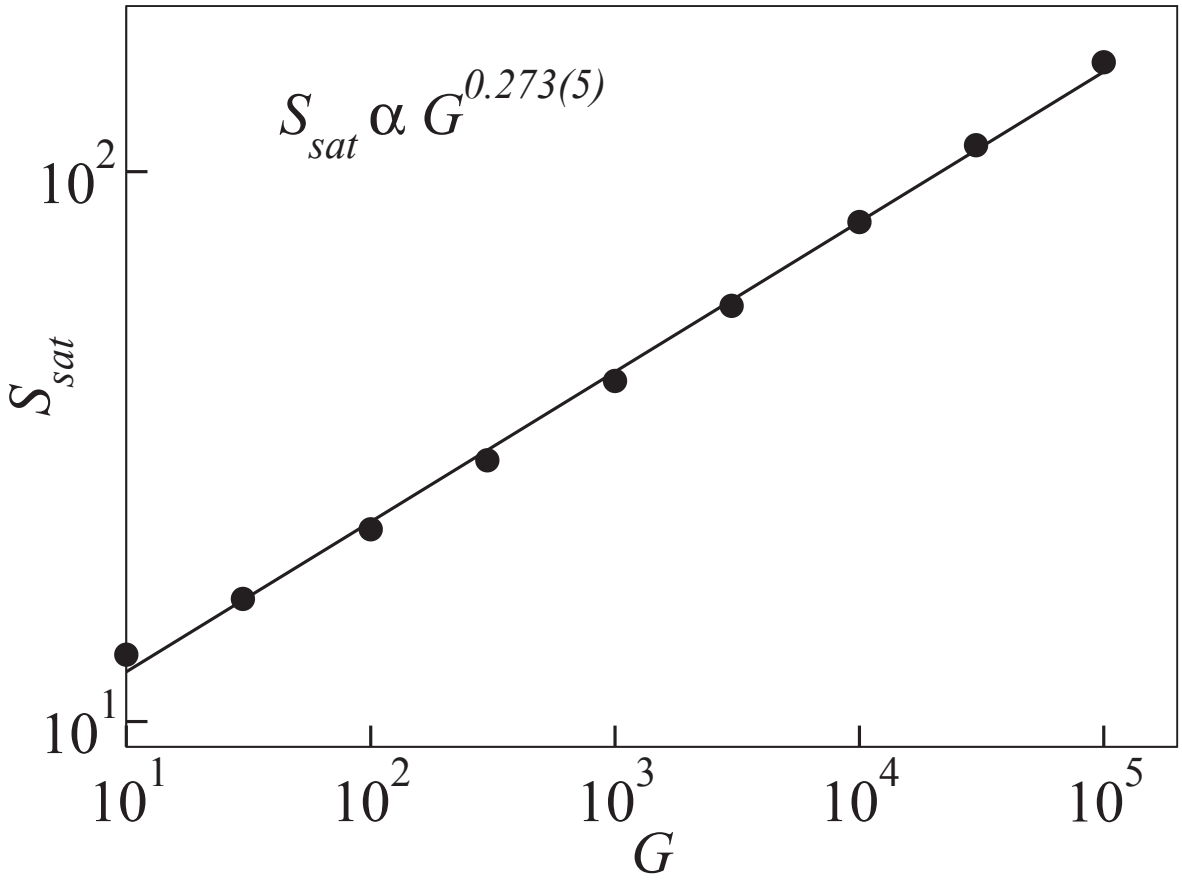

Figure 5.2: The variation of mean chain length in saturation regime (S_{sat}) as a function of G. A straight line fit on the log-log plot indicates a power law increase of S_{sat} with G, the error in the exponent was obtained from the curve fit.

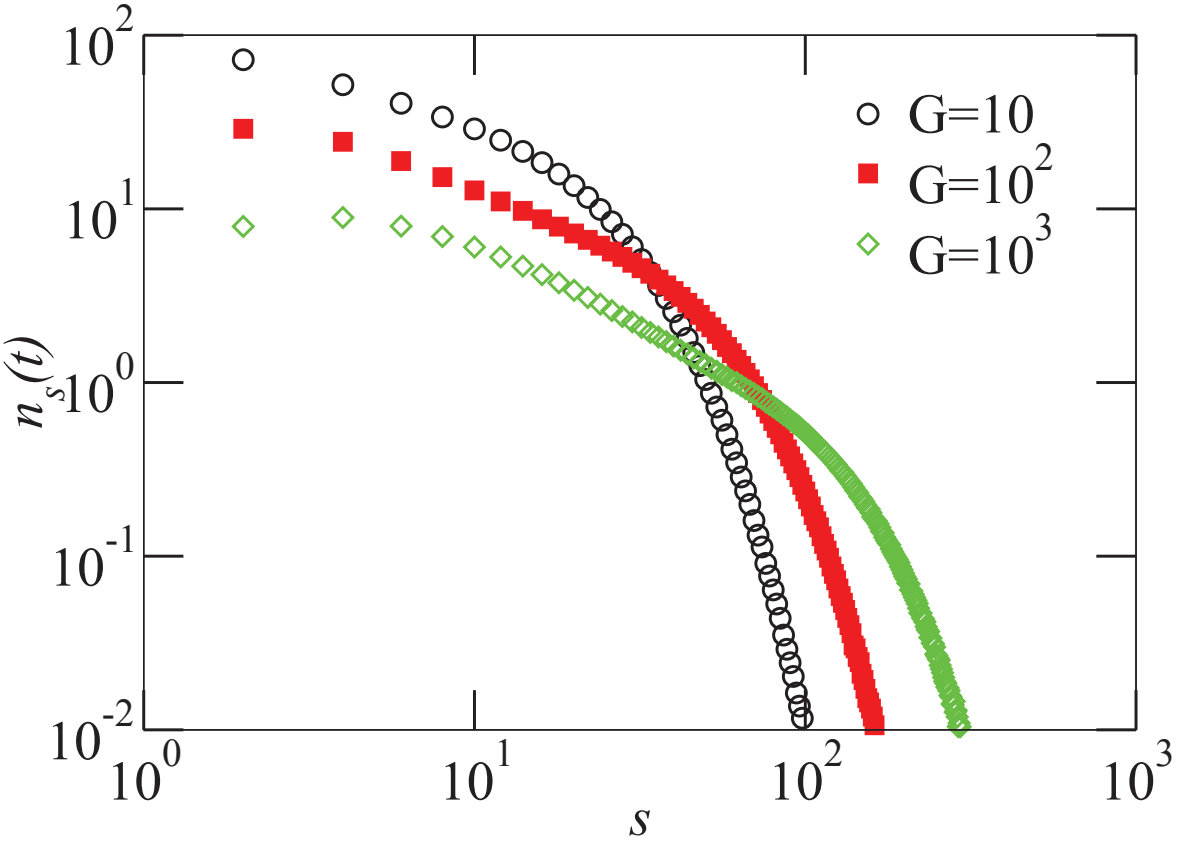

Figure 5.3: Plots of polymer chain length distribution $n_s(t)$ as a function of G for $L = 200$ and $T = 10 \times 10^3$. The statistical error of the mean is smaller than the symbol sizes.

performed VDP simulations for very long deposition times of $t = 10^4$ using $G = 10$, 10^2, and 10^3. The average estimates for $n_s(t)$ were obtained from multiple independent runs. In Fig. 5.3 we show the data for $n_s(t)$ versus s for $G = 10$, 10^2, and 10^3. In Fig. 5.3 we find that the behavior of $n_s(t)$ versus s looks qualitatively similar for all the studied G. Basically, for a given G, the $n_s(t)$ starts off at its maximum value for the smallest chains ($s = 2$) and gradually decreases as longer polymer chains are encountered in the system. This behavior indicates that $n_s(t)$ is largest for smallest chain and the probability of finding longer chains keeps reducing for longer chains. Apart from the discussed similarity in the behavior of $n_s(t)$, it is interesting to study the differences in the characteristics of $n_s(t)$ as G was increased from 10 to 10^3. In Fig. 5.3, as G was increased from 10 to 10^3, an increase in the lateral spread of $n_s(t)$ data was observed. This systematic increase in the range of s indicates that as G is increased, the VDP system tends to have greater number of long polymer chains. This finding can be understood by noting that, with an increase in G, the monomers present in the film have a higher probability to diffuse and reach the active ends of the chains. This promotes polymer chain propagation and results in the appearance of longer chains in the system. In contrast, for a lower value of $G = 10$, the monomers in the system do not have a higher diffusion probability and tend to initiate new chains (dimers) by reacting with newly deposited monomers. A large number of chain initiations at lower values of G results in higher values of $n_s(t)$ for shorter chains as observed in Fig. 5.3.

5.2.2 Dependence on s and t

In this section we discuss the characteristics of $n_s(t)$ as function of parameters t and s. Firstly, we study the dependence of $n_s(t)$ on s for $t = 10^3$, 5×10^3, 10^4. The Fig. 5.4 shows the variation of $n_s(t)$ as a function of s for indicated t , and $G = 10$. In Fig. 5.4, for a given t, the $n_s(t)$ distribution was observed to decrease to zero for increasing chain lengths s. Similar behavior was observed for a range of G varying from 10 to 10^3 and was shown

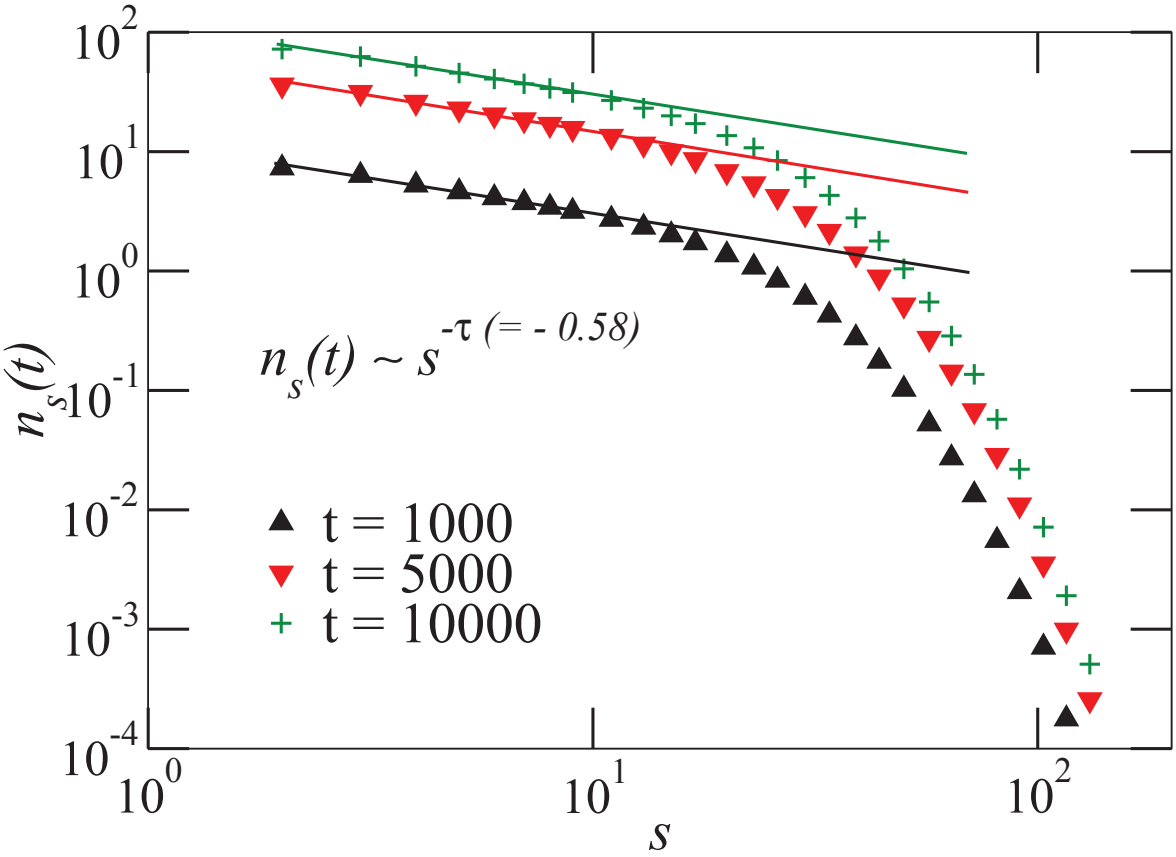

Figure 5.4: Plots of polymer chain length distribution $n_s(t)$ as a function of s for $L = 200$ and $G = 10$ at $t = 10^3$, 5×10^3, and 10×10^3. The straight lines have a slope $\tau = -0.58(2)$ and indicate a power-law dependence of $n_s(t)$ on s. The error in the exponent was obtained from the curve fit.

in Fig. 5.3. It can also be seen that as t was increased from 10^3 to 10^4, the average $n_s(t)$ increased for all chain sizes; and for all s, an increase in t is seen to increase the numerical value of $n_s(t)$ without much effecting the length of the largest polymer chains present in the system. This finding is contrary to the conventional growth studies of diffusion-limited cluster aggregation and reaction-limited cluster aggregation studied in Refs. [68, 100, 104] where, with an increase in t , the smaller clusters are observed to merge and form larger clusters. This feature of Fig. 5.4 is a consequence of restricting the polymer propagation to the active ends only. Similar behavior of $n_s(t)$ can be expected in VDP growth of other linear polymers where all the chains are constrained to grow at either of their active ends only. From Fig. 5.4 it can be seen that the critical value of s at which the power law decay cuts off does not vary much with an increase in t. The quantitative information about the growth of polymers can be obtained by observing the straight line behavior on the log-log plots in Fig. 5.4 that correspond to a power-law decay of $n_s(t)$,

$$n_s(t) \sim s^{-\tau}, \tag{5.2}$$

with an average exponent $\tau = 0.58(2)$ for indicated t. In Fig. 5.4, for $G = 10$, the exponent τ was found to be invariant for $t = 10^3$, 5×10^3, 10^4. Also, the τ was found to be ≈ 0.58 for other values of G from 10 to 10^4.

After having studied the variation of $n_s(t)$ with s, we now concentrate on the temporal evolution of polymer chain densities to understand how $n_s(t)$ varies with t for polymer chains with varying s. For $G = 10$, Fig. 5.5 shows the evolution of $n_s(t)$ as deposition time t was increased from 0 to 10^4, for representative chains with $s = 10$, 20, 40, and 50. For indicated s and t, the $n_s(t)$ distribution was observed to follow a power law given by,

$$n_s(t) \sim t^{\omega}, \tag{5.3}$$

with an average exponent $\omega = 1.01(2)$ that can be used to quantify the rate of increase in $n_s(t)$ with t. The power law increase in $n_s(t)$ with t observed in Fig. 5.5 explains the presence

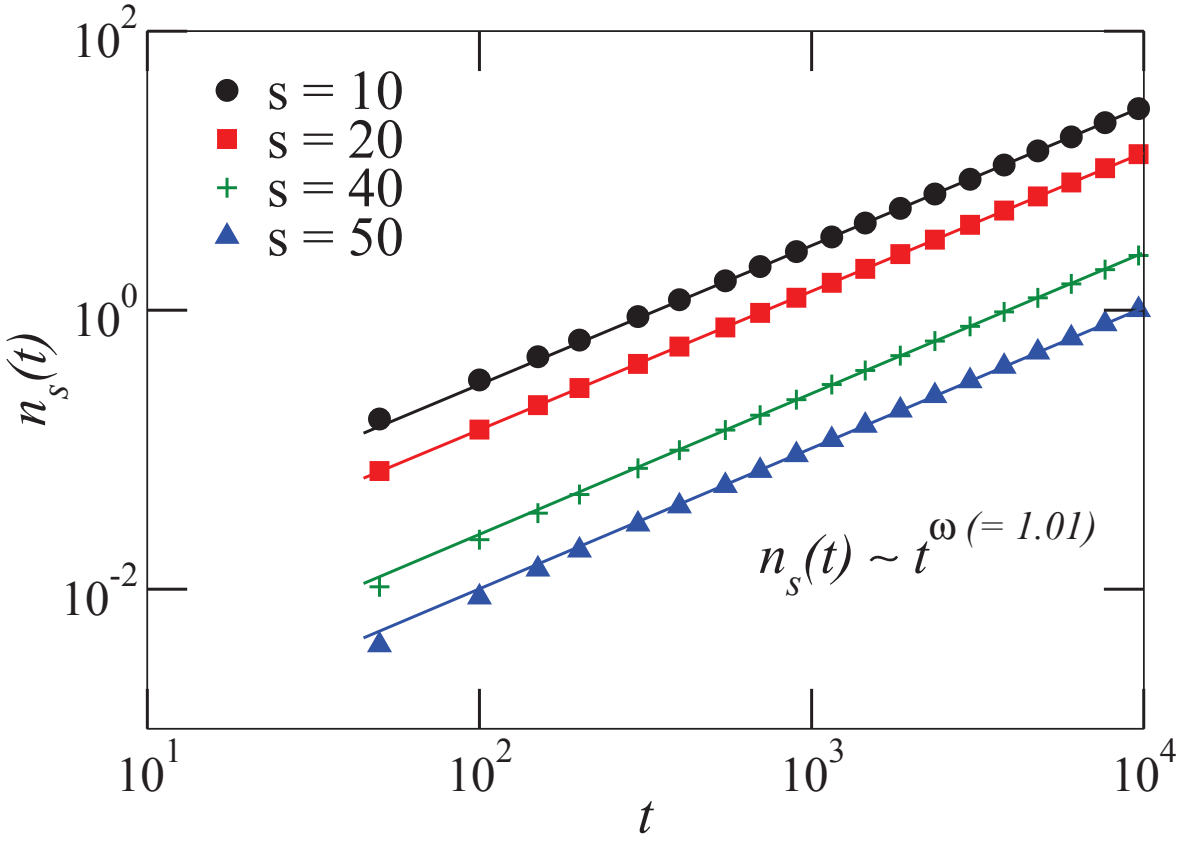

Figure 5.5: Plots of chain length distribution $n_s(t)$ as a function of t for $L = 200$, $G = 10$, and selected chain lengths $s = 10$, 20, 40, and 50. The straight lines have a slope $\omega = 1.01(2)$ and indicate a power law increase of $n_s(t)$ with t. The error in ω was obtained from the curve fit.

of smaller chains throughout the VDP growth process (seen earlier in Fig. 5.4) and indicates that the smaller polymers do not have the tendency to merge and form larger chains in spite of the polymer merger move present in our simulations. From Fig. 5.5, we see that $n_s(t)$ keeps increasing with an increase in t. Moreover, the rate of increase of $n_s(t)$ with t, that was quantified by ω was found to be independent of polymer chain length s as seen in Fig. 5.5.

From above discussions, it can be understood that $n_s(t)$ increases with t for all polymer chains in the VDP system. Another way of determining the temporal growth rate of $n_s(t)$ is by counting the total number of polymer chains $N_{total}(t)$ in the system and studying the evolution of $N_{total}(t)$ with time for varying G. In Fig. 5.6, we show the variation of $N_{total}(t)$ in the system as a function of t for $G = 10$,10^2, and 10^3. Here too, we observed a power law increase in $N_{total}(t)$ given by, $N_{total}(t) \propto t^{0.9962(4)}$ that corroborates our finding of power law increase in $n_s(t)$ for $s = 10$, 20, 40, and 50, shown earlier in Fig. 5.5. The power law exponent calculated in Fig. 5.6 was found to be $= 0.9962(4)$ and is the same (to with in error-bars) as the exponent $\omega = 1.01(2)$ obtained in Fig. 5.5.

5.3 Dynamic Scaling of Chain Aggregates

Typically in the experimental studies of aggregation processes, a quantity referred to as "coverage" $\theta = F \times t$ is often used to quantify the number of particles present on the substrate. The θ used in this section is different from the deposition angle θ used in the earlier Section 3.3. As θ is more convenient for comparison of simulational results with the experiments, we expressed the time dependence of $n_s(t)$ and other relevant quantities in terms of θ. We define the total polymer chain density N_{total} (excluding monomers) and the coverage θ as,

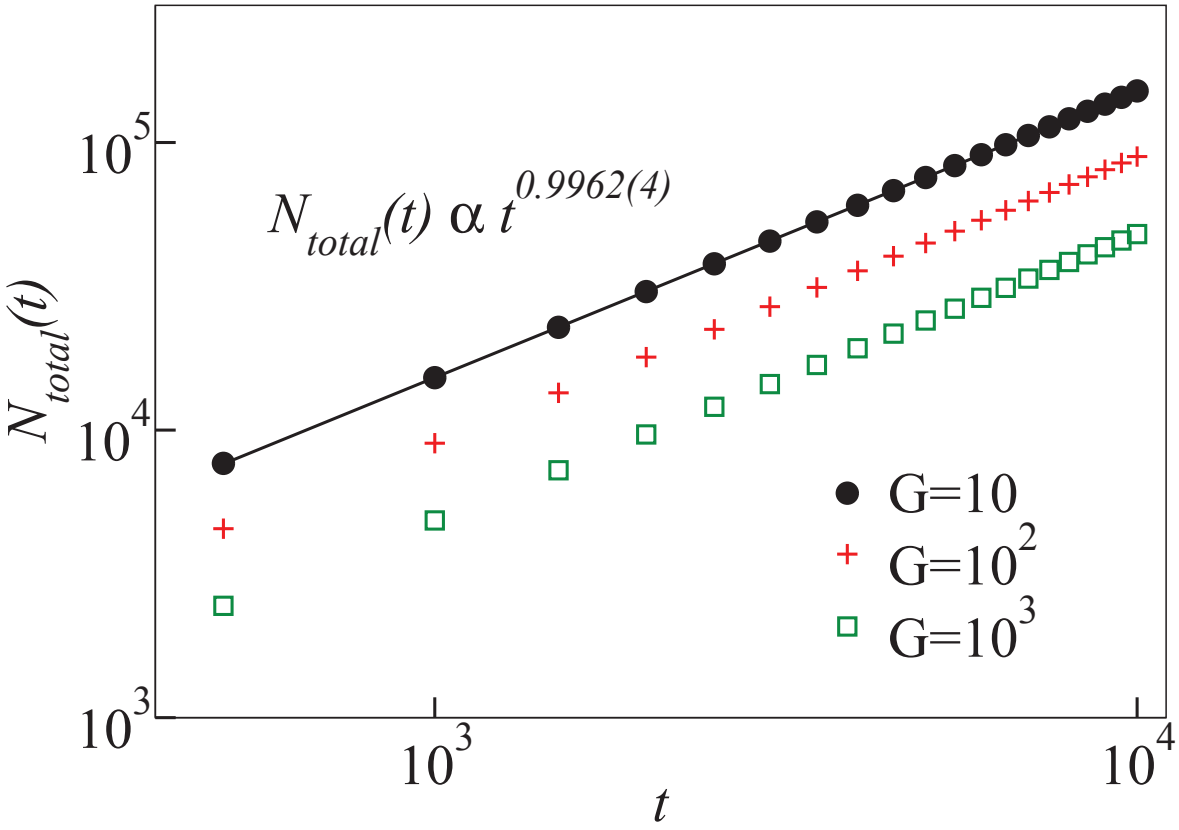

Figure 5.6: Plots of the total number of polymer chains N_{total} as a function of t for $L = 200$, $G = 10$. The straight line through the $G = 10$ data has a power law exponent of 0.9962(4). The power law exponent of N_{total} versus t was found to be same as ω (within error bars) obtained from Eqn. (5.3). The error in exponent of the curve-fit data was obtained from regression analysis.

$$N_{total} = \sum_{s \geq 2} n_s(\theta), \tag{5.4}$$

and

$$\theta = \sum_{s \geq 1} s n_s, \tag{5.5}$$

such that the average linearized chain length $S(t)$ defined earlier in Eqn. (5.1) can be rewritten as a function of θ as,

$$S = \frac{\sum_{s>1} n_s(t) s}{\sum_{s>1} n_s(t)} = \frac{(\theta - N_1)}{N_{total}} \tag{5.6}$$

where N_1 is the number of monomers in the system.

According to the dynamic scaling of aggregates [68], there exists only one characteristic size in the system, which in our VDP model is the mean island size $S(\theta)$ defined in Eqn. (5.6). This implies that $n_s(\theta)$ scales with $S(\theta)$, and we can write,

$$n_s(\theta) = A(S, \theta) f(s/S), \tag{5.7}$$

where $f(s/S)$ is referred to as a *scaling function* for the polymer chain distribution. Using the definition of θ and the scaling form for $n_s(\theta)$ shown in Eqn. (5.7), we can write,

$$\theta = \sum_{s \geq 1} s n_s(\theta), \tag{5.8}$$

we now substitute back the expression for $n_s(\theta)$ from Eqn. (5.7) and replace the summation by integration over s (because $f(s/S)$ is a continuous function),

$$\theta = \int_0^\infty s A(S, \theta) f(s/S) ds. \tag{5.9}$$

By changing the variable of integration from (s/S) to u we get

$$\theta = A(S, \theta) S^2 \int_0^\infty f(u) u du, \tag{5.10}$$

which implies $A(S,\theta) \sim \theta/S^2$. By taking $A(S,\theta) = \theta/S^2$, we can write the general scaling form as,

$$n_s(\theta) = \theta S^{-2} f(s/S) \qquad \text{for} \qquad s \geq 2, \tag{5.11}$$

where the scaling function $f(u)$ satisfies the following properties,

$$\int_0^\infty f(u) u du = 1, \tag{5.12}$$

$$f(u) \sim u^\omega \qquad \text{for} \qquad u \ll 1. \tag{5.13}$$

In a recently published study of the nucleation and growth dynamics during submonolayer VDP of Poly(chloro-p-xylylene) (PPX-C) films on a silicon oxide substrate, Lee et al. [93] used the dynamic scaling theory (discussed above) to study the scaling functions of aggregation mechanism. With an increase in the coverage, the bell-shaped monomodal chain distribution function (characteristic of Diffusion Limited Aggregation) gradually disappeared and became a monotonically decreasing function with extended tails approximately following a power law. The substantial change in the behavior of the scaling function of chain aggregates was attributed to the strong chemical reactivity involved in the polymerization process. The authors Lee et al. [93] obtained the scaling functions of VDP-grown aggregates and reported the power law scaling of chain density function in the large chain regime $(s/S_{sat}) \geq 1$ rather than for small chain region $(s/S_{sat}) \ll 1$ as shown in Eqn. (5.13).

The availability of a directly related experimental result was our motivation to analyze our simulational $n_s(t)$ data. We followed the procedure outlined by the scaling theory [68] and plotted the rescaled quantity $n_s(t) \times S_{sat}^2$ versus s/S_{sat} in Fig. 5.7 for $t = 8 \times 10^3$, 9×10^3, 10^4, and $G = 10$, 10^4. For a given G, the aforementioned rescaling shifts $n_s(t)$ shown in Fig. 5.4 such that all data points for varying t and s collapse onto a single curve, referred to as the *scaling function*. The scaling functions obtained for $G = 10$ and 10^4 are shown in Fig. 5.7. In Fig. 5.7 the values of $n_s(t) \times S_{sat}^2$ were observed to decrease for increasing values of s/S_{sat}. Our results are in agreement with the experimental work of Lee et al. [93] where

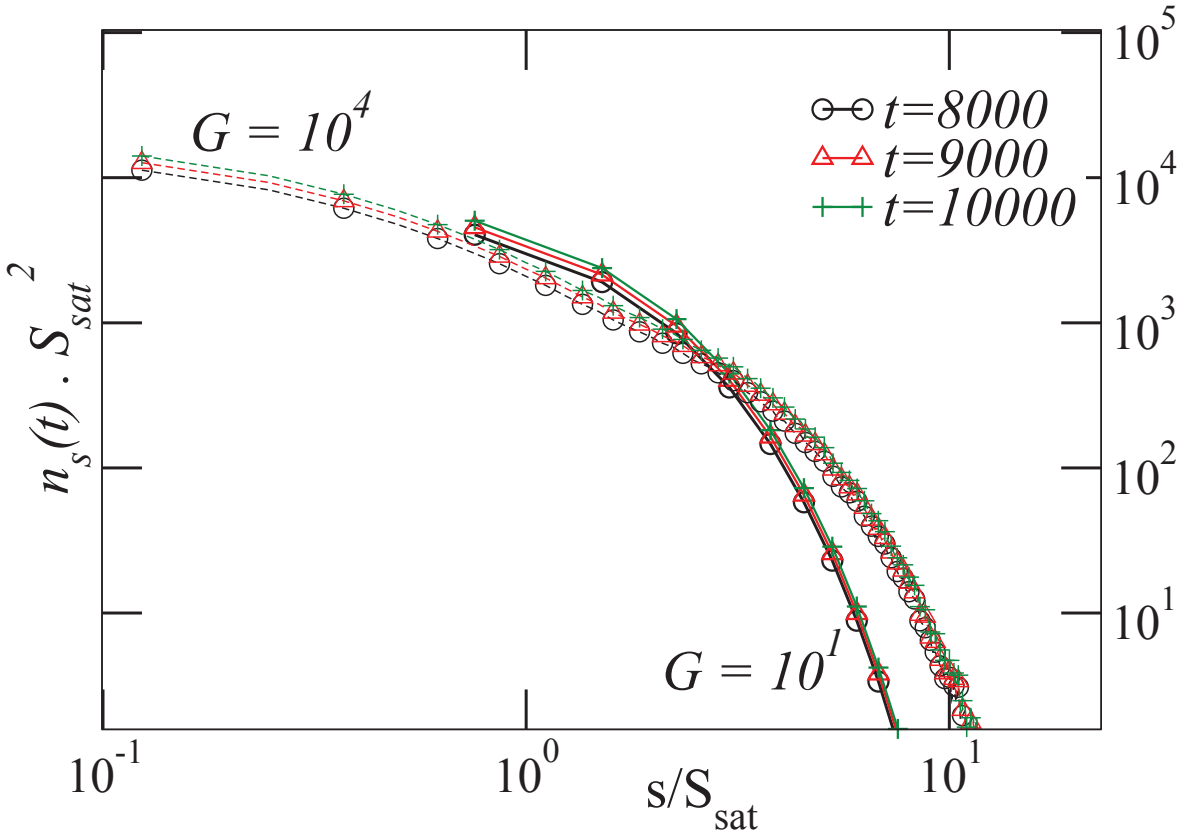

Figure 5.7: Comparison of scaled chain length distributions for $L = 200$ and $G = 10$ and 10^4. For a given G and $t = 8 \times 10^3$, 9×10^3, and 10×10^3 the rescaled plots collapse onto a single scaling function. However, a variation in G affects the behavior of scaling functions of $n_s(t)$ and produces non-overlapping curves at varying G. The connecting lines are guide for the eyes.

authors noticed a power law scaling of island density distribution in the large island regime ($s/S_{sat} \geq 1$) instead of an exponentially decaying function observed for the usual reaction-limited colloid aggregation. The scaling functions shown in Fig. 5.7 are different from the conventionally studied monomodal (bell-shaped) curves obtained in atomistic growth models [68, 101]. This difference in the behavior of scaling functions in VDP is can be attributed to an increase in the number of polymer chains (of all sizes) in the system. This accumulation of chains results in a diverging $n_s(t)$ as a function of t (see Fig. 5.5).

In Fig. 5.7 we find that the scaling functions corresponding to $G = 10$ and 10^4 do not collapse onto a unique master curve. We thus note that G is an important parameter in determining the dynamic scaling of polymer chain aggregates. We hope that our observation of non-overlapping scaling functions in Fig. 5.7 merits itself a careful further study on understanding the changes in the aggregation mechanism brought about by G.

5.4 Conclusions

In this chapter, by varying the ratio G, we studied the role of surface diffusion in determining the dynamic scaling of polymer chain distribution function $n_s(t)$ found in our VDP growth model. The ratio G has a direct influence on the behavior of scaling functions that characterize the aggregation process. By performing a systematic study of the dependence of $n_s(t)$ on G and t, we found noticeable differences between the properties of $n_s(t)$ found in VDP and conventional diffusion-limited cluster aggregation and diffusion-mediated island growth models. In particular, for $G = 10$, we found the time dependence of $n_s(t)$ to be a power law, given by $n_s(t) \sim t^{\omega}$ with $\omega = 1.01(2)$. The positive exponent $\omega > 0$ means that the shorter polymer chains continue to be present in the system instead of merging to longer chains. Also, the exponent ω was found to remain a constant ($= 1.01(2)$) as the ratio G was varied from 10 to 10^3. However, for $G = 10$, and 10^4, we observed that the scaling functions obtained for chain aggregates did not collapse onto a single universal curve, and a variation

in G inhibited the appearance of a unique scaling function for the aggregation process in VDP.

In our VDP model, the linear polymer growth happens via chain propagation and polymer-merger processes. Since these two growth mechanisms depend on polymerization reaction at either of the two active ends of the chains, the temporal evolution of $n_s(t)$ can be thought to strongly depend on the chemical binding nature of the precursors involved in VDP. Also, the complicated screening action resulting from a limited bonding nature of monomer is also thought to bring about a significant modification to the aggregation mechanism observed in our study.

Chapter 6

Polymer Chain Structural Properties

Although the fundamental property of bulk polymers is their degree of polymerization, the overall physical (conformational) structure of the chain is also an important factor that determines the macroscopic properties of the polymer films. Typically, the terms configuration and conformation are commonly used in describing the geometric structures of polymer chains. More often than not, these two terms are intermingled in usage and it is good practice to clarify our usage of these two properties with respect to polymer chains. The term configuration refers to the differences in polymer structures arising from the order of the constituting chemical bonds and a chain configuration cannot be altered unless the bonds are broken and re-made. On the other hand, the term conformation refers to a property that arises from relative positions of monomers within the polymer chain. Since we do not allow bond breaking and re-making in our VDP simulations, we concentrate on the conformational properties of the polymer chains that are present in the system during VDP growth.

Since the beginning of the 1980s, fractal geometry analysis [105] has been an effective tool in the description of complex growing structures. It has been successfully applied in obtaining valuable information about the physical mechanisms of many growth processes including diffusion limited aggregation (DLA), cluster-cluster aggregation, and percolation systems [106]. Many growth models that follow general cluster-cluster aggregation mechanism are known to exhibit a fractal dimension. In this chapter we discuss the geometrical characteristics of polymer chains grown via VDP. We present the conformational properties of polymers of varying chain lengths, grown at G varying from 10 to 10^4.

6.1 Radius of Gyration and Fractal Dimension of Chains

A popular quantity that is used in measuring the space occupied by a polymer chain is expressed in terms of the radius of gyration R_g, defined as an average distance from the center of mass of the chain to the chain itself. It is calculated as the root mean square distance of the polymer chain's constituent monomers from its center of mass:

$$R_g(s) = \sqrt{\frac{\sum_{i=1}^{s}(r_i - r_{cm})^2}{s}}. \tag{6.1}$$

Since the chain conformations of growing polymers are constantly changing over time, the $R_g(s)$ calculations need to be averaged over all polymer chains in the system. That is, our calculations of $R_g(s)$ were obtained after averaging over an ensemble of chains found in the system. One of the reasons that $R_g(s)$ is an interesting property to analyze is that it can be determined experimentally by using static light scattering [107], small angle neutron- and x-ray scattering and the simulational estimates of $R_g(s)$ allows our computational model to be compared to the experimental data.

In general, for many cluster growth models including polymer growth, the radius of gyration $R_g(s)$ is known to follow power law scaling with s given by [49],

$$R_g(s \gg 1) \propto s^{\beta} \tag{6.2}$$

Using the exponent β and from Eqn. (6.2) the fractal dimension D_β of the chain aggregates can be calculated by [108],

$$D_\beta = \frac{1}{\beta} \tag{6.3}$$

We selected a representative substrate of length $L = 200$ and performed 500 independent simulations for deposition times of $t = 10^4$ to study the behavior of various conformational properties of the chains present in the system.

In Fig. 6.1 we show the variation of R_g as a function of s for simulations performed with $G = 10$, 10^2, 10^3, and 10^4. As seen in Fig. 6.1, for both shorter ($s < 20$) and longer

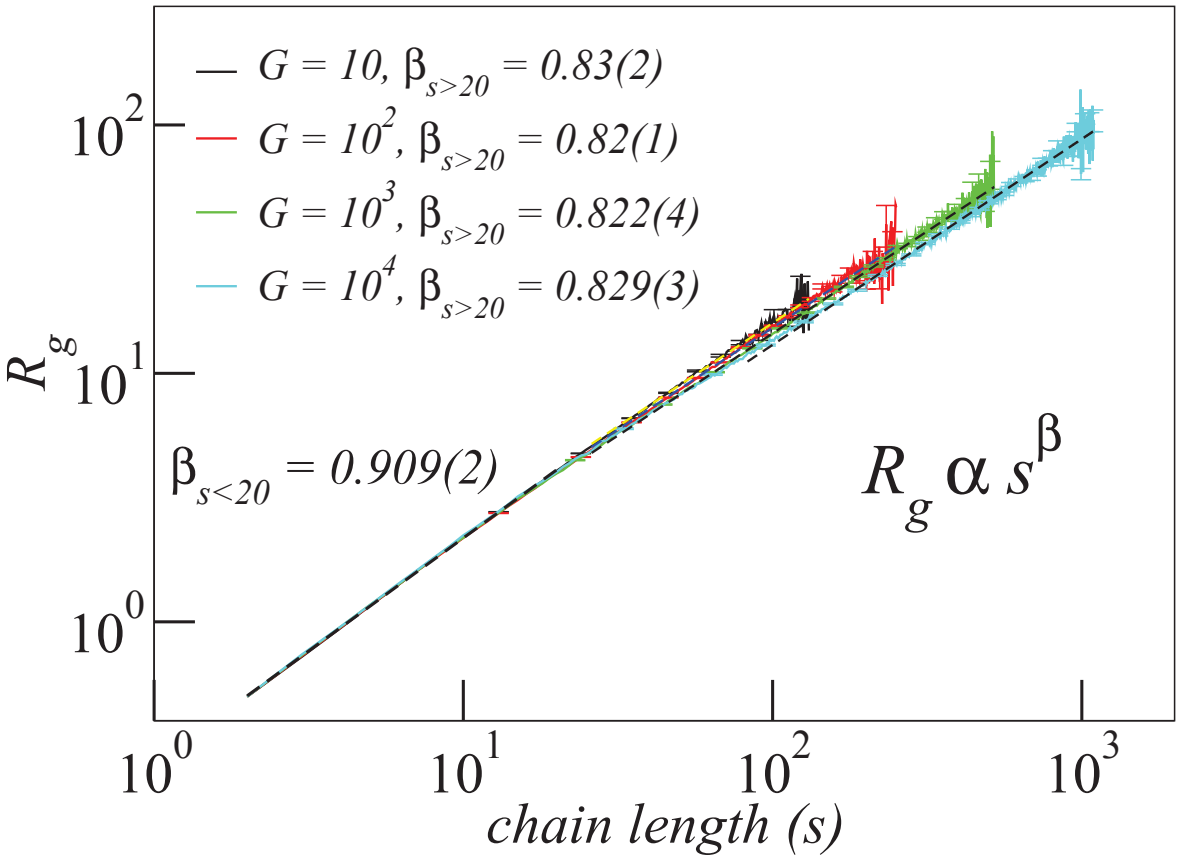

Figure 6.1: The plots of radius of gyration R_g versus chain length s for the polymer films grown using $L = 200$, $G = 10$, and $t = 10 \times 10^3$. The data are averaged over 500 independent runs and the statistical error of the mean are shown in the plots.

chains ($s > 20$) in the system, R_g depends on s according to the power law given in Eqn. (6.2). However, for shorter chains with $s < 20$ we found $\beta = 0.909(2)$, invariant for $G = 10$, 10^2, 10^3, and 10^4. Whereas, for longer chains with $s > 20$, $\beta = 0.825(3)$, that also remained invariant (with in error-bars) with an increase in G from 10 to 10^4. In our calculations of R_g, we found the power law exponent β to depend on the chain length ($s < 20$ or $s > 20$) and to be independent of G used in the simulations. This observation implies that at large $t = 10^4$ when the system is in a steady state growth regime, the fractal dimension $D_\beta = \frac{1}{\beta}$ of polymer chains in the system depends on their chain length and remains invariant to G used in the simulations. By using $L = 200$ and $t = 10^4$, we found $D_\beta(s < 20) = \frac{1}{(\beta = 0.909(2))} = 1.100(1)$ for chains with $s < 20$, and for longer chains with $s > 20$ the fractal dimension was found to be, $D_\beta(s > 20) = \frac{1}{(\beta = 0.825(3))} = 1.212(1)$ as shown in Fig. 6.1.

6.2 Spatial Distribution of Polymer Chains

The above discussion on $R_g(s)$ provided the insights about the geometric arrangements of the chains in $1 + 1D$ space of VDP growth. In this section we study the spatial distribution of polymer chains in x and y directions separately by calculating the root mean square fluctuations in the horizontal and the vertical positions of the monomers relative to the center of mass of the polymer. We label the fluctuations of the monomer positions in the x-direction and y-directions as $\Delta x_{CM}(s)$ and $\Delta y_{CM}(s)$ respectively, and use the definition,

$$\Delta x_{CM}(s) = \sqrt{\frac{\sum_{i=1}^{s}(x_i - x_{CM})^2}{s}}, \tag{6.4}$$

$$\Delta y_{CM}(s) = \sqrt{\frac{\sum_{i=1}^{s}(y_i - y_{CM})^2}{s}}, \tag{6.5}$$

to study the evolution of spatial fluctuations of polymer chains along two orthogonal directions of our growth system. We are interested in studying if there exists a bias in the growth direction of the polymers and how this bias (if it exists) in the preferred growth direction

depends on G. To this effect, we chose $L = 200$, $t = 10^4$ and performed simulations by varying G from 10 to 10^4. The data were averaged over 500 independent runs and the standard error of the mean was used as the error estimate of $\Delta x_{CM}(s)$ and $\Delta y_{CM}(s)$.

In Figs. 6.2(a) and 6.2(b) we show the fluctuations in monomer positions along horizontal (x) and vertical (y) directions respectively. In both plots of Fig. 6.2, the statistical errors in $\Delta x_{CM}(s)$ and $\Delta y_{CM}(s)$ increase as the chain length s increases. This is due to the decrease in the sample size of the longer chains in the system. We also note that in both plots of Fig. 6.2 the range of s is seen to increase with an increase in G; this is due to the presence of longer polymer chains at higher G. The dependence of s on G was discussed earlier in Section 5.1.2.

We now focus on studying the effect of G on the possible bias in the spatial distribution of monomers present in the chains growing via VDP. We chose $L = 200$ and two extreme values $G = 10$ and 10^4 and performed simulations to study the values of $\Delta x_{CM}(s)$ and $\Delta y_{CM}(s)$ for $t = 10 \times 10^3$. The Figs. 6.3(a) and 6.3(b) show the variation in the spatial spread of polymers along the two normal directions of our $1+1D$ growth model. The Fig. 6.3(a) shows the rms fluctuations $\Delta x_{CM}(s)$ and $\Delta y_{CM}(s)$ for $G = 10$, in this figure we found the values of $\Delta x_{CM}(s)$ and $\Delta y_{CM}(s)$ to be numerically very close for polymers with same chain length s. As s increases in the system, the corresponding $\Delta x_{CM}(s)$ and $\Delta y_{CM}(s)$ were also observed to increase proportionately to each other. In contrast, for $G = 10^4$, Fig. 6.3(b) shows the differences in $\Delta x_{CM}(s)$ and $\Delta y_{CM}(s)$ values for varying chain length polymers present in the system. In the higher diffusion case with $G = 10^4$ shown in Fig. 6.3(b), as s increases the average $\Delta y_{CM}(s)$ measured is found to be larger than $\Delta x_{CM}(s)$ for all chains with $s > 200$.

These observations from Figs. 6.3(a) and 6.3(b) substantiates our earlier finding that, as G increases in the simulations, the chains tend to grow in the direction perpendicular (y) to the substrate. This biased growth direction along y axis explains the accelerated growth rate of average film height h_{avg} discussed in Section 4.2.

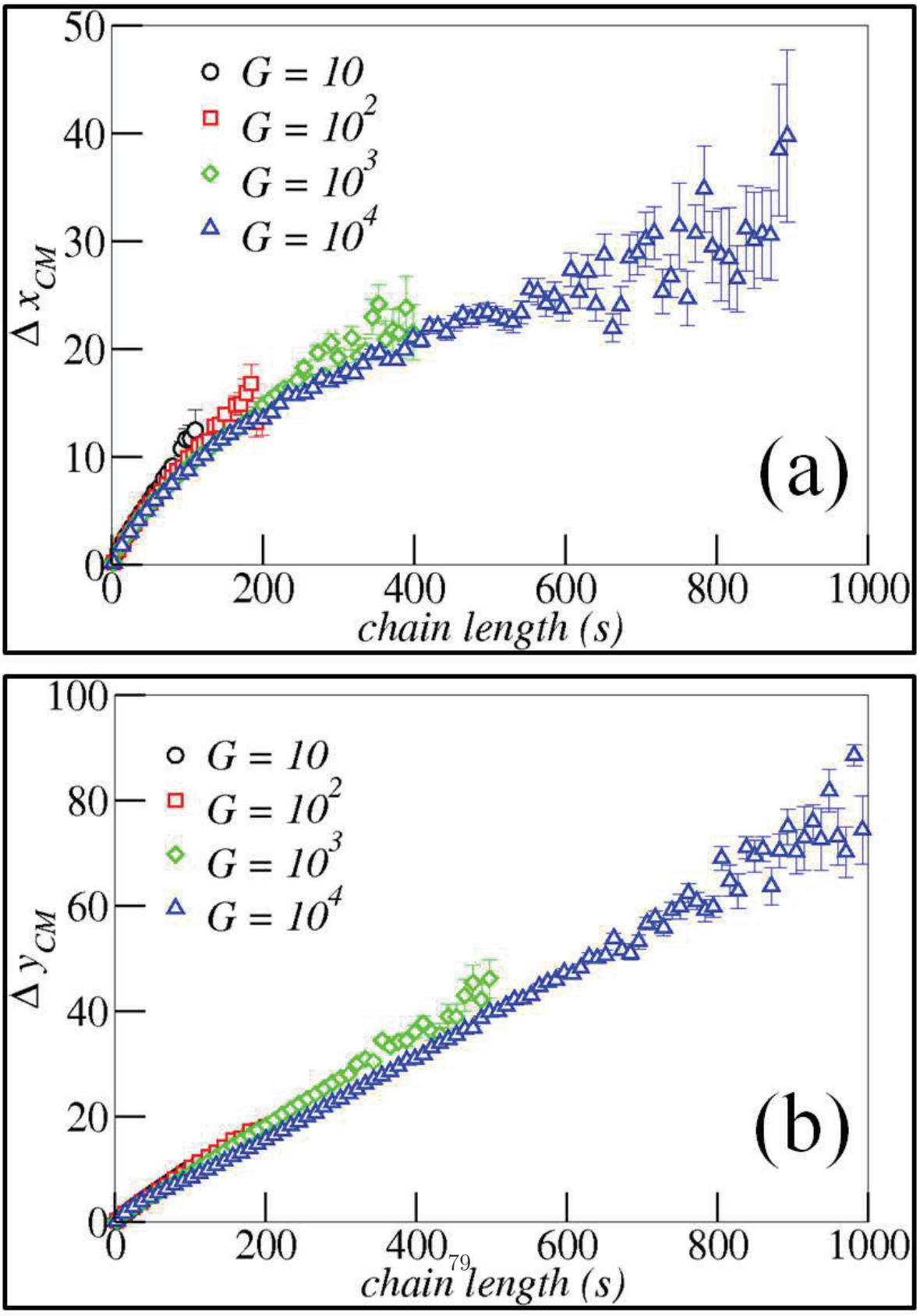

Figure 6.2: The plots of (a):$\Delta x_{CM}(s)$ and (b):$\Delta y_{CM}(s)$ of the monomers present in polymer chains. The data were obtained for $L = 200$, and $t = 10 \times 10^3$. The error-bars in data were calculated using the standard error of the mean obtained from 500 independent simulations.

6.3 Conclusions

In this chapter, the conformational properties of polymer chains growing in a VDP system were studied. In particular, we calculated the radius of gyration R_g of the polymers with varying chain length s. The quantity R_g increases with s in accordance with a power law given by Eqn. (6.3). However instead of finding a single exponent β, we obtained two distinct exponents β depending on the chain lengths used in the curve-fit. For chains with $s < 20$, β was found to be 0.909(2) whereas for longer chains with $s > 20$ we found $\beta = 0.825(3)$. We also studied the spatial distributions of chains along x and y directions of the growth model. With an increase in G, the monomer positions in the chains were found to have more rms fluctuations along the y axis, such that $\Delta y_{CM}(s) > \Delta x_{CM}(s)$ for chains with $s > 200$. This difference in the spatial distributions of the chains explained the bias in the over all chain growth along the y direction as G is increased in the system.

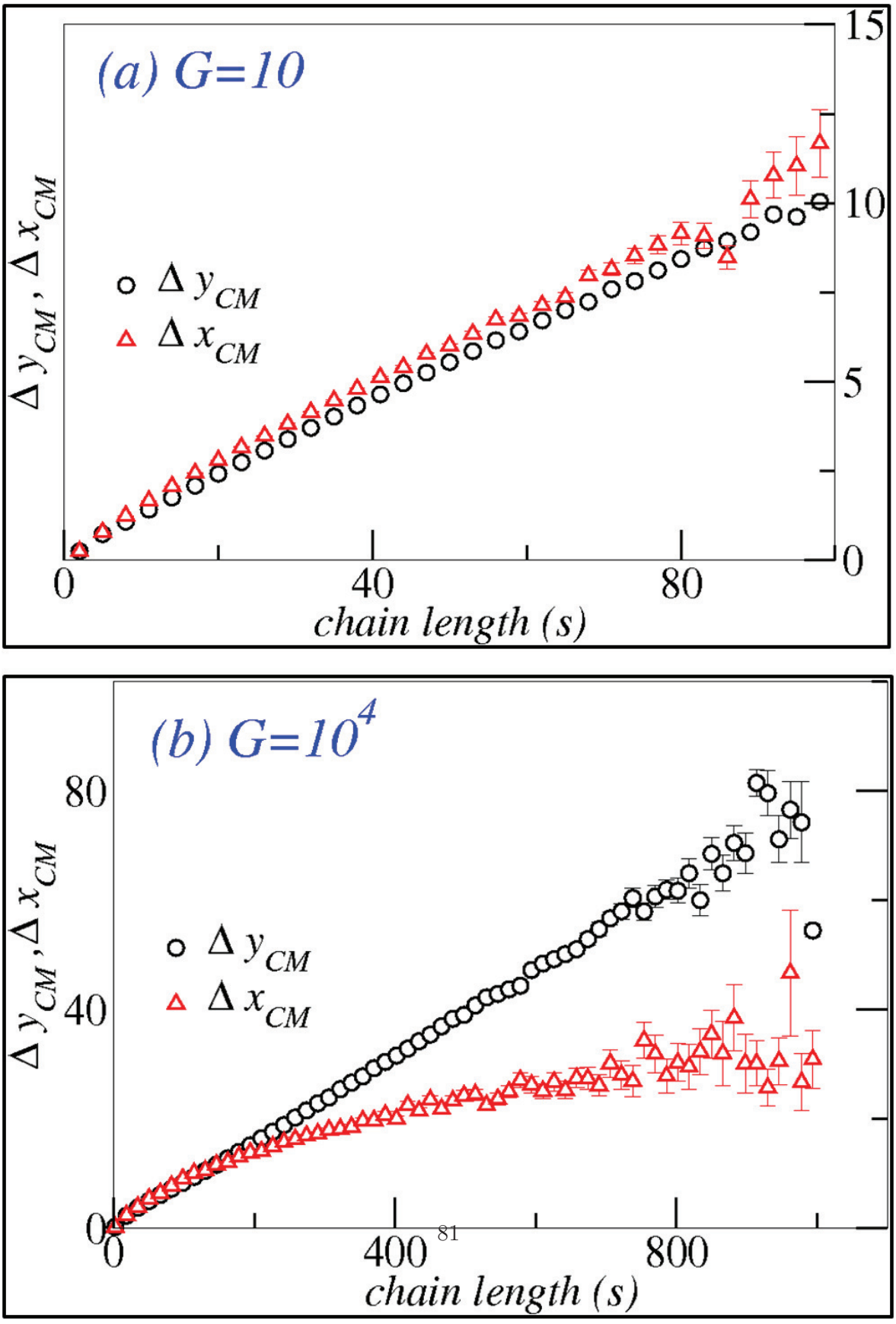

Figure 6.3: The plots of $\Delta x_{CM}(s)$ and $\Delta y_{CM}(s)$ for two extreme cases of diffusion (a):$G = 10$ and (b):$G = 10^4$. The data were obtained for $L = 200$, and $t = 10 \times 10^3$. The error-bars were calculated using the standard error of the mean obtained from 500 independent simulations.

Chapter 7

Conclusions

Polymer films continue to be a rich and active field of study, due to their importance in both basic research and a wide array of technological applications. The experimental technique referred to as vapor deposition polymerization (VDP) is considered to be advantageous in growing polymer films due to its ease and practical feasibility in both laboratory set-up and industrial mass productions. We therefore, performed a Monte Carlo based simulational study and used a coarse-grain approximation to simulate the polymers grown in VDP. The polymer growth simulations were performed on a $1 + 1D$ lattice by using a parameter $G = D/F$ that determined the competition between the deposition rate and diffusion rate of monomers during the VDP growth. The broad areas of our investigations of VDP growth focussed on (a) the interface width characteristics of films, (b) aggregation mechanism of polymer chains, and (c) understanding the structural properties of the chains. A principal outcome of our research is an understanding that the ratio G is a critical parameter that determines various properties of the films grown via VDP. Our study provides a basis for understanding the film growth under varying rates of surface diffusion and shows the importance of surface diffusion of monomers while explaining the fundamental differences between the films grown using VDP and physical vapor deposition (PVD).

The results section of this dissertation begin with the discussion on the properties of polymer films. Our simulations indicated that at any given time t, the average height of the deposited films was proportional to G, and for larger G ($> 10^5$) the growth rate of the average film height $r(G)$ was found to obey a power law, $r(G) \propto G^{0.162(3)}$. The dependence of $r(G)$ on

G explained the appearance of compact films at low G and the appearance of more porous films at large G. This behavior was noted to be a characteristic of VDP growth as our observations were in contrast to conventional PVD growth where higher diffusion results in films being less porous and more compact. Calculation of lateral film density $\rho(y)$ at varying t was carried out and it provided information about the existence of three distinct growth regions prevalent in VDP growth. The three different growth regimes were noted to be: interface, bulk film, and the growth front. We performed extensive studies of the growth front region by calculating the interface width $w(L,t)$ and height-height correlation functions $H(r,t)$ of the film surface. The finite length scaling was used to study the roughening behavior of the films at global length scales and we found that Dynamic Scaling Theory was valid at global length scales. However, at local length scales, the analysis of $H(r,t)$ revealed the presence of anomalous scaling in the films grown using VDP. The scaling functions that characterize the behavior of $w(L,t)$ and $H(r,t)$ were also calculated for two representative diffusion cases of $G = 10$ and 10^3. For obtaining a quantitative measure of the film morphology, we measured the average column-separation λ for the $2D$ tree-like structures obtained in our simulations. The time evolution of λ obeyed a power law given by $\lambda \propto t^p$ and the exponent p was seen to depend on the G used in the simulation.

The next phase of our study included the investigation of the aggregation mechanism of the polymer chains at varying diffusion conditions. The average chain length $S(t)$ was calculated to study the time evolution of chain aggregates. With an increase in t, we found the presence of a saturation region in the growth of chain aggregates where the $S(t)$ was observed to attain a saturation value S_{sat}. The overall size of the chain aggregates in saturation region S_{sat} was found to follow a power with G, given by $S_{sat} \propto G^{0.273(5)}$. Another interesting feature we observed in the chain length distribution functions $n_s(t)$ was a systematic deviation in their behavior as G was increased from 10 to 10^3. We found that as G was increased, the system was seen to have longer chains; the increase in the chain length

s of the polymers with G was understood to be arising from the high diffusion probabilities of monomers. With an increase in t, we observed a power law increase in the values of $n_s(t)$ for all polymer chain sizes present in the system. The time evolution studies of chain length distribution $n_s(t)$ for varying G showed the presence of a power law given by, $n_s(t) \propto t^{1.01(2)}$. This feature was found to be novel to the aggregation process in VDP as the polymer chains did not show the tendency of merging with each other to form larger chains. The reduced probability of polymer chain merger is in contrast to island aggregations observed in many diffusion mediated growths.

We applied the theory of dynamic scaling of aggregates to the polymer chains found in VDP and found that the scaling functions obtained for $G = 10$ and $G = 10^4$ did not overlap onto a single universal curve as expected by the theory. The ratio G was seen to bring about a systematic change in the behavior of the scaling functions that prevented the appearance of a single "data collapse" curve for varying G. This observed feature of the polymer aggregation mechanism was also noted to be a characteristic of VDP.

Lastly, we studied the structural properties of polymer chains by calculating the radius of gyration R_g and spatial distribution of chains using the rms fluctuations $\Delta x_{CM}(s)$ and $\Delta y_{CM}(s)$. The fractal dimension D_β of the chains was found to depend on the chain length s. We found $D_\beta = 1.100(1)$ for chains with $s < 20$ and $D_\beta = 1.212(1)$ for longer chains with $s > 20$ and the variation in G did not show any effect on the values of D_β for $L = 200$ and $t = 10^4$. However, the ratio G was seen to have a noticeable effect on the values of $\Delta x_{CM}(s)$ and $\Delta y_{CM}(s)$. With an increase in G from 10 to 10^4, the fluctuations in the monomer positions along y ($\Delta y_{CM}(s)$) were found to be larger than $\Delta x_{CM}(s)$. The difference in the spatial distributions of the monomers constituting the chains was found to account for the bias in the growth of chains along the y direction in our growth model.

In conclusion, the results presented in this dissertation have furthered the theoretical understanding of VDP growth used in the growth of linear polymer films. Although a sig-

nificant amount of results have been presented here, our model is in need of experimental data to validate the effects of surface diffusion and particle transport on the bulk films and polymer chain aggregates. In recent times as vapor deposition methods are of heightened interest we hope that our simulations will initiate new experimental and simulational studies of VDP and provide direct and improved measurements of particle diffusion and its effects on the evolution of polymer aggregates and overall film properties. We anticipate the insights provided by our research will benefit ongoing and future studies of this important film deposition technique.

Bibliography

[1] M. Anthamatten and K. K. S. Lau, *Encyclopedia of Chemical Processing*, Taylor & Francis (2009).

[2] S. Rogojevic, J. A. Moore, and W. N. Gill, "Modeling vapor deposition of low-k polymers: Parylene and polynaphthalene," *Journal of Vacuum Science & Technology A* **17**(1), 266–274 (1999).

[3] D. Y. Zhong, M. Hirtz, W. C. Wang, R. F. Dou, L. F. Chi, and H. Fuchs, "Kinetics of island formation in organic film growth," *Phys. Rev. B* **77**, 113404 (2008).

[4] S. Tangirala, D. P. Landau, and Y.-P. Zhao, "Dynamic scaling study of vapor deposition polymerization: A monte carlo approach," *Phys. Rev. E* **81**(1), 011605 (2010).

[5] J. Lahann, "Vapor-based polymer coatings for potential biomedical applications," *Polymer International* **55**(12), 1361–1370 (2006).

[6] G. W. Collins, S. A. Letts, E. M. Fearon, R. L. McEachern, and T. P. Bernat, "Surface roughness scaling of plasma polymer films," *Phys. Rev. Lett.* **73**, 708–711 (1994).

[7] F. Biscarini, P. Samor'i, O. Greco, and R. Zamboni, "Scaling behavior of anisotropic organic thin films grown in high vacuum," *Phys. Rev. Lett.* **78**, 2389–2392 (1997).

[8] J. Fortin and T. Lu, "A model for the chemical vapor deposition of poly(para-xylylene) (parylene) thin films," *Chemistry of Materials* **14**, 1945–1949 (2002).

[9] T.-M. Lu and J. A. Moore, "Vapor deposition of low-dielectric-constant polymeric thin films," *Mater. Res. Soc. Bull* **20**, 28 and references therein (1997).

[10] C. P. Wong, *Polymers for Electronic and Photonic Application*, Academic Press, Boston, MA (1993).

[11] J. Lahann, "Vapor-based polymer coatings for potential biomedical applications," *Polymer International* **55**, 1361–1370 (2006).

[12] B. W.F., L. C., B. D.R., and O. R. Austin T.M. and, *Encyclopedia of Polymer Science and Engineering*, Wiley, New York (1989).

[13] A. Gusev, K. Mailyan, A. Pebalk, I. Ryzhikov, and S. Chvalun, "Prospects for the application of nanostructured polymer and nanocomposite films based on poly-p-xylylene for micro-, opto-, and nanoelectronics," *Journal of Communications Technology and Electronics* **54**, 833–843 (2009).

[14] M.Soriaga, *Thin Films: Preparation, Characterization, and Applications*, Springer, New York (2002).

[15] M.Ohring, *Materials Science of Thin Films: Deposition and Structure*, Academic, San Diego (2002).

[16] V. Shalaev, *Nonlinear Optics of Random Media: Fractal Composites and Metal-Dielectric Films*, Springer, Berlin (2000).

[17] S.Ogale, *Thin Films and Heterostructures for Oxide Electronics*, Springer, Berlin (2005).

[18] J. H. S. Jackson and D. Lennon, *Catalysis in Application*, Royal Society of Chemistry, Cambridge (2003).

[19] J. Thomas, *Principles and Practice of Heterogeneous Catalysis*, Wiley, New York (1997).

[20] T.-M. Lu and J. A. Moore, "Vapor deposition of low-dielectric constant polymeric thin films," *MRS Bulletin* **22** (1997).

[21] W. R. Dolbier and W. F. Beach, "Parylene-af4: a polymer with exceptional dielectric and thermal properties," *Journal of Fluorine Chemistry* **122**(1), 97 – 104 (2003).

[22] K. Kim, M. Y. Jung, G. L. Zhong, J.-I. Jin, T. Y. Kim, and D. J. Ahn, "Morphology of poly(p-phenylenevinylene) thin films prepared directly on the surface of silicon wafers by the chemical vapor deposition polymerization," *Synthetic Metals* **144**(1), 7 – 11 (2004).

[23] H. Usui, "Deposition of polymeric thin films by ionization-assisted method," in *Proceedings of 1998 International Symposium on Electrical Insulating Materials*, 577–582 (1998).

[24] H. Biederman, V. Stelmashuk, I. Kholodkov, A. Choukourov, and D. Slavnsk, "Rf sputtering of hydrocarbon polymers and their derivatives," *Surface and Coatings Technology* **174**, 27–32 (2003).

[25] D. B. Chrisey and G. K. Hubler, Eds., *Pulsed Laser Deposition of Thin Films*, Wiley-Interscience (1994).

[26] A. Piqu, R. C. Y. Auyeung, J. L. Stepnowski, D. W. Weir, C. B. Arnold, R. A. McGill, and D. B. Chrisey, "Laser processing of polymer thin films for chemical sensor applications," *Surface and Coatings Technology* **163**, 293–299 (2003).

[27] F. Schreiber, "Organic molecular beam deposition: Growth studies beyond the first monolayer," *Physica Status Solidi Applied Research* **201**, 1037–1054 (2004).

[28] P. giles De Gennes, *Scaling Concepts in Polymer Physics*, Cornell University Press, Ithaca, N.Y (1979).

[29] P. J. Flory, *Principles of Polymer Chemistry*, Cornell University Press, Ithaca, N.Y (1953).

[30] B. K. and p. W. , "Monte carlo simulations of polymer dynamics: Recent advances," *Journal of Polymer Science Part B: Polymer Physics* **35**(1), 1–31 (1997).

[31] J. Baschnagel1, K. Binder, W. Paul, M. Laso, U. Suter, I. Batoulis, W. Jilge, and T. Burger, "On the construction of coarsegrained models for linear flexible polymer chains: Distribution functions for groups of consecutive monomers ," *J. Chem. Phys.* **95**(8), 6014–6025 (1991).

[32] K. Kremer and K. Binder, "Monte Carlo Simulations of Lattice Models for Macromolecules," *Computer Physics Reports* **7**(6), 259–310 (1988).

[33] D. M. and E. S. F., *The Theory of Polymer Dynamics*, Clarendon Press, Oxford (1986).

[34] de Gennes P. G., "Vapor deposition of low-dielectric constant polymeric thin films," *J. Chem. Phys.* **69** (1972).

[35] I. Carmesin and K. Kremer, "The bond fluctuation method - A new effective algorithm for the dynamics of polymers in all spatial dimensions," *Macromolecules* **21**(9), 2819–2823 (1988).

[36] W. Paul, K. Binder, D. Heermann, and K. Kremer, "Crossover scaling in semidilute polymer-solutions - A Monte Carlo test ," *Journal de Physique II* **1**(1), 37–60 (1991).

[37] W. Paul, K. Binder, K. Kremer, and H. D.W., "Structure property correlation of polymers, a Monte Carlo approach," *Macromolecules* **24**(23), 6332–6334 (1991).

[38] W. Paul and N. Pistoor, "A mapping of realistic onto abstract polymer models and an application to 2 Bisphenol polycarbonates," *Macromolecules* **27**(5), 1249–1255 (1994).

[39] Y. Xu, D. Xu, and J. Liang, *Computational Methods for Protein structure Prediction and Modeling: Structure Prediction*, Oxford University Press (2007).

[40] J. Skolnick, A. Kolinski, D. Kihara, M. Betancourt, P. Rotkiewicz, and M. Boniecki, "Ab initio protein structure prediction via a combination of threading, lattice folding, clustering, and structure refinement," *Proteins: Structure, Function, and Bioinformatics* **45**(S5), 149–156 (2001).

[41] M. Szwarc, "Poly-Para-Xylelene - Its chemistry and application in coating technology," *Polymer Engineering and Science* **16**(7), 473–479 (1976).

[42] M. Szwarc, "New monomers of the quinoid type and their polymers," *Journal of Polymer Science* **6**(3), 319–329 (1951).

[43] M. Szwarc, "New monomers of the quinoid type and their polymers," *Journal of Chemical Physics* **16**(2), 128 (1948).

[44] W. F. Gorham, "A new, general synthetic method for the preparation of linear poly-p-xylylenes," *Journal of Polymer Science Part A-1: Polymer Chemistry* **4**(12), 3027–3039 (1966).

[45] J. B. Fortin and L. Toh-Ming, *Chemical Vapor Deposition Polymerization: The Growth and Properties of Parylene Thin Films*, Kluwer Academc Publishers, Boston (2004).

[46] W. F. Beach, "A model for the vapor deposition polymerization of p-xylylene," *Macromolecules* **11**(1), 72–76 (1978).

[47] D. M. Mattox, *Handbook of Physical Vapor Deposition (PVD) Processing*, Noyes Publications, Berkshire, UK (1998).

[48] A.-L. Barabasi and H. E. Stanley, *Fractal Concepts in Surface Growth*, Cambridge University Press, Cambridge, England (1995).

[49] P. Meakin, *Fractals, scaling, and growth far from equilibrium*, Cambridge University Press, Cambridge, England (1998).

[50] S. Pal and D. P. Landau, "Monte carlo simulation and dynamic scaling of surfaces in mbe growth," *Phys. Rev. B* **49**, 10597–10606 (1994).

[51] Y. Shim, D. P. Landau, and S. Pal, "Domain growth and surface roughening in monte carlo simulations of $a0.5b0.5$ film growth," *Phys. Rev. E* **58**(6), 7571–7579 (1998).

[52] Y.-P. Zhao, A. R. Hopper, G.-C. Wang, and T.-M. Lu, "Monte carlo simulation of submonolayer vapor-deposition polymerization," *Phys. Rev. E* **60**(4), 4310–4318 (1999).

[53] W. Bowie and Y. P. Zhao, "Monte carlo simulation of vapor deposition polymerization," *Surface Science* **563**(8), L245–L250 (2004).

[54] A. Greiner, S. Mang, O. Schafer, and P. Simon, "Poly(p-xylylene)s: Synthesis, polymer analogous reactions, and perspectives on structure-property relationships," *Acta Polymerica* **48**(1-2), 1–15 (1997).

[55] P. Simon, S. Mang, A. Hasenhindl, W. Gronski, and A. Greiner, "Poly(p-xylylene) and its derivatives by chemical vapor deposition: Synthesis, mechanism, and structure," *Macromolecules* **31**(25), 8775–8780 (1998).

[56] N. Tung, Y. Yu, K. Kim, S. Joo, and J. Jin, "Synthesis of poly(p-xylylene) from alpha,alpha-bis(alkoxy or aryloxy)-p-xylenes by chemical vapor deposition polymerization," *Bulletin of the Korean Chemical Society* **25**(1), 31–32 (2004).

[57] D. R. Strel'tsov, A. I. Buzin, E. I. Grigor'ev, P. V. Dmitryakov, K. A. Mailyan, A. V. Pebalk, and S. N. Chvalun, "Scaling analysis of the morphology of nanostructured poly (p-xylylene) films synthesized by vapor deposition polymerization," *Nanotechnologies in Russia* **3**, 494–501 (2008).

[58] Y.-P. Zhao, J. B. Fortin, G. Bonvallet, G.-C. Wang, and T.-M. Lu, "Kinetic roughening in polymer film growth by vapor deposition," *Phys. Rev. Lett.* **85**(15), 3229–3232 (2000).

[59] I. J. Lee, M. Yun, S.-M. Lee, and J.-Y. Kim, "Growth mechanisms of vapor-born polymer films," *Phys. Rev. B* **78**(11), 115427 (2008).

[60] K. Smalara, A. Gieldon, M. Bobrowski, J. Rybicki, and C. Czaplewski, "Theoretical Study of Polymerization Mechanism of p-Xylylene Based Polymers," *Journal of Physical Chemistry A* **114**(12), 4296–4303 (2010).

[61] I. Y. Gotlib, E. M. Piotrovskaya, and S. W. de Leeuw, "Molecular dynamics simulation of poly(p-xylylene): Bulk phase and a single molecule," *Journal of Physical Chemistry C* **111**(18), 6613–6620 (2007).

[62] S. Tangirala and D. P. Landau, "Role of diffusion in scaling of polymer chain aggregates found in vapor deposition polymerization," *Phys. Rev. E (communicated)* (2010).

[63] G. Marsaglia, "Random number generators," *J. Mod. Appl. Statist. Methods* **2**(1), 2–13 (2003).

[64] J. Yu and J. G. Amar, "Dynamical scaling behavior in two-dimensional ballistic deposition with shadowing," *Phys. Rev. E* **66**(2), 021603 (2002).

[65] J. Evans, P. Thiel, and M. Bartelt, "Morphological evolution during epitaxial thin film growth: Formation of 2d islands and 3d mounds," *Surface Science Reports* **61**(1-2), 1 – 128 (2006).

[66] S. Das Sarma and P. Tamborenea, "A new universality class for kinetic growth: One-dimensional molecular-beam epitaxy," *Phys. Rev. Lett.* **66**(3), 325–328 (1991).

[67] D. E. Wolf and J. Villain, "Growth with surface diffusion," *Europhysics Letters* **13**(5), 389 (1990).

[68] J. G. Amar, F. Family, and P.-M. Lam, "Dynamic scaling of the island-size distribution and percolation in a model of submonolayer molecular-beam epitaxy," *Phys. Rev. B* **50**(12), 8781–8797 (1994).

[69] J. T. Drotar, Y.-P. Zhao, T.-M. Lu, and G.-C. Wang, "Surface roughening in shadowing growth and etching in $2+1$ dimensions," *Phys. Rev. B* **62**(3), 2118–2125 (2000).

[70] M. Pelliccione, T. Karabacak, and T.-M. Lu, "Breakdown of dynamic scaling in surface growth under shadowing," *Phys. Rev. Lett.* **96**(14), 146105 (2006).

[71] R. P. U. Karunasiri, R. Bruinsma, and J. Rudnick, "Thin-film growth and the shadow instability," *Phys. Rev. Lett.* **62**(7), 788–791 (1989).

[72] G. S. Bales and A. Zangwill, "Growth dynamics of sputter deposition," *Phys. Rev. Lett.* **63**(6), 692 (1989).

[73] Y.-P. Zhao, J. T. Drotar, G.-C. Wang, and T.-M. Lu, "Roughening in plasma etch fronts of si(100)," *Phys. Rev. Lett.* **82**(24), 4882–4885 (1999).

[74] J. T. Drotar, Y.-P. Zhao, T.-M. Lu, and G.-C. Wang, "Surface roughening in low-pressure chemical vapor deposition," *Phys. Rev. B* **64**(12), 125411 (2001).

[75] A.-L. Barabási and T. Vicsek, "Multifractality of self-affine fractals," *Phys. Rev. A* **44**(4), 2730–2733 (1991).

[76] F. Family and T. Vicsek, Eds., *Dynamics of Fractal Surfaces*, (Singapore), World Scientific (1991).

[77] J. Asikainen, S. Majaniemi, M. Dubé, J. Heinonen, and T. Ala-Nissila, "Dynamical scaling and kinetic roughening of single valued fronts propagating in fractal media," *Eur. Phys. J. B* **30** (2002).

[78] J. Krug, "Turbulent interfaces," *Phys. Rev. Lett.* **72**(18), 2907–2910 (1994).

[79] J. J. Ramasco, J. M. López, and M. A. Rodríguez, "Generic dynamic scaling in kinetic roughening," *Phys. Rev. Lett.* **84**(10), 2199–2202 (2000).

[80] J. H. Jeffries, J.-K. Zuo, and M. M. Craig, "Instability of kinetic roughening in sputter-deposition growth of pt on glass," *Phys. Rev. Lett.* **76**(26), 4931–4934 (1996).

[81] S. Das Sarma, S. V. Ghaisas, and J. M. Kim, "Kinetic super-roughening and anomalous dynamic scaling in nonequilibrium growth models," *Phys. Rev. E* **49**, 122–125 (1994).

[82] J. G. Amar, P.-M. Lam, and F. Family, "Groove instabilities in surface growth with diffusion," *Phys. Rev. E* **47**(5), 3242–3245 (1993).

[83] M. Schroeder, M. Siegert, D. E. Wolf, J. D. Shore, and M. Plischke, "Scaling of growing surfaces with large local slopes," *Europhys. Lett.* **24**(7), 563–568 (1993).

[84] J. M. López, M. A. Rodríguez, and R. Cuerno, "Superroughening versus intrinsic anomalous scaling of surfaces," *Phys. Rev. E* **56**(4), 3993–3998 (1997).

[85] R. Baiod, D. Kessler, P. Ramanlal, L. Sander, and R. Savit, "Dynamical scaling of the surface of finite-density ballistic aggregation," *Phys. Rev. A* **38**(7), 3672–3679 (1988).

[86] F. Family and T. Vicsek, "Scaling of the active zone in the eden process on percolation networks and the ballistic deposition model," *Journal of Physics A* **18**(2), L75–L81 (1985).

[87] J. M. Kim and J. M. Kosterlitz, "Growth in a restricted solid-on-solid model," *Phys. Rev. Lett.* **62**(19), 2289–2292 (1989).

[88] F. Family, "Scaling of rough surfaces: effects of surface diffusion," *Journal of Physics A* **19**(8), L441–L446 (1986).

[89] Y. Zhao, G.-C. Wang, and T.-M. Lu, *Characterization of amorphous and crystalline rough surface : principles and application*, Academic Press, San Diego, CA (2001).

[90] J. M. López, M. A. Rodríguez, and R. Cuerno, "Power spectrum scaling in anomalous kinetic roughening of surfaces," *Physica A: Statistical and Theoretical Physics* **246**(3-4), 329 – 347 (1997).

[91] S. Ganguli, H. Agrawal, B. Wang, J. F. McDonald, T. M. Lu, G.-R. Yang, and W. N. Gill, "Improved growth and thermal stability of parylene films," *Journal of Vacuum Science and Technology: A* **15**(6), 3138–3142 (1997).

[92] W. F. Beach, "A model for the vapor deposition polymerization of p-xylylene," *Macromolecules* **11**(1), 72–76 (1978).

[93] I. Lee and M. Yun, "Island nucleation and growth dynamics during submonolayer vapor deposition polymerization," *Macromolecules* **43**(12), 5450–5454 (2010).

[94] R. Iwamoto, R. Bopp, and B. Wunderlich, "Crystallization during polymerization of Ploy-P-Xylylene. III. Crystal-structure and molecular-orientation as a function of temperature," *Journal of Polymer Science:B - Polymer Physics* **13**(10), 1925–1938 (1975).

[95] d. Kirkpatrick and B. Wunderlich, "Thermal-analysis of the phase-transitions of Ploy(Para-Xylynene)," *Makromolekulare Chemie-Macromolecular Chemistry and Physics* **186**(12), 2595–2607 (1985).

[96] S. Kubo and B. Wunderlich, "The unit cell of poly-p-xylylene and the structure of solution-grown crystals," *Die Makromolekulare Chemie* **162**(1), 1–7 (1972).

[97] S.-W. Son, M. Ha, and H. Jeong, "Anomalous scaling behavior in polymer thin film growth by vapor deposition," *Journal of Statistical Mechanics: Theory and Experiment* **2009**(02), P02031 (2009).

[98] M. A. Albao, M. M. R. Evans, J. Nogami, D. Zorn, M. S. Gordon, and J. W. Evans, "Monotonically decreasing size distributions for one-dimensional ga rows on si(100)," *Phys. Rev. B* **72**(3), 035426 (2005).

[99] M. Brinkmann, F. Biscarini, C. Taliani, I. Aiello, and M. Ghedini, "Growth of mesoscopic correlated droplet patterns by high-vacuum sublimation," *Phys. Rev. B* **61**(24), R16339–R16342 (2000).

[100] T. Vicsek and F. Family, "Dynamic scaling for aggregation of clusters," *Phys. Rev. Lett.* **52**(19), 1669–1672 (1984).

[101] M. C. Bartelt and J. W. Evans, "Scaling analysis of diffusion-mediated island growth in surface adsorption processes," *Phys. Rev. B* **46**(19), 12675–12687 (1992).

[102] G. H. Lathe and C. R. Ruthven, "The separation of substances and estimation of their relative molecular sizes by the use of colums of starch in water.," *Biochem. J.* **62**(4), 665–674 (1956).

[103] F. Leyvraz and S. Redner, "Scaling theory for migration-driven aggregate growth," *Phys. Rev. Lett.* **88**(6), 068301 (2002).

[104] A. Moncho-Jordá, F. Martínez-López, and R. Hidalgo-Álvarez, "Simulations of aggregation in 2d. a study of kinetics, structure and topological properties," *Physica A: Statistical Mechanics and its Applications* **282**(1-2), 50 – 64 (2000).

[105] B. B. Mandelbrot, *The Fractal Geometry of Nature*, W. H. Freeman, 1 ed. (1982).

[106] V. T., *Fractal Growth Phenomena*, World Scientific, Singapore (1989).

[107] A. J. Barrett and J. Skolnick, "On the apparent radius of gyration of linear polymers and the experimental determination of the excluded-volume parameter," *Macromolecules* **21**(4), 1141–1145 (1988).

[108] P. Meakin, "Diffusion-limited polymerization and surface growth," *Phys. Rev. A* **37**(7), 2644–2659 (1988).